UNIVERSITA' DEGLI STUDI DI PARMA

Dottorato di ricerca in Progettazione e Sintesi di
Composti Biologicamente Attivi

Ciclo XXIV

Structure-based drug design of molecules influencing fatty acid derivatives signal pathways

Coordinatore:
Chiar.mo Prof. Marco Mor

Tutor:
Chiar.mo Prof. Marco Mor

Dottorando: Luigi Capoferri

Contents

1. Ligand-protein interactions modelling in drug design

Drug development is a long route that aims at the introduction of a new drug on the market. This process starts when scientists identify new pharmacological targets and confirm their role in diseases (Target validation). Once the target is validated and specific assays are successfully developed, screening of compound libraries are generally performed to find biologically active compounds, the hits. These small molecules are then optimized in order to improve their drug-like properties, obtaining the lead compounds. The resulting drug candidate undergos preclinical trials, that preliminary establish their safety profile on animal model. Before the registration of a new drug on the market, the three phases of clinical trials must finally assure its efficacy and safety on humans. In this long process, computational chemistry contribute in different ways to the early steps of hit and lead identification and of lead optimization.

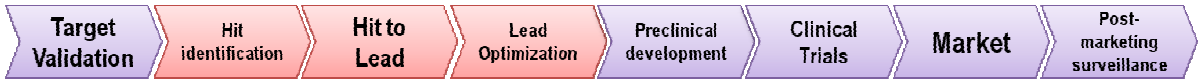

Figure 1.1 Critical steps in drug development process

One of the basic principles of medicinal chemistry is that biological activity of a compound depends on the three-dimensional placement of specific functional groups that must ensure the optimal supramolecular interactions with the specific target. On this light, it becomes clear why many efforts are spent to elucidate the relationships between the chemical or 3D structure of a molecule and its biological activity (Structure activity relationships – SAR).

Molecular modeling places exactly on the representation and manipulation of the structure of molecules, and of properties that are dependent upon the three-dimensional structures, such as geometries, energies, electronic and spectroscopic properties. Tools provided by this discipline can be used, in conjunction with traditional research techniques, to examine the structural properties of known

compounds and to develop hypothesis which relates these characteristics to experimental observations, in order to predict activities for new chemical entities.

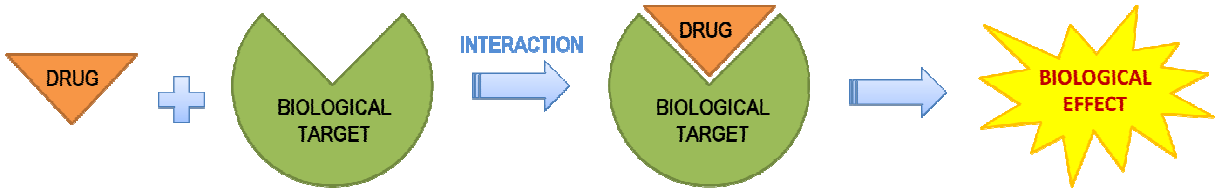

Figure 1.2 Specific interactions between the drug and its target are essential to elicit a biological effect. The occupancy of the target is defined by the affinity, while efficacy indicates the ability to give a biological response.

Ligand - target interactions modelling

The selective binding of a small-molecule ligand to a particular protein is determined by mutual structural and energetic recognition. These interactions can be either covalent or non-covalent.

The rapid increase in available structural information about target proteins, obtained by NMR and crystallography, together with the creation of specific computational tools, provided the possibility to obtain insights at atomistic level about these interactions. “Structure-based drug design” is a popular modus operandi where the three-dimensional structure of a target interacting with small molecules is used to guide drug discovery.

Non-covalent interactions

Non-covalent association of receptor (R) and ligand (L) to form a receptor-ligand complex (RL) generally occurs in an aqueous, electrolyte-containing solution.

$$R + L \underset{K_d}{\overset{K_a}{\rightleftarrows}} RL \qquad \textit{(eq. 1.1)}$$

Under thermodynamic equilibrium conditions, this reaction is determined by the standard Gibbs free energy of binding ΔG_0.

$$K_a = K_d^{-1} = \frac{[RL]}{[R][L]} \qquad \textit{(eq. 1.2)}$$

$$\Delta G_0 = \Delta H_0 - T\Delta S = -RT\ ln(K_a) \qquad \textit{(eq. 1.3)}$$

This quantity is related to the experimentally determined association or affinity constant K_a (or its reciprocal dissociation constants, K_d) and is composed of an enthalpic (ΔH_0) and an entropic ($T\Delta S$) portion, where T refers to the absolute temperature.

In place of ΔG_0, the term (binding) affinity is used to describe the tendency of a molecule to form a complex with another one. Therefore ΔG_0 can be understood as a function that describes the stability of the complex with respect to free ligand and uncomplexed receptor.

Experimentally determined dissociation constants fall into a range between 10^{-2} and 10^{-12} M, which corresponds to a Gibbs free energy of binding of -10 to -70 kJ mol^{-1} at 298 K. A change in free enthalpy of 5.7 kJ mol^{-1} at this temperature alters the affinity constant by one order of magnitude[1]. It is generally accepted that electrostatic interactions play a major role in non-covalent ligand-receptor binding. They comprise salt bridges, hydrogen bonds, dipole-dipole interactions, and interactions with metal ions. Furthermore, also solvation and desolvation contributions, and the mutual spatial complementarity in van der Waals interactions are of most importance.

Molecular modeling offers methods to calculate free energies of binding, providing insights at a molecular level about protein–ligand interactions which are valuable for rationalizations and predictions in the drug design process.

At best, ΔG_0 is determined by statistical thermodynamics resulting in a master equation that considers all contributing effects. The most theoretically convincing approaches are elaborate methods such as free energy perturbation (FEP), thermodynamic integration (TI) or the path sampling[2]. In these methods, derived directly from statistical mechanics, extensive simulations are employed to sample all the degrees of freedom along a reaction coordinates that correspond to an alchemical (FEP and TI) or configurational (path sampling) modification of the

system. In the first case perturbations are made to convert one ligand to another using the thermodynamic cycle involving a coupling parameter that causes one molecule to be smoothly mutated to the other; in the latter case, biasing potential are used to obtain a PMF along the dissociation path. Application of these methods are reported by Kollman and Merz, that published a rare prospective FEP result on the binding of an inhibitor to thermolysin. Pearlman performed a retrospective analysis on congeneric series of 16 kinase inhibitors. In addition, Reddy and Erion have used FEP calculations to evaluate contributions of heteroatoms and small groups to binding. Jorgensen performed several substituent optimization on COX-2/COX-1 selectivity, and studied the effects of HIV-RT mutations on the activities of NNRTIs[3].

Unfortunately these methods are computationally too demanding for a widespread use. In order to obtain fast computational methods, various levels of approximations have been considered, particularly the treatment of electrostatics, of the solvent or the estimation of configurational entropy. Generally, these methods are based on the generally assumption that the binding affinity can be parted into several additive terms: a number of empirically derived contributions is fitted to a data set of experimental observation and their sum constitute the empirical regression-based scoring functions. Actually, this approach is the basis of widely used techniques such as Linear Interaction Energy (LIE) or Docking.

When the structure of the target is known, a preliminary virtual screening approach allow to prioritize compounds for experimental testing. By docking, libraries of potential ligands are built in the computer, optimally positioned in the binding site, and scored for potential activity. Some particularly notable examples are the discovery of DNA gyrase inhibitors after HTS failed and the findings of much higher hit rates for docking than HTS in two comparative studies for tyrosine phosphatase 1B[4].

Covalent interactions

During drug development, covalent interaction of the candidate with several biological entities must be taken into account.

It is widely acknowledged that nonspecific covalent binding should be avoided or minimized when optimizing drug properties, to reduce the potential for organ toxicity or idiosyncratic reactions. These side reactions can be easily avoided filtering out screening hits containing potentially reactive functionality.

Less obvious is to predict the metabolism of a drug by an enzyme, that can potentially reduce its pharmacokinetics profile, sometimes depending from genetic polymorphisms, or lead to toxic metabolites.

Alternatively, there are instances where controlled, target-specific covalent modification has proven useful, as demonstrated by a number of available drugs acting in covalent way (e.g. penicillins, proton-pump inhibitors, aspirine)[5].

In a chemical reaction, $\Delta G_{activation}$ is the energy of activation necessary to raise the reactants into a high energy state (transition state), that represents the intermediate between the reactants and the products. Enzyme are biological systems that are able to reduce the $\Delta G_{activation}$ for specific reactions, by stabilization of the transition states. $\Delta G_{activation}$ for enzymatic catalyzed reactions are include between 50 and 90 kJ·mol^{-1} [6].

Enzymatic reactions are generally assumed to take place in two main steps: initial recognition between enzyme and substrate leads to the rapid formation of a reversible complex, the so-called Michaelis complex, while in a slower chemical step, the chemical modification takes place[7].

$$E + S \underset{k_{-1}}{\overset{k_1}{\rightleftarrows}} E \cdot S \qquad \textit{(eq. 1.4)}$$

$$E \cdot S \xrightarrow{k_{CAT}} E + P \qquad \textit{(eq. 1.5)}$$

$$k_{CAT} = \frac{[E]\cdot[P]}{[ES]} \qquad \textit{(eq. 1.6)}$$

Using the steady-state approximation, other important parameters can be calculated: the V_{max}, the enzyme's maximum rate, and the Michaelis-Menten constant, K_M, that represents the concentration at which the rate of the enzyme

reaction is half V_{max}. The ratio k_{CAT}/K_M is a measure of catalytic efficiency (diffusion process determines the efficiency theoretical limit of 10^8 M^{-1} s^{-1}). It is an apparent second rate constant that takes into account the free energy difference between the dissociated enzyme-substrate and the transition state of the catalytic reaction[8].

$$K_M = \frac{k_{-1}+k_{CAT}}{k_1} \qquad \textit{(eq. 1.7)}$$

$$\Delta G_{activation} = -RT\ ln\left(\frac{k_{CAT}}{K_M}\right) \qquad \textit{(eq. 1.8)}$$

In less simple cases, an intermediate reaction exists and the intermediate compound is converted into product in a second step. In this instance we have a very similar equation where k_{CAT} depends on the two reactive steps:

$$E + S \underset{k_{-1}}{\overset{k_1}{\rightleftarrows}} E \cdot S \qquad \textit{(eq. 1.9)}$$

$$E \cdot S \xrightarrow{k_2} EI \qquad \textit{(eq. 1.10)}$$

$$EI \xrightarrow{k_3} E + P \qquad \textit{(eq. 1.11)}$$

$$k_{CAT} = \frac{k_2 \cdot k_3}{k_2 + k_3} \qquad \textit{(eq. 1.12)}$$

Covalent modifiers, in ideal case, must be poorly reactive with solution nucleophiles under physiological conditions but, upon appropriate positioning, they should selectively react within the target protein. In this case, the covalent modifier kinetics are similar to the two-step enzymatic kinetics: 1) recognition between ligand and target, 2) formation of the covalent adduct and, depending of its stability, 3) hydrolysis of the covalent complex. Modulation of all these three steps is essential during the development of a covalent modifier.

Generally, compounds designed to act in a covalent way are inhibitors (I) that target specific enzymes (E). Their kinetics, when inhibitor is irreversible and its concentration is higher than that of the enzyme, are described by the equation of Kitz and Wilson.

$$K_i = \frac{k_1}{k_{-1}} \qquad \textit{(eq. 1.13)}$$

$$k_{obs} = \frac{k_2}{1+\frac{K_i}{[I]}} \qquad \textit{(eq. 1.14)}$$

This equation can also be written in a linearized form:

$$\frac{1}{k_{obs}} = \frac{K_i}{k_2 \cdot [I]} + \frac{1}{k_2} \qquad \textit{(eq. 1.15)}$$

K_i is the dissociation constant of the enzyme-inhibitor complex, and k_2 is the maximum (or limiting) inhibition rate if the enzyme is saturated with inhibitor. This is a first-order rate constant. The ratio k_2/K_i is a second-order inhibition rate, similar to k_{CAT}/K_M, and is the most commonly used parameter to report inhibition data. Another important parameter is the IC_{50} value, the inhibitor concentration necessary to effect 50% inhibition of the enzyme. With a covalent inhibitor this parameter clearly depends on the conditions of the enzyme assay and on the time during which the enzyme is incubated with the inhibitor[9].

Simulations and modelling of enzyme-catalyzed reaction mechanisms offer the potential of uniquely detailed, atomic-level insight into the fundamental processes of biological catalysis. Intermediates and transition states structures can provide useful structural information for the design of analogues of the transition states that act as inhibitor. On the other hand, energy profiles for the reactions for covalent modifiers can be suitable for prediction of their reactivity and for SAR studies[10].

While modeling a reaction, it is often desirable to calculate the energy and the structures of the system at several stages of the chemical change, typically, the equilibrium and the transition states. A theoretically accurate approach consists of the calculation of the potential of mean force (PMF) along the minimum energy reaction path (MERP), that connect the two minima on the free energy surface representing the reactants and the products. This can be done by a molecular dynamics (MD) or statistical Monte Carlo (MC) extensive sampling, but, since the treatment of the system by Quantum Mechanics (QM) is required to sample the chemical changes, the computation of the free energy surface is often too expensive.

A typical approach, when entropic contribute variation is negligible, is to approximate the problem to a potential energy question: this approach include geometry optimization of equilibrium structures and searching for TS by minimization algorithms, eventually applying an entropic correction factor about the vibrational frequency of the system. Optimization methods allow to find the minimum energy structures with reasonably accuracy and performance, but less trivial is the search for TS.

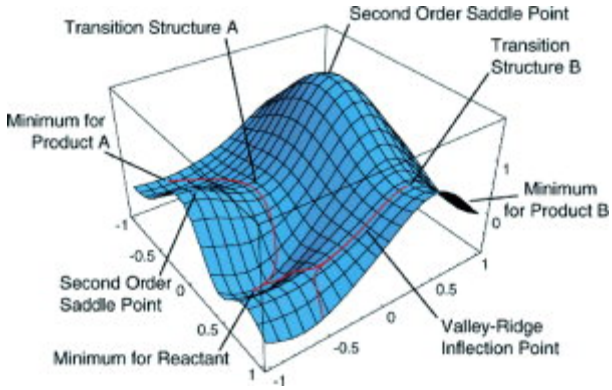

Figure 1.3 Model potential energy surface showing minima, transition states, a second-order saddle point, reaction paths, and a valley ridge inflection point (from ref.11)

A transition state is a stationary point on a potential energy surface that corresponds to a saddle point (Figure 1.3). It is a maximum in one and only one direction and a minimum in all other perpendicular directions. Several minimization methods can be adapted to find transition states, imposing one and only one negative eigenvalue in the initial Hessian where the corresponding eigenvector must be a suitable approximation to the transition vector (i.e., pointing from one valley to the other).

Other methods permits to find the minimum energy path (MEP) that connect two minima. After a TS has been located following reaction path can be applied. For example, intrinsic reaction coordinate (IRC) is an accurate method that permits to search for the MEP. Adopting a mass-weighted steepest descent method, from the TS the path orthogonal to the isopotential surface is reconstructed till reaching the minima. However for biomolecules these methods can be computationally demanding, since they require the calculation of the Hessian matrix.

If a priori definition of a reaction coordinate is known, a more general alternative to climb from reactants or products to the transition state is the coordinate driving or adiabatic mapping method: a chosen variable is stepped while optimizing the remaining ones[12].

Although enzymes are generally regarded as targets, the main examples of enzymatic reaction modeling applied to drug design focus on drug metabolism and toxicology (ADME–TOX). For example, a huge number of mechanistic studies was performed to enlight the catalytic mechanisms of P450 isozymes CYP3A5 and CYP2D6, that metabolize more than 70% of the drugs in humans, and several reviews describe the numerous *in silico* methods developed to predict the site-of-metabolism of drug-like compounds[13,14,15]. Other examples of QM/MM applied to drug discovery is the modeling of the mechanism of antibiotic breakdown in β-lactamase, bacterial resistance enzymes, to describe the critical interactions to avoid to develop stable β-lactam antibiotics[16].

[1] Gohlke, H.; Klebe, G. Angewandte Chemie (International ed. in English) 2002, 41, 2644-76.
[2] de Ruiter, A.; Oostenbrink, C. Free energy calculations of protein-ligand interactions. Current opinion in chemical biology 2011, 15, 547-552.
[3] Jorgensen, W. L. Efficient drug lead discovery and optimization. Accounts of chemical research 2009, 42, 724-33.
[4] Jorgensen, W. L. The many roles of computation in drug discovery. Science (New York, N.Y.) 2004, 303, 1813-8.
[5] Singh, J.; Petter, R. C.; Baillie, T. a; Whitty, A. The resurgence of covalent drugs. Nature reviews. Drug discovery 2011, 10, 307-17.
[6] Daniel, R. M.; Peterson, M. E.; Danson, M. J.; Price, N. C.; Kelly, S. M.; Monk, C. R.; Weinberg, C. S.; Oudshoorn, M. L.; Lee, C. K. The molecular basis of the effect of temperature on enzyme activity. The Biochemical journal 2010, 425, 353-60.
[7] Bugg, T. D. H. The development of mechanistic enzymology in the 20th century. Natural Product Reports 2001, 18, 465-493.
[8] Warshel A. Computer modeling of chimica reactions in enzymes and solutions. Wiley professional: New York, 1991.
[9] Powers, J. C.; Asgian, J. L.; Ekici, O. D.; James, K. E. Irreversible inhibitors of serine, cysteine, and threonine proteases. Chemical reviews 2002, 102, 4639-750.
[10] Mulholland, A. J. Modelling enzyme reaction mechanisms, specificity and catalysis. Drug Discovery Today 2005, 10, 1393-1402.
[11] Schlegel, H. B. In Modern Electronic Structure Theory; Yarkony, D. R., Ed.; World Scientific Publishing: Singapore, 1995.

[12] Schlegel, H. B. Exploring potential energy surfaces for chemical reactions: an overview of some practical methods. Journal of computational chemistry 2003, 24, 1514-27.

[13] Loew, G. H.; Harris, D. L. Role of the heme active site and protein environment in structure, spectra, and function of the cytochrome p450s. Chemical reviews 2000, 100, 407-20.

[14] Shaik, S.; Kumar, D.; de Visser, S. P.; Altun, A.; Thiel, W. Theoretical perspective on the structure and mechanism of cytochrome P450 enzymes. Chemical reviews 2005, 105, 2279-328.

[15] Shaik, S.; Cohen, S.; Wang, Y.; Chen, H.; Kumar, D.; Thiel, W. P450 enzymes: their structure, reactivity, and selectivity-modeled by QM/MM calculations. Chemical reviews 2010, 110, 949-1017.

[16] Hermann, J. C.; Hensen, C.; Ridder, L.; Mulholland, A. J.; Höltje, H.-D. Mechanisms of antibiotic resistance: QM/MM modeling of the acylation reaction of a class A beta-lactamase with benzylpenicillin. Journal of the American Chemical Society 2005, 127, 4454-65.

2. Aim of this thesis

This PhD project is aimed at the development of molecular models useful for the elucidation of mechanistic aspects and structure-activity relationships (SAR)s for a class of covalent inhibitors of fatty acid amide hydrolase (FAAH), one of the main component of the endocannabinoid system and an emerging target for the treatment of chronic pain, inflammation, immunological diseases, psychiatric conditions, metabolic and cardiovascular diseases[1].

In the recent years, the search for selective and potent inhibitors of FAAH has been the subject of an intense medicinal chemistry effort. Many promising inhibitors identified so far are covalent modifiers of the enzyme such as *O*-aryl carbamates and tertiary ureas. *O*-aryl carbamates, including the reference compound cyclohexylcarbamic acid 3′-carbamoylbiphenyl-3-yl ester (URB597) , inhibited FAAH through carbamoylation of Ser241, following a mechanism similar to those of substrates. Mass spectrometry and X-ray crystallography experiments have recently shown that also tertiary ureas, including the piperidinyl derivative PF-750 or the piperazinyl one, N-phenyl-4-(3-phenyl-1,2,4-thiadiazol-5-yl)-1-piperazine-carboxamide (JNJ1661010), inhibit FAAH through carbamoylation of Ser241. Indeed, the aniline moiety of these compounds served as a leaving group during catalysis, with the piperidine(piperazine)-1-carboxylic acid fragment forming a tertiary carbamate with Ser241.

Recognition of a carbamate-based inhibitor at an enzyme catalytic site depends on its overall size, shape, lipophilicity, and electronic complementarity with the binding cavity, whereas its intrinsic reactivity influences the rate of reaction with the catalytic residue. This general behavior applies both to the desired targets of carbamate-based inhibitors and to other off-target proteins involved in side effects or metabolic degradation. As a consequence, modulation of carbamate reactivity should be considered during pharmacodynamic and pharmacokinetic optimization of such compounds.

For the class of N-cyclohexyl carbamic acid biphenyl-3-yl esters developed as FAAH inhibitors by the University of Parma, in collaboration with Univerisity of Urbino and University of California-Irvine, a recent SAR investigation has demonstrated that is possible to modulate the reactivity of the inhibitor preserving inhibitor potency[2]. In particular, this study has shown that conjugated electron-donor groups on the biphenyl scaffold (which increase electron density around the carbamate carbon) reduce the interaction with plasma and liver carboxylesterases without affecting FAAH-inhibitor potency in vitro. The overall effect of this chemical modification is thus an enhanced in vivo potency and a reduced inhibition of off-targets[3,4]. With this in mind, the covalent modification of FAAH by three differently substituted cyclohexyl carbamic acid biphenyl-3yl esters was here modeled by means of a hybrid QM/MM scheme previously validated for FAAH by our lab.

Anticipating the results of this computational study, the calculations clearly showed that the peculiar catalytic mechanism of FAAH, leading to the formation of an exceptionally strong nucleophile, is able to overcome the difference in reactivity of these inhibitors. Thus at least for the considered class of compounds, the intrinsic reactivity can be tuned in order to increase the selectivity of these carbamates towards possible off-targets

Reversibility is another key aspect of enzyme inhibition, as it controls the time-course of the inhibition, and therefore both in vivo potency and efficacy. Generally, carbamoylating compounds blocks the catalytic activity of serine hydrolases by trapping the nucleophile residue of the enzyme within an acylenzyme-like intermediate that, differently from the substrate-based one, is resistant to chemoenzymatic hydrolysis.

Recently, scientists at Johnson&Johnson have pointed out that in the case of FAAH, the ability of the carbamoylated enzyme to recover activity depends on the chemical structure of the inhibitor[5]. Indeed, while the FAAH-URB597 adduct failed to recover amidase activity after 18-hrs dialysis, the FAAH-JNJ1661010 one recovered activity in the same condition, suggesting a release of the carbamoylating fragment from the active site.

To elucidate the chemical determinant of reversibility of the inhibition, the hydrolysis of the covalent adduct of FAAH with the irreversible carbamate inhibitor (URB597), the prototypical reversible urea (JNJ1661010) and a substrate were modeled and compared by means of a QM/MM approach.

The study demonstrated that an additional interaction between the irreversible inhibitor fragment and the catalytic site is able to increase the stability of the covalent adduct, preventing its hydrolysis.

In order to obtain more accurate results, the last study was carried out applying the self-consistent charge-density functional tight binding (SCC-DFTB) quantum Hamiltonian. Although semi-empirical in its conception, the SCC-DTB has proven to be excellent for geometries and energetics, performing well as DFT hybrid calculations in the best cases. Since it remains a parameterized method its reliability on this biological system was assessed by an extensive test on FAAH, by investigating its acylation in presence of oleylamide and oleylmethylester substrates.

The results here discussed have been recently reported in the following papers:

Lodola, A.; Capoferri, L.; Rivara, S.; Chudyk, E.; Sirirak, J.; Dyguda-Kazimierowicz, E.; Andrzej Sokalski, W.; Mileni, M.; Tarzia, G.; Piomelli, D.; Mor, M.; Mulholland, A. J. *Understanding the role of carbamate reactivity in fatty acid amide hydrolase inhibition by QM/MM mechanistic modelling.* Chemical communications (Cambridge, England) 2011, 47, 2517-9.

Capoferri, L.; Mor, M.; Sirirak, J.; Chudyk, E.; Mulholland, A. J.; Lodola, A. *Application of a SCC-DFTB QM/MM approach to the investigation of the catalytic mechanism of fatty acid amide hydrolase*. Journal of molecular modeling 2011, 17, 2375-83.

[1] Kathuria, S.; Gaetani, S.; Fegley, D.; Valiño, F.; Duranti, A.; Tontini, A.; Mor, M.; Tarzia, G.; La Rana, G.; Calignano, A.; Giustino, A.; Tattoli, M.; Palmery, M.; Cuomo, V.; Piomelli, D. Modulation of anxiety through blockade of anandamide hydrolysis. Nature medicine 2003, 9, 76-81.

[2] Tarzia, G.; Duranti, A.; Gatti, G.; Piersanti, G.; Tontini, A.; Rivara, S.; Lodola, A.; Plazzi, P. V.; Mor, M.; Kathuria, S.; Piomelli, D. Synthesis and structure-activity relationships of FAAH inhibitors: cyclohexylcarbamic acid biphenyl esters with chemical modulation at the proximal phenyl ring. ChemMedChem 2006, 1, 130-9.

[3] Vacondio, F.; Silva, C.; Lodola, A.; Fioni, A.; Rivara, S.; Duranti, A.; Tontini, A.; Sanchini, S.; Clapper, J. R.; Piomelli, D.; Mor, M.; Tarzia, G. Structure-property relationships of a class of carbamate-based fatty acid amide hydrolase (FAAH) inhibitors: chemical and biological stability. ChemMedChem 2009, 4, 1495-504.

[4] Clapper, J. R.; Vacondio, F.; King, A. R.; Duranti, A.; Tontini, A.; Silva, C.; Sanchini, S.; Tarzia, G.; Mor, M.; Piomelli, D. A second generation of carbamate-based fatty acid amide hydrolase inhibitors with improved activity in vivo. ChemMedChem 2009, 4, 1505-13.

[5] Karbarz, M. J.; Luo, L.; Chang, L.; Tham, C.-S.; Palmer, J. A.; Wilson, S. J.; Wennerholm, M. L.; Brown, S. M.; Scott, B. P.; Apodaca, R. L.; Keith, J. M.; Wu, J.; Breitenbucher, J. G.; Chaplan, S. R.; Webb, M. Biochemical and biological properties of 4-(3-phenyl-[1,2,4] thiadiazol-5-yl)-piperazine-1-carboxylic acid phenylamide, a mechanism-based inhibitor of fatty acid amide hydrolase. Anesthesia and analgesia 2009, 108, 316-29.

3. Biological target

The endocannabinoid system

Cannabis sativa is a plant indigenous of central and south Asia and evidences of its use in ceremonial practices can be found since the 3rd millennium BC. In Europe, medicinal properties of this plant appear described by the Greek Discoride in his book *Materia Medica*, at the time of ancient Rome, while Indian and Chinese written documents accurately report its physiological effects centuries before him[22].

Nowadays is known that these effects, that include a combination of euphoria, relaxation, reflex tachycardia and hypothermia, are mainly produced by the dibenzopyrane derivative delta-9-tetrahydrocannabinol (delta9-THC).

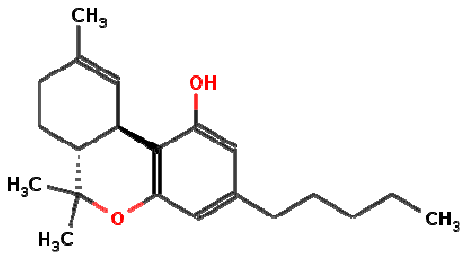

Figure 3.1 Chemical structure of delta-9-tetrahydrocannabinol (Δ 9-THC)

This agent exerts its biological effects acting on particular receptors belonging to the so-called endocannabinoid system (ECS). ECS refers to a group of receptors (which most characterized are CB1 and CB2), their endogenous ligands (the endocannabinoids) and a network of proteins involved in their metabolism, that modulates the synaptic signal of several neural networks.

Differently than other neurotransmitters, endocannabinoids are lipids and they are not stored in vesicles, but they are synthesized and released in the synaptic gap on demand. The increase of Ca^{2+} concentration and/or the activation of neurotransmitter receptors on the post-synaptic neuron trigger the bio-synthesis of the endocannabinoids in the plasmalemma. The subsequent release may be mediated by passive diffusion or by lipid-binding proteins. On the pre-synaptic axon, the

cannabinoid receptors are coupled to multiple cellular signaling pathways, including inhibition of adenylyl cyclase activity, inhibition of voltage-activated calcium channel and activation of potassium channels. The resulting effect is a pre-synaptic inhibition that reduces the impact of incoming synaptic input. Activity of the endocannabinoids is terminated by specific transporters and enzymes that internalize and degradate them.

The wide distribution of the endocannabinoids and their receptors suggests an extensive modulatory role for the endocannabinoid system, responsible for regulating a number of tasks. This system is not limited to the CNS but it is also concerned with peripheral processes and could act modulating neurotransmitter release and action from autonomic and sensory nerve fibers.

Central functions influenced by ECS include cognitive functions, emotional reactivity, motor activity, pain modulation and regulation of temperature, feed and blood pressure. Peripherically functions within control of immunological, gastrointestinal, reproductive and cardiovascular performance are also indicated[23].

Endocannabinoids

Endocannabinoids are lipid derivatives that share two common structural motifs: a polyunsatured fatty acid moiety (e.g. arachidonic acid) and a polar head group, consisting of an alcohol or an amine. Generally they are produced through cleavage of the phospholipid precursors that are present in the membranes of neurons, glia and other cells.

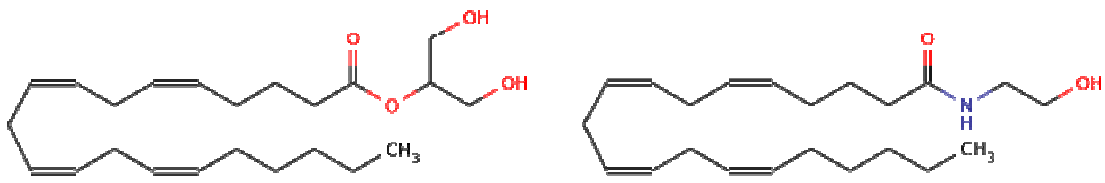

Anandamide 2-Arachidonoylglycerol

Figure 3.2 Molecular structures of main endocannaboids.

Anandamide (N-arachidonoylethanolamide, or AEA) and 2-arachidonoyl-glycerol (2-AG) are the most characterized endocannabinoids, but several other analogues with activity at cannabinoid receptors have been isolated.

Anandamide (AEA)

In 1992, Mechoulam and coworkers discovered the first endogenous compound with cannabinoid binding activity. It was the ethanolamide of arachidonic acid and they named this novel compound anandamide, after the Sanskrit “ananda”, inner bliss[24].

AEA is a partial agonist at both CB_1 (K_i= 61 nM) and CB_2 (K_i= 1930 nM) receptors, with higher affinity for the first. It was found to be widely distributed in the brain and peripheral tissues. In human brain it is present both in regions with high (e.g. hippocampus, cerebellum, striatum) and low (thalamus) expression of CB_1 receptors. Peripherically, AEA was found in human spleen and heart and in rat skin, whereas only traces were detected in human serum, plasma and cerebrospinal fluid.

The postulated biosynthetic pathway for AEA involves the hydrolysis of the phospholipid precursors N-arachidonoyl phosphatidylethanolamine (N-ArPE), catalyzed by a specific phospholipase D (NAPE-PLD). The precursor N-ArPE may be resynthesized by N-acyltransferase (NAT), which transfer arachidonate group from *sn*-1 glycerol ester position of phospholipids to the primary amino group of PE. Both reactions are supposed to proceed in parallel after they are initiated by an intracellular Ca^{2+} increase[25].

Once AEA is released in the synaptic cleft, it is rapidly inactivated by re-uptake and degradation in neurons and glia. Mechanism of AEA degradation involves an intracellular membrane-bound protein, Fatty Acid Amide Hydrolase (FAAH), that hydrolyzes AEA in arachidonic acid and ethanolamine[26]. A more detailed disquisition about this enzyme will be provided subsequent in the text. While the degradation mechanism of AEA is well characterized, the mechanism of how AEA is removed from the synaptic space and is shuttled to FAAH, that is anchored to inner-compartment membranes, remained molecularly uncharacterized for a long time. Since several years was demonstrated an energy-independent carrier-mediated

transport of AEA, characterized by saturability, fast rate, temperature dependence, substrate selectivity and stereospecific inhibition. Only in 2011, Piomelli and co-workers characterized the FLAT(FAAH-like anandamide transporter), a soluble splicing variant of FAAH with no amidase activity, that is able to desorb AEA from the plasmalemma and deliver it to intracellular organelles where FAAH is located[27]. Besides this knowledge, the mechanism adopted by AEA to pass the cytoplasmatic membrane remains uncharacterized.

2-Arachidonoyl-glycerol (2-AG)

2-Arachidonoyl-glycerol was isolated from canine gut and identified as CB agonist by Mechoulam in 1995[28], but its role as endocannabinoid was accepted only in 1997, when Piomelli and coworkers demonstrated its presence in rat brain[29]. 2-AG is the most abundant endocannabinoid in brain and its concentrations are ~170-fold greater than those of AEA. Beside its abundance, two pharmacological properties make it essentially different than AEA: it binds to both CB_1 and CB_2 receptors with comparable affinity, and acts as full agonist.

Highest concentrations of 2-AG in brain were found in brainstem, medulla, limbic forebrain, striatum and hippocampus, while lower levels were detected in the cortex, diencephalon, mesencephalon, hypothalamus and cerebellum. 2-AG was detected also in the peripheral nervous system, such as in sciatic nerve, lumbar spinal cord, lumbar dorsal root ganglion and also in rat and bovine retinas.

2-AG biosynthesis occurs by two possible routes in neurons. Hydrolysis of membrane phospholipids by phospholipase C (PLC) may produce diacylglycerol (DAG), which may be subsequently converted to 2-AG by diacylglycerol lipase (DAGL). Alternatively, phospholipase A_1 (PLA_1) may generate a lysophospholipid, which may be hydrolyzed to 2-AG by lyso-PLC activity. Experiments suggested that synthesis of 2-AG is initiated by elevating intracellular Ca^{2+} levels or by electric stimulation. The strongly enhanced synthesis of 2-AG in presence of a cholinergic agonist carbachol, after activation of cortical neuron cultures by Ca^{2+} influx, indicates that some neurotransmitter receptors may be linked to 2-AG accumulation. In the

intestine, 2-AG formation is catalyzed by pancreatic lipases during the digestion of triglycerides and phospholipids.

Similarly to AEA, degradation of 2-AG takes place in a two-step mechanism: uptaking of the neurotransmitter into the cell and enzymatic hydrolysis. Experimental evidences suggest that the two endocannabinoids may compete for the same transport system, since they are accumulated with similar kinetic properties (K_M, and V_{max}), they can prevent each other's transport, and their accumulation is prevented by the same inhibitor (AM404). On the other hand is known that 2-AG transport is not influenced by FLAT and that incubation with arachidonic acid can decrease the 2-AG uptake, without influencing AEA accumulation. Intracellular degradation of 2-AG is carried out by monoacylglycerol lipase (MGL)[30]. MGL is a soluble serine hydrolase that converts monoglycerides in fatty acid and glycerol. In rat, it is found in all organs, and has a heterogeneous distribution in the brain, with highest levels in the regions where CB_1 receptor is abundant. Since the high concentration of 2-AG in brain, MGL play an important role in the modulation exerted by ECS.

Others

Besides the two most widely accepted, AEA and 2-AG, three other endogenous cannabimimetic molecules have thus far been identified (Noladine – 2AGE, Virodamine and N-arachidonoyl dopamine – NADA) while other candidate molecules are being investigated. Nevertheless, physiological relevance and metabolic pathway of these molecules are still subject of ongoing investigations[31].

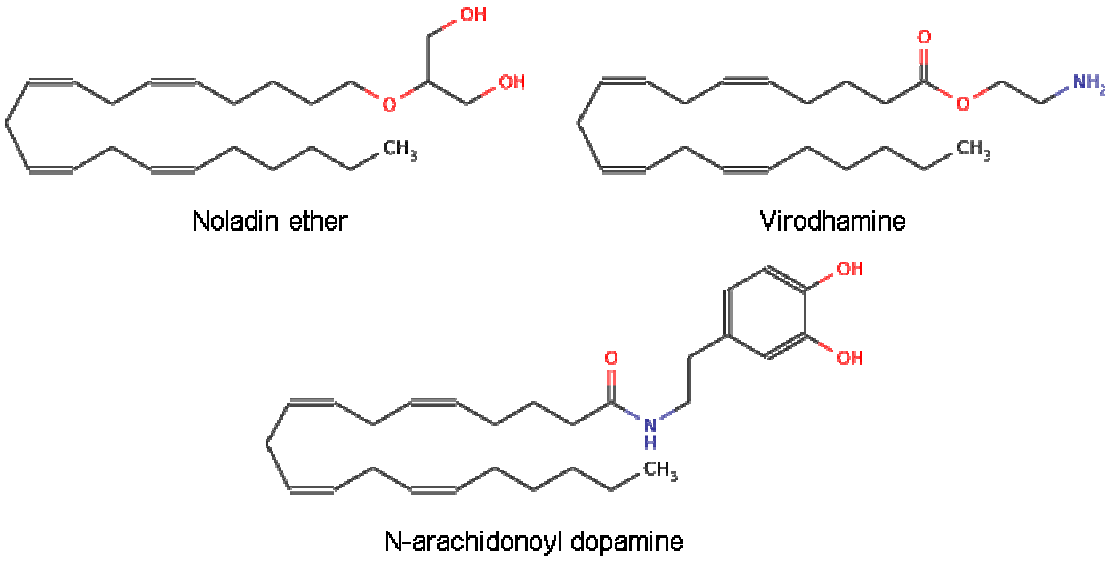

Figure 3.3 Molecular structures of endogenous lipids that activate brain cannabinoid receptors. As the most studied AEA and 2-AG, they share common structural motifs: a polyunsatured fatty acid chain moiety and a polar head.

The receptors

To date, three protein sites that binds endocannabinoids have been identified by molecular cloning; these are the G protein-coupled receptors cannabinoid type 1 (CB_1)[32] and type 2 (CB_2)[33] and the ion channel vanilloid type 1 receptor (TRPV1)[34]. Both CB_1 and CB_2 are lipid receptors that recognize acylethanolamide analogues, but, while CB_1 is predominantly found in neurons, CB_2 is highly concentrated in immune cells and does not appear in the CNS; on the other hand, TRPV1 is a polymodal channel, activated by physical and chemical stimuli. However, the lack of affinity of some cannabinoids at CB_1/CB_2 and studies performed with $CB_1^{-/-}$ and $CB_2^{-/-}$ mice have indicated that certain effects of cannabinoids on tissues must be mediated also by other receptors.

CB_1

Cannabinoid type 1 receptor was encoded in 1990 by Matsuda. The coupling with the inhibition of adenylyl cyclase activity, leads to the modulation of the protein expression, by inactivation protein kinase A (PKA) phosphorylation pathway, or stimulation of mitogen-activated protein kinase (MAPK). Instantaneus effects are also

exerted by the $G_{\beta\gamma}$–subunit that directly inhibits the voltage-dependent calcium channel (VDCC) and positively influence the inwardly rectifying potassium channels (IRK), reducing the neuron excitability.

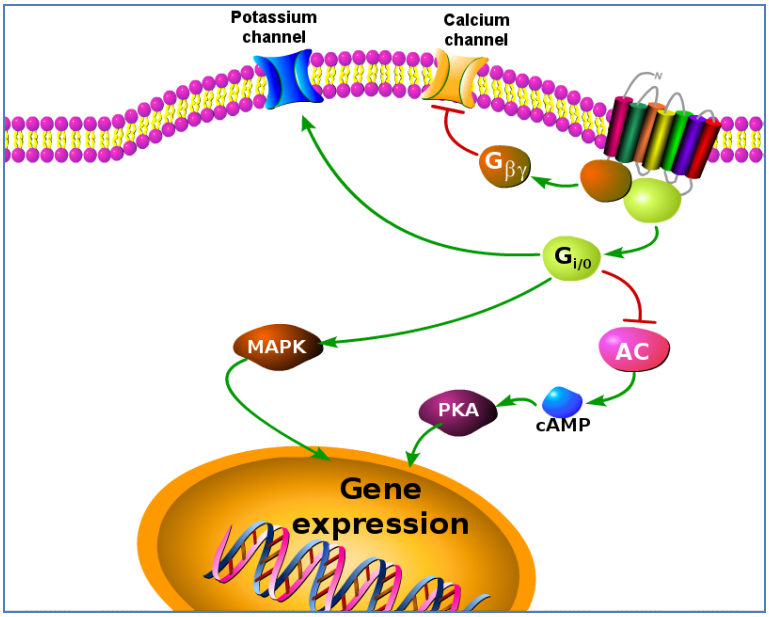

Figure 3.4 Major signalling pathways associated to CB1 activation.

It is distributed throughout the body, but is mainly expressed in central and peripheral nervous system. Expression of CB_1 receptor gene is restricted to specific cell types, subserving distinct functional roles in certain neural networks. High expression of CB_1 receptor are found in many cortical regions. Moderate levels of expression are present in the striatum and in the cerebellum, while weak expression of CB_1 are widespread throughout the brain. At lower level is also present in testis, heart, vascular tissue, and immune cells. Genetic deletion studies confirmed that it is the major responsible of the behavior effects of cannabimimetic drugs, while the peripherical role is less relevant.

CB_2

Cannabinoid type 2 receptor was identified in 1992 by Munro. Low identity with CB_1 (44%) indicates that the two receptor subtypes diverged long ago in evolution. Also CB_2 is negatively coupled with the adenylate cyclase activity but, differently than

CB_1, does not present activity on VDCC and IRK. It is expressed at peripheral level, predominantly at immune and hematopoietic cells, and is present in the CNS during the inflammatory states. Its primarily involved in inflammatory reactions and the immune response.

TRPV1

Transient vanilloid receptor type 1, also known as the capsaicin receptor and the vanilloid receptor 1, is a ligand-gated, non-selective cation channel expressed predominantly by sensory neurons. It is activated mainly by capsaicin, low pH and heat. In 1999, Högestätt demonstrated the affinity of AEA for this receptor. This receptor is highly expressed in the sensor neurons, where it plays an important role in the transduction of noxious thermal and chemical stimuli. TRPV1 is also expressed in the cardiovascular system, immune cells and in the CNS, where AEA, that is a low-affinity agonist of this receptor with a tissue-dependent efficacy, is supposed to be the endogenous ligand.

Others candidates

It is now established that phytocannabinoids, endocannabinoids, and synthetic cannabinoids have multiple in vivo sites-of-action additional to CB_1, CB_2 and TRPV1, since these classical cannabinoid receptors do not explain the observed pharmacology in some cases. These additional targets have come to be known collectively as non-CB1/CB2 receptor. Non-CB_1/CB_2 sites were be found in the vasculature, where AEA and analogues mediate vasodilatation; in the CNS has been observed that AEA can stimulate GTPγS binding in brain slices from $CB_1^{-/-}$ mice, and inhibits the EPSC in areas where CB1 is absent; on immune cells, experiments with $CB_1^{-/-}$ and $CB_2^{-/-}$ mice support the existence of additional cannabinoid targets.

Between the potential non-CB_1/CB_2 receptors, the orphan GPCR GPR55, has so far been reported as novel cannabinoid receptor. GPR55 has been demonstrated to interact with chemically unrelated cannabinoid ligands; although the endogenous agonist and physiological relevance of GPR55 are not yet clear, it could mediate the

unexplained vasodilatatory effects of AEA and the reduced mechanical nociception following inflammatory or neuropathic challenge[35].

Physiological processes

It is widely assessed that endocannabinoids system act as a presynaptic way modulating both excitatory and inhibitory neurotransmission. In particular, endocannabinoids in the CNS intervene in both short-term and long-term forms of synaptic plasticity, including depolarization-induced suppression, long-term potentiation and depression, and long-term depression of inhibition.

The abundance of both CB_1 receptors and endocannabinoids in the basal ganglia and cerebellum makes targeting this signaling system an ideal way to modulate movement and posture. The neuromodulatory actions of endocannabinoids in the sensory and autonomic nervous systems also result, mostly through CB_1 receptors, in the regulation of pain perception and of cardiovascular, gastrointestinal and respiratory functions; their effects on the release of hypothalamic hormones and peptides, and the regulation of their levels by steroid hormones, lead to modulation of food intake and of the pituitary–hypothalamus–adrenal axis, as well as of both female and male reproduction[23].

CB_2 were originally described in cells of immune system, where they are implicated in immunomodulatory and neuroprotective roles. Evidence for their expression in human primary sensory neurons, and increased levels of CB_2 receptors in human peripheral nerves after injury, explain the antinociceptive effects in models of inflammatory and nociceptive pain elicited by CB_2 receptor agonists[36].

ECS pharmacological modulation

Mechanisms of action of cannabinoids are complex, not only involving interaction at the cannabinoid receptor, but also activation of vanilloid receptors, increase of endocannabinoid concentration, antioxidant activity, metabolic interaction with other compounds, and several others.

The CB_1 receptor antagonists, e.g. rimonabant, had been in clinical use for the treatment of obesity and were under investigation for the treatment of nicotine and other dependencies. These drugs, basically, turn off the pleasure center that causes people to crave food, but at the same time, cause psychiatric adverse reactions in patients. In 2007 rimonabant was retired from the market, and other treatments acting on the same target were retired from clinical trials.

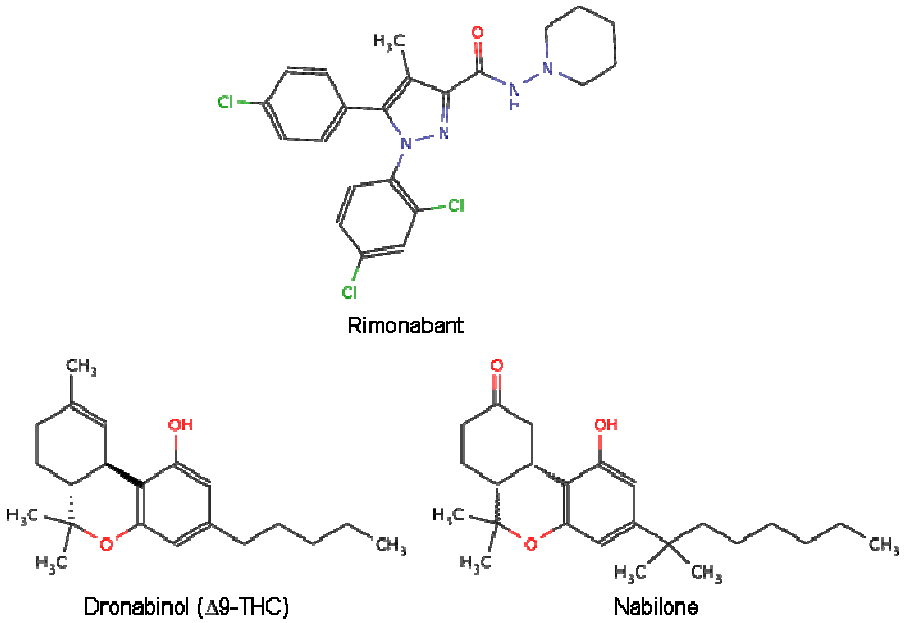

Figure 3. 5 Molecular structures of the CB1 antagonist Rimonabant, retired from market because of its side effects, and the CB agonists Dronabilon and Nabilone.

Currently two CB agonists, dronabinol and nabilone, and a cannabis extract (Sativex®), are in medical use. In addition, cannabis herb produced according to pharmaceutical standards is legalized for medical use in several states. Dronabinol (Marinol®)is the international non-proprietary name for Δ9-THC, the main psychoactive compound of cannabis. It is approved for nausea and vomiting associated with cancer chemotherapy in patients that had failed to respond adequately to conventional anti-emetic treatments. Furthermore it is administrated for anorexia associated with weight loss in patients with AIDS. More recently, Sativex® was also indicated for symptomatic relief of neuropathic pain and spasticity in multiple sclerosis. Nabilone (Cesamet®) is a synthetic derivative of Δ9-THC approved for the treatment of nausea and vomiting associated with chemotherapy[37].

However, a major limitation to the use of direct cannabinoid agonists as therapeutic agents is the undesirable profile of side effects, which includes dysphoria, dizziness and effects on motor coordination and memory. In particular, the cognitive effects of these agents appear to be sufficiently aversive to markedly limit their use.

One attractive approach to elicit the desirable effects of cannabinoid activation, while avoiding the negative effects of global CB_1 stimulation, is to manipulate endogenous cannabinoid signaling through the inhibition of FAAH and related enzymes, since resting concentrations of endocannabinoids in the CNS are very low because of their rapid hydrolysis. Inhibition of degrading enzyme would be expected to elevate the endogenous concentrations of endocannabinoids and consequently prolong and potentiate their biological effects.

Such potentiation, acting preferentially on active pathways, might be expected to have a reduced risk of psychotropic effects compared with global activation of cannabinoid receptors by exogenously applied agonists. Concerning AEA, direct evidences for such upregulation of synthesis in a context relevant to nociception was demonstrated by the intraplantar injection of formalin, that led to release of this endocannabinoid selectively in the periaqueductal gray region of the brain, an area associated with nociceptive processing[38]. AEA synthesis is also up-regulated following physiological stress, and it has been proposed that an increased endocannabinoid tone under stressful physiological situations may represent an endogenous neuroprotective mechanism[39].

FAAH

In 1984 Schmid and collaborators identified, for the first time, an hydrolase activity in dog brain homogenates that catalyzes the hydrolysis of fatty acid ethanol amides to free fatty acid and ethanolamine. In 1996, Cravatt and co-workers isolated and cloned this enzyme, the fatty acid amide hydrolase (FAAH), demonstrating its role in AEA hydrolysis[40].

Experimental evidences indicates that FAAH is the main responsible of AEA degradation and resting concentrations of AEA in the CNS are very low because of its rapid hydrolysis. In addition FAAH controls the levels of other lipid mediators, such

as OEA or PEA, that exert their analgesic and anti-inflammatory effects via non-cannabinoid pathways. FAAH knock-out mice have elevated resting brain concentrations of AEA and manifest an analgesic phenotype in both carrageenan model of inflammatory pain and formalin model of spontaneous pain; furthermore, several studies show reduced inflammatory responses in $FAAH^{-/-}$ mice, as well as improvements in slow wave sleep and memory acquisition[41].

Development of selective FAAH inhibitors permitted to validate the enzyme as pharmaceutical target. In-vivo pharmacological evaluation of URB597, the best pharmacologically characterized inhibitor, developed by Mor and co-workers, showed that the block of FAAH activity elevates AEA levels in rat brains, without inducing catalepsy, hypothermia or hyperphagia, the typical effects of exogenous cannabinoids. On the other side, FAAH inhibition produces antinoceptive effects at hot-plate test and analgesic effects in the inflammatory and neuropathic models. Positive effects towards anxiety and depression in animal models are also observed[42].

Currently, there are several therapeutic areas in which alterations in endocannabinoids processing may be beneficial: treatment of pain, immunological diseases, psychiatric conditions, metabolic and cardiovascular disorders, drug addiction and inflammation.

Comparative genomics

FAAH is a member of amidase-signature (AS) family that hydrolyses N-acylethanolamides. The AS sequence consists in highly conserved serine residues and moderately conserved cysteine residues originally identified in several amidases of fungi and bacteria. AS enzymes catalyse the hydrolysis of amide bonds (CO-NH) and they are generally characterized by a Ser-Ser-Lys catalytic triad, although this family has diverged widely with regard to substrate specificity and function. Nonetheless, these enzymes maintain a core alpha/beta/alpha structure, where the topologies of the N- and C-terminal halves are similar. Peculiar features of FAAH, the first known mammalian member of the AS family, are preferential hydrolysis of lipid

compounds and, opposite to the other members, a N-terminal transmembrane binding domain that anchors this enzyme to internal membranes.

FAAH was isolated for the first time from the rat liver cytoplasmic membrane. In humans and in other vertebrates, that, remarkably, do not include mice and rats, two genes encoding for different variants of FAAH were found. The two human FAAH enzymes shares less than 20% sequence identity and are referred as FAAH-1 and FAAH-2[43]. They hydrolyze primary fatty acid amide substrates (e.g. oleamide) at equivalent rates, whereas FAAH-1 exhibits greater activity with N-acyl ethanolamines (e.g. anandamide) and N-acyl taurines. Both enzymes are sensitive to the principal classes of FAAH inhibitors synthesized to date, including O-aryl carbamates and alpha-keto heterocycles. The overlapping substrate specificity, but distinct tissue distributions of FAAH-1 and FAAH-2, suggest that these proteins may collaborate to control fatty acid amide catabolism in primates.

Human FAAH-1, referred simply as FAAH hereafter, shares ~82% sequence identity with rat FAAH[44]. Sequence comparison identified six amino acids that differ between rat FAAH and human FAAH in the active sites: L192F, F194Y, A377T, S435N, I491V, V495M. However, beside the strong degree of sequence homology, rat and human FAAHs were found to share many biochemical and enzymological features, including membrane association, apparent molecular size, substrate selectivity and inhibitor sensitivity.

Since human FAAH has proven difficult to express and purify, as an alternative strategy, a “humanized” version of rat FAAH was created converting the protein's active site in order to match the human enzyme. The generated humanized rat (h/r) FAAH protein can be expressed at levels similar to rFAAH in E.coli and showed inhibitory sensitivity profiles that matched the human enzyme[45]. This mutated enzyme is generally used as a surrogate for hFAAH for structural studies.

Structural Biology

In 2002 Stevens obtained the first crystal structure of rat FAAH, which overall fold was essentially identical to the that observed for the later h/rFAAH structures. It revealed a dimeric enzyme, which dimer interface buries about 1560 $Å^2$ of molecular

surface area per monomer. The protein core is characterized by a twisted beta sheet consisting of 11 mixed strands, which are surrounded by 24 alpha helices of various length[46].

Analysis of primary sequence predicted a trans-membrane (TM) domain including the first alpha helix, composed by residues 9-29 at N-terminus. Deletion of residues 1-30 resulted in an enzyme (ΔTM-FAAH) with normal amidase activity, but still strongly associated to the membrane[47]. In fact the two helices 18 and 19, rich in hydrophobic residues, lie on the membrane side and are supposed to be dipped into the plane of the membrane, forming the membrane binding region, with the TM one.

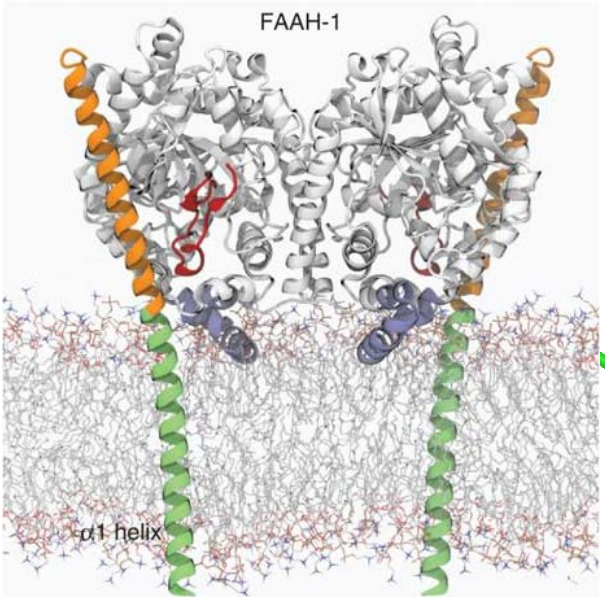

Figure 3.6 Model of rat FAAH in membrane, based on the structure of FAAH-ΔTM. α1 (green) and α19-18 helices (blue) are the proposed membrane binding region of the enzyme (picture from ref. 27).

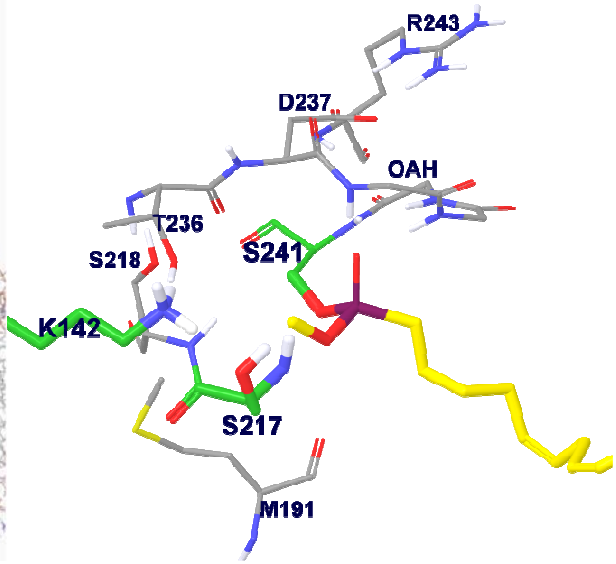

Figure 3.7 Catalytic site of FAAH (PDB code:1MT5). Catalityc Triad is shown in green. The substrate analogue inhibitor MAPF is depicted in yellow, covalently attached to S241. Elements of the oxyanion hole and other important residues are also evidenced.

Catalytic site of FAAH is buried deep into the enzyme. The catalytic triad is composed by the nucleophile Ser241, and the residues Ser217 and Lys142[48,49]. The catalytic lysine lie between Thr236 and Ser218, each of which accepts an Hbond from the lysine amino group. Adjacent to the nucleophilic serine, the four peptidic NH groups of Ile238, Gly239, Gly240 and Ser241 lie in circle, forming the oxyanion hole (OAH) that interact with the carbonyl oxygen of the substrates. On the side of the OAH opposite to the substrate sits the side chain of Asp237, an highly conserved position among amidase, that is in tight interaction with Arg243. On the opposite side

of the catalytic site the peptidic CO group of Met191 can interact with the amidic hydrogen of the substrates.

Access to the catalytic site

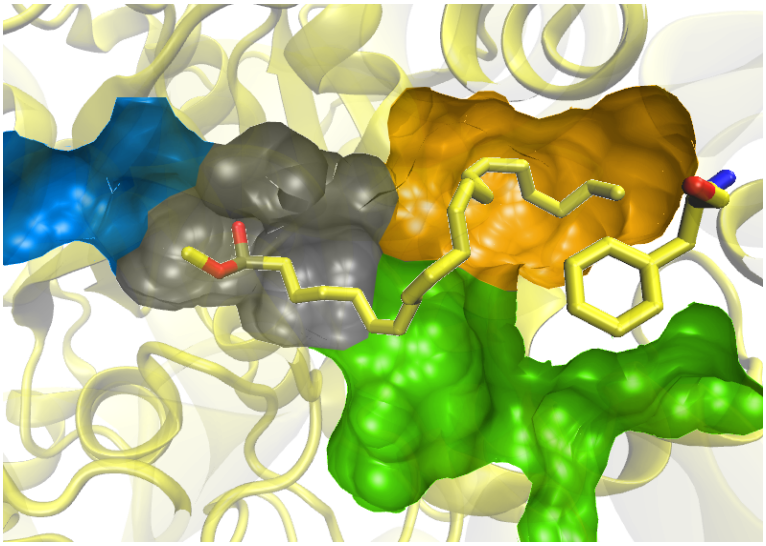

Figure 3. 8 Interior channels of FAAH active site, modelled with MAPF (PDB code 1MT5). In blue, cytoplasmatic access channel points toward cytoplasm. On the right side, pointing toward the membrane, F432 (shown in yellow) splits the channel in the membrane access channel, depicted in green, and the acyl chain binding, orange.

Catalytic site is accessible by two narrow channels: one is more hydrophilic, being defined by Ser217, Lys142 and other polar residues such as Thr236, and wider than the second. This channel leads to the cytoplasm and it is the putative path for water molecules to access the catalytic centre and also the path for polar leaving groups (e.g. ethanolamine, ammonia) from the substrate to exit FAAH.

The second channel is narrower, longer and more hydrophobic, pointing toward the membrane. Leading away from the catalytic machinery, in proximity of Phe492, it splits into two sub-channels, lining helices 18 and 19 on the two sides. One leads to an entrance defined by residues that are both hydrophobic (Ile407 and Ile530) and charged (Arg486 and Asp403). It is called Membrane Access Channel (MAC). The latter subchannel is capped by polar residues that are on the surface of FAAH:

Tyr335, Glu373 and Arg428. Since this pocket hosts the lipophilic chain of the most of co-crystallized FAAH-inhibitors, it was called Acyl-chain Binding Pocket (AcBP).

Two theories try to explain how the fatty chain could reach the second sub-channel: one possibility is that the substrates enter FAAH through the charged pore, pass over the catalytic machinery and then reach the second channel reversing and consequently to Phe432 rearrangement. On the other hand, according to the second hypothesis, the residues that line the back of the AcBP could undergo a sidechain rearrangement, providing an entrance for substrates[50].

Catalytic mechanism

FAAH is able to hydrolize both amides and esters at comparable rates, with preferences toward primary amides and unsatured fatty chains, at a basic pH (optimum at pH=9).

Substrate	K_M (μM)	k_{CAT} (s^{-1})	k_{CAT}/K_M ($\mu M^{-1}s^{-1}$)	Substrate selectivity (k_{CAT}/k_{CAT}OA)
Oleamide	37 ± 7	9 ± 1	0.24	1
Oleylmethyl amide	9 ± 2	1.9 ± 0.1	0.21	0.2
Oleylphenyl amide	22 ± 3	0.17 ± 0.02	$7.7 \cdot 10^{-3}$	0.02
Oleylmethyl ester	21 ± 3	2.8 ± 0.1	0.13	0.3

Table 3.1 FAAH substrate specificity related to amide and esters. Tested on WT-ratFAAH at pH 9.[49]

Substrate	K_M (μM)	k_{CAT} (s^{-1})	k_{CAT}/K_M ($M^{-1}s^{-1}$)	Substrate selectivity (k_{CAT}/k_{CAT}OleylpNA)
Hexanoyl pNA	>2000	>0.38	170 ± 10	0.05
Heptanoyl pNA	410 ± 20	0.46 ± 0.02	1120 ± 50	0.31

Octanoyl pNA	220 ± 30	0.73 ± 0.07	3320 ± 170	0.91
Nonanoyl pNa	74 ± 10	0.60 ± 0.04	8100 ± 700	2.22
Decanoyl pNA	57 ± 2	0.56 ± 0.03	9800 ± 200	2.69
Lauroyl (C12) pNA	65 ± 6	0.46 ± 0.03	7100 ± 300	1.94
Myristoyl (C14) pNA	99 ± 14	0.29 ± 0.02	2900 ± 200	0.80
Palmitoyl (C16) pNA	74 ± 7	0.27 ± 0.03	3600 ± 100	1.00
Oleoyl (C18, 9Z) pNA	74 ± 8	0.27 ± 0.02	3600 ± 200	1.00
Arachidonoyl (C20, 5,7,9,11Z) pNA	∓0 ± 8	0.48 ± 0.05	8000 ± 200	2.19

Table 3.2 FAAH substrate specificity related to acylchain length. Tested on ΔTM rFAAH at pH 9 (pNA = paranitroanilide). [51]

Mutagenesis studies and the pH-activity profile strongly suggest a mechanism of hydrolysis catalyzed by FAAH where Lys142 serves as a key acid and base in distinct steps of the catalytic cycle. As a base, Lys142 activates the Ser241 nucleophile for attack on the substrate carbonyl. As an acid, Lys142 readily protonates the substrate leaving group leading to its expulsion. The impact of Lys142 on Ser241 nucleophile strength and leaving group protonation occurs indirectly, via the bridging Ser217 of the triad, which acts as a "proton shuttle"[52].

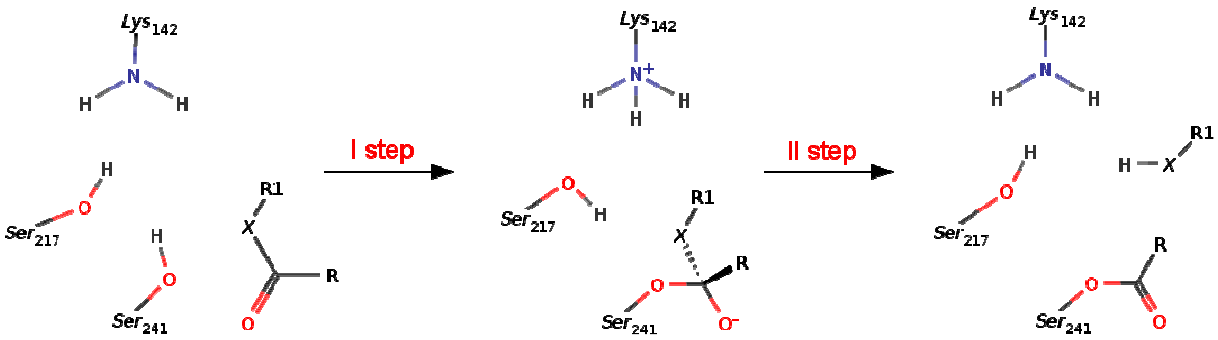

Figure 3.9 Mechanism of substrate hydrolisis by FAAH (X= NH, O; R_1= H,Me).

Mutagenesis and functional studies have displayed that other residues play important roles in the catalysis. In fact, single mutations of Ser218, Arg243 and Asp237 decrease the amidase activity of FAAH greater than 100-fold without detectably impacting the structural integrity of the enzyme.

Natural variant of FAAH has a marked selectivity towards amides hydrolysis. Consistently with the different chemical reactivity of the amide and ester group, the punctual mutation of the residue Lys142, that prevents the formation of a strong nucleophile, generates a catalytically compromised enzyme that hydrolyzed esters hundreds-fold faster than amides. Of comparable effects, the mutant Arg243Ala, displayed uncompromised esterase activity but severely reduced amidase activity, indicating its important role in the transition state stabilization, during catalysis[53].

Concerning the acyl chain binding specificity, FAAH exhibits a strong preference for unsatured acyl chains nine carbons in length or longer. In rat, the substrate specificity for medium-chain pNA substrates (7-12 carbons) is strongly influenced by Ile491, that participates in hydrophobic binding interactions with medium-chain FAAH substrates[51].

QM/MM calculations

In 2005 Lodola et al., published the first QM/MM modelling of the oleamide hydrolysis catalyzed by FAAH. The hydrolysis mechanism proposed by Cravatt was modelled by a static approach, exploring the potential energy surfaces at B3LYP//PM3-CHARMM27 potential. Consistently with the experimental data, the study supported a mechanism where Lys142 and Ser217 cooperate in the activation of the nucleophile Ser241: the initial proton exchange occurs when Lys142 deprotonates Ser217, resulting in a zwitterionic intermediate. Subsequently, Ser217 activates the nucleophile Ser241, and the addiction takes place with the subsequent tetrahedral intermediate formation. Furthermore, this study identified the nucleophile activation dominating the transition state.[54]

In further studies, this QM/MM protocol was shown to be able to reproduce the substrate selectivity of FAAH towards amide and esters, identifying also for both cases, that leaving group expulsion represents the rate limiting step of the hydrolysis.[55]

This QM/MM framework was interestingly and successfully applied in order to solve a drug design question: docking experiments showed that cyclohexyl-3yl carbamates, covalent inhibitors of FAAH (e.g. URB597) present two possible orientations within the FAAH catalytic site. The QM/MM modelling of the inhibition reaction was able to identify a specific energetically preferred orientation two years before the crystallographic structure of the carbamoylated adduct was resolved.[56]

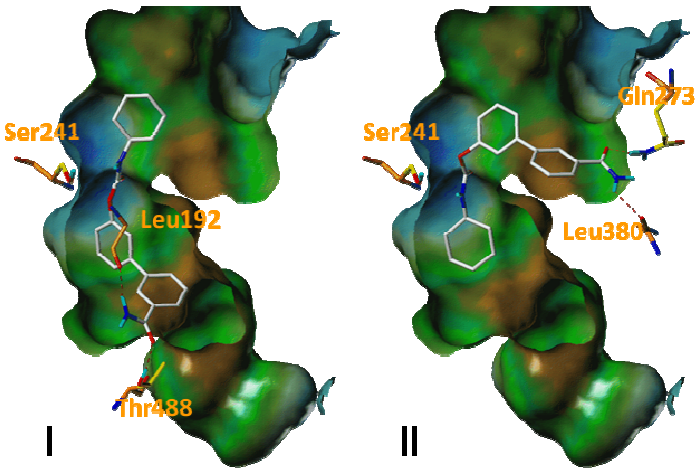

Figure 3.10 Representation of compound URB597 docked into the FAAH binding site in two alternative orientations. Carbons of the inhibitor are in white, those of FAAH in orange. Docking studies results indicate that both orientation I and II are equiprobable. Modelling of the covalent modification identified the orientarion II as the productive binding pose.

In 2006, Jorgensen and co-workers modelled the hydrolysis of OA and OME by FAAH and by the K142A-mutant FAAH. Calculating the free-energy of the reaction by Monte Carlo simulations with PDDG-PM3/OPLS-AA potential, comparable results with the previous static model were obtained. Also this approach was able to reproduce the experimental data about the substrate specificity of the enzyme, but differently from the previous reported, indicated the TI formation as the rate limiting step of the catalytic reaction.[57]

Faah inhibitors

A number of FAAH inhibitors have been described, including fatty-acid trifluoromethylketones, fluorophosphonates, alphaketo esters and alphaketo amides, bromoenol lactones, and non-steroidal antiinflammatory drugs. These compounds lack, however, the target selectivity and/or biological availability required neither by a template for drug design or by chemical probes[58].

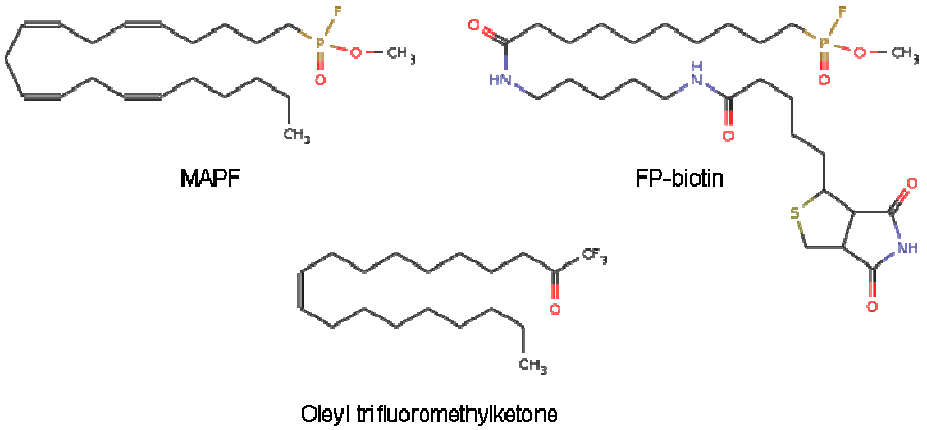

Figure 3.11 Early inhibitors of FAAH.

An emerging second generation of FAAH inhibitors comprises several structurally diverse groups of compounds. These include substituted alpha-ketoheterocycles, carbamates and urea based inhibitors.

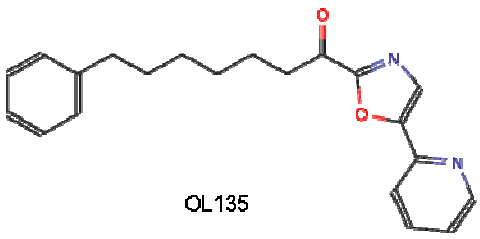

Figure 3.12 Reference inhibitor of the class of alpha-ketoheterocycles.

Alpha-keto heterocycles were developed at the Scripps Research Institute, the prototype of this class is OL135 (2-pyridyl-5-yl-oxazol-2-yl-phenhexyl ketone), that acts covalently binding the nucleophile serine of FAAH in a reversible manner[59]. This class derives from the early oleyl trifluoromethylketone, where the essential electron-

withdrawing character of the trifluoromethyl group is mimed by the heterocycle, assuring the ectrophilicity of the carbonyl carbon. On the other hand, the oleyl chain is substituted by a less lipophilic group, increasing the solubility of the compound. These modification made OL-135 the first tool for the investigation of FAAH pharmacology. Notwithstanding the nanomolar in-vitro potency (OL-135 potency 4.7nm) and the relative selectivity towards other hydrolases, this class of compounds displayed only transient elevation of AEA in vivo, probably due to their rapid metabolism.

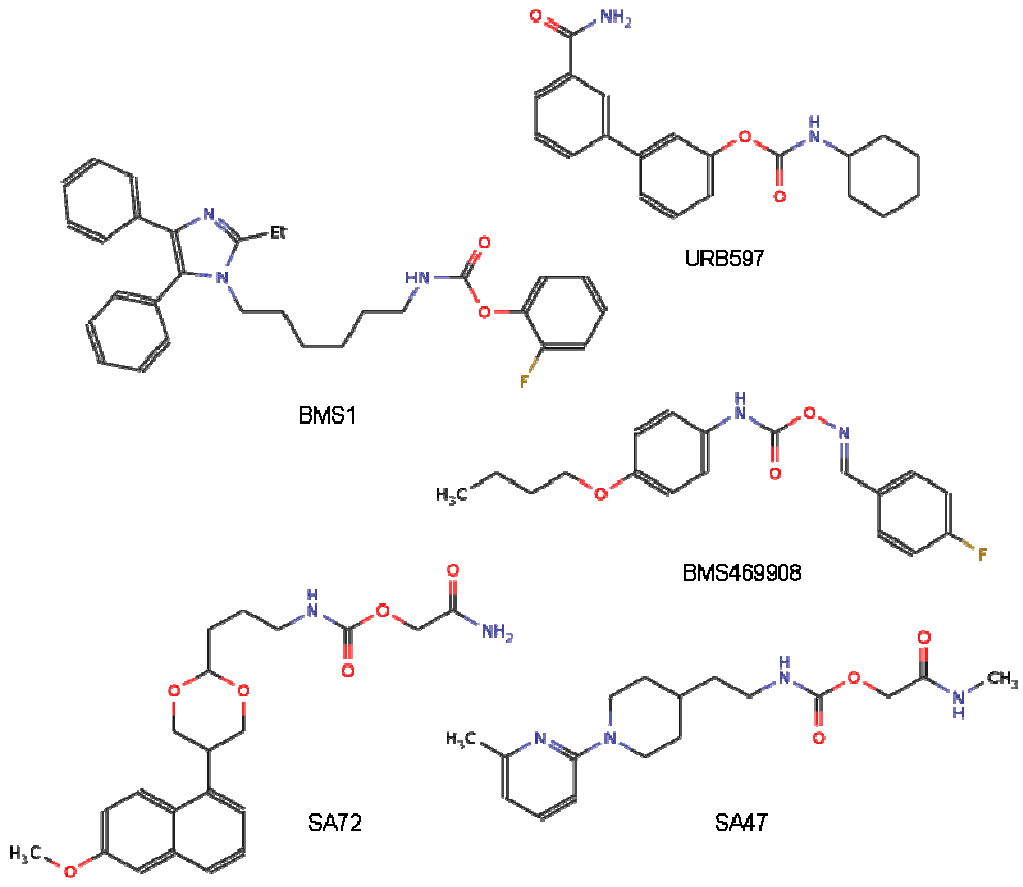

Figure 3.13 Carbamate FAAH inhibitors.

First class of carbamate inhibitors is a series of cyclohexylcarbamic acid biphenyl esters (e.g. URB597) published in 2003 by Mor and co-workers[60]. These compounds inhibit FAAH with a non-competitive mechanism consisting of persistent carbamoylation of the nucleophilic serine at the active site, with the concurrent expulsion of the ester moiety. Other carbamate-based inhibitors were patented at

Bristol-Myers Squibb (eg. BMS469908, BMS1) and Sanofi Aventis (eg SA47, SA72), and some of these are in clinical trials for the treatment of pain.

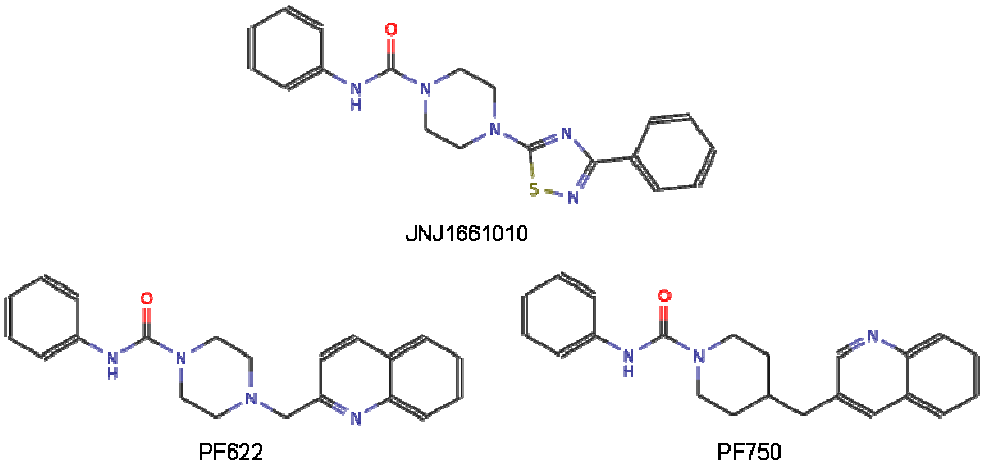

Figure 3.14 Urea FAAH inhibitors.

In 2006 a new class of arylurea inhibitors was reported by Takeda and Johnson & Johnson (eg. JNJ1661010)[61]. Since the high stability of ureas to hydrolisis, it was surprising that these compounds act carbamoylating the nucleophile Ser241 of FAAH, similarly to the more reactive carbamates. Other urea based inhibitors were later development at Pfizer and Scripps (PF750, PF622)[62].

Cyclohexylcarbamic acid biphenyl esters

Cyclohexylcarbamic acid biphenyl esters were developed in collaboration between University of Parma, Urbino and California-Irvine. Starting from a FAAH-inactive acetyl cholinesterase inhibitor, an initial series of compounds was obtained modifying the O- and N-termini of the carbamic template by alkyl or aryl groups. A first SAR study indicated that the nitrogen must bear an aliphatic group while the moiety on the oxygen should be aromatic to retain FAAH activity. Supposing the aromatic substituent would mimic the binding conformation of the FAEs chain, exploration of the steric requirements at this level by designing conformationally constrained O-aryl moieties, indicated that compounds endowed with a bent shape are much more potent than the straight ones. The most potent compound identified in this study was the m-biphenyl derivative (IC_{50} = 63 nM), known as URB524[60].

Further SAR campaigns were carried out by modulation of steric and electronic features at both N- and O- portions of URB524. The introduction of a carbamoyl group in meta position of the distal phenyl ring of ester moiety, that allows the formation of two Hbond with the backbone carbonyl of Leu380 and with the side-chain NH_2 of Gln273, gave the most potent compound of the series, URB597 (IC_{50} = 4 nm)[63].

Insertion of groups with different electronic properties at the para positions of the proximal phenyl ring of URB524 should directly affect the reactivity of the carbamic carbon. While the introduction of an electron donor group, such as NO_2, increases the reactivity of the molecule, leading to chemical instability, the insertion of an electron withdraw group, such as OH or NH_2, that reduce the reactivity of the compound, does not affect the in-vitro activity on FAAH. This fact can be explained by two hypothesis or a combination of both: 1) small polar substituents at this position can accept a hydrogen bond from the NH group of Cys269 with or without the interposition of a water molecule, leading to an improved recognition step of the inhibition process; 2) the intrinsic catalytic mechanism of FAAH is able to overcome the differences in reactivity of these compounds[64].

These observations lead to the synthesis of a new derivatives of URB597, substituted in para position of the proximal phenyl ring. This study showed that introduction of both carbamoyl group in meta to the distal phenyl ring and electrondonor group in para position to the proximal phenil ring does not lead to a synergic nor cumulative effect on potency. Most interestingly, the hydroxyl substituted compound (URB937) is a target of an efflux pump at the brain blood barrier, leading to the first peripherally restricted inhibitor of FAAH. Pharmacological evaluation of this compound demonstrated that, despite its inability to access brain and spinal cord, it retains antiinflammatory and antinociceptive effects[65].

Modification of the N-alkyl structure heavily affect the recognition events. Synthesis of compounds with long aliphatic chain at this position confirmed the orientation of this class inhibitors in the FAAH catalytic site, with the biphenyl moiety oriented in the CA and the N-portion located into the AcBP, as previously predicted by a QM/MM study[66].

		IC50 (nM)	ID50 (mg/Kg)
	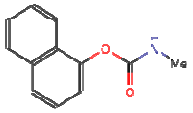	Inactive	
	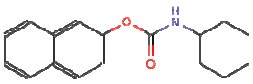	324	
URB524	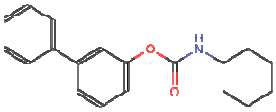	63	0.81
URB597	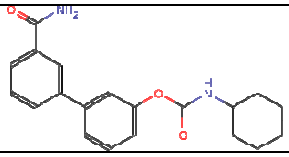	4.6	0.22
	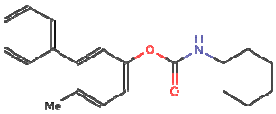	176	
URB694	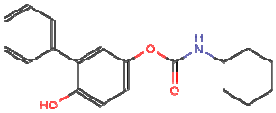	45	0.16
URB618	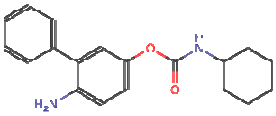	52	0.18
	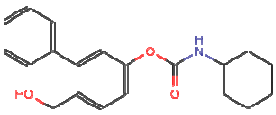	46	
URB937	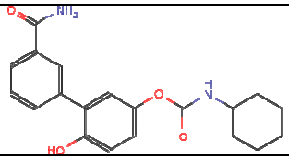	27	
	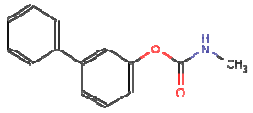	13900	
	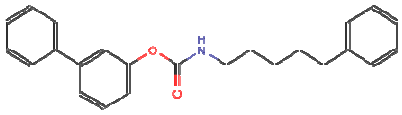	13	

Table 3.3 O-aryl cyclohexyl carbamate FAAH-inhibitors. Some examples from the SAR studies.

The potent and selective inhibitor URB597, early became the reference compound for the functional studies on FAAH. It inhibits FAAH with IC_{50}=4nm without affecting the activity of a broad panel of enzymes. In-vivo administration of the selective FAAH

inhibitor URB597 cause an elevation of brain anandamide levels, which correspond to anxiolytic, antidepressant and analgesic effects[42].

[22] Russo, E. B. History of cannabis and its preparations in saga, science, and sobriquet. Chemistry & biodiversity 2007, 4, 1614-48.

[23] Freund, T. F.; Katona, I.; Piomelli, D. Role of endogenous cannabinoids in synaptic signaling. Physiological reviews 2003, 83, 1017-66.

[24] Devane, W. A.; Hanus, L.; Breuer, A.; Pertwee, R. G.; Stevenson, L. A.; Griffin, G.; Gibson, D.; Mandelbaum, A.; Etinger, A.; Mechoulam, R. Isolation and structure of a brain constituent that binds to the cannabinoid receptor. Science (New York, N.Y.) 1992, 258, 1946-9.

[25] Basavarajappa, B. S. Critical enzymes involved in endocannabinoid metabolism. Protein and peptide letters 2007, 14, 237-46.

[26] Natarajan, V.; Schmid, P. C.; Reddy, P. V.; Schmid, H. H. Catabolism of N-acylethanolamine phospholipids by dog brain preparations. Journal of neurochemistry 1984, 42, 1613-9.

[27] Fu, J.; Bottegoni, G.; Sasso, O.; Bertorelli, R.; Rocchia, W.; Masetti, M.; Guijarro, A.; Lodola, A.; Armirotti, A.; Garau, G.; Bandiera, T.; Reggiani, A.; Mor, M.; Cavalli, A.; Piomelli, D. A catalytically silent FAAH-1 variant drives anandamide transport in neurons. Nature neuroscience 2011, 1-8.

[28] Mechoulam, R.; Ben-Shabat, S.; Hanus, L.; Ligumsky, M.; Kaminsky, N. E.; Schatz, A. R.; Gopher, A.; Almog, S.; Martin, B. R.; Compton, D. R.; Pertwee, R. G.; Griffin, G.; Bayewitch, M.; Barg, J.; Vogel, Z. Identification of an endogenous 2-monoglyceride, present in canine gut,that binds to cannabinoid receptors. Science 1995, 50, 83-90.

[29] Stella, N.; Schweitzer, P.; Piomelli, D. A second endogenous cannabinoid that modulates long-term potentiation. Nature 1997, 388, 773-8.

[30] Dinh, T. P.; Carpenter, D.; Leslie, F. M.; Freund, T. F.; Katona, I.; Sensi, S. L.; Kathuria, S.; Piomelli, D. Brain monoglyceride lipase participating in endocannabinoid inactivation. Proceedings of the National Academy of Sciences of the United States of America 2002, 99, 10819-24.

[31] Walker, J. M.; Krey, J. F.; Chu, C. J.; Huang, S. M. Endocannabinoids and related fatty acid derivatives in pain modulation. Chemistry and physics of lipids 2002, 121, 159-72.

[32] Matsuda, L. A.; Lolait, S. J.; Brownstein, M. J.; Young, A. C.; Bonner, T. I. Structure of a cannabinoid receptor and functional expression of the cloned cDNA. Nature 1990, 346, 561-4.

[33] Munro, S.; Thomas, K. L.; Abu-Shaar, M. Molecular characterization of a peripheral receptor for cannabinoids. Nature 1993, 365, 61-65.

[34] Zygmunt, P. M.; Petersson, J.; Andersson, D. a; Chuang, H.; Sørgård, M.; Di Marzo, V.; Julius, D.; Högestätt, E. D. Vanilloid receptors on sensory nerves mediate the vasodilator action of anandamide. Nature 1999, 400, 452-457.

[35] Brown, a J. Novel cannabinoid receptors. British journal of pharmacology 2007, 152, 567-75.

[36] Atwood, B. K.; Wager-Miller, J.; Haskins, C.; Straiker, A.; Mackie, K. Functional selectivity in CB2 cannabinoid receptor signaling and regulation: implications for the therapeutic potential of CB2 ligands. Molecular pharmacology, doi 10.1124/mol.111.074013.

[37] Gerra, G.; Zaimovic, A.; Gerra, M. L.; Ciccocioppo, R.; Cippitelli, A.; Serpelloni, G.; Somaini, L. Pharmacology and toxicology of Cannabis derivatives and endocannabinoid agonists. Recent patents on CNS drug discovery 2010, 5, 46-52.

[38] Walker, J. M.; Huang, S. M.; Strangman, N. M.; Tsou, K.; Sañudo-Peña, M. C. Pain modulation by release of the endogenous cannabinoid anandamide. Proceedings of the National Academy of Sciences of the United States of America 1999, 96, 12198-203.

[39] Veldhuis, W. B.; van der Stelt, M.; Wadman, M. W.; van Zadelhoff, G.; Maccarrone, M.; Fezza, F.; Veldink, G. A.; Vliegenthart, J. F. G.; Bär, P. R.; Nicolay, K.; Di Marzo, V. Neuroprotection by the endogenous cannabinoid anandamide and arvanil against in vivo excitotoxicity in the rat: role of vanilloid receptors and lipoxygenases. The Journal of neuroscience : the official journal of the Society for Neuroscience 2003, 23, 4127-33.

[40] Cravatt, B. F.; Giang, D. K.; Mayfield, S. P.; Boger, D. L.; Lerner, R. A.; Gilula, N. B. Molecular characterization of an enzyme that degrades neuromodulatory fatty-acid amides. Science 1996, 384, 83-87.

[41] Cravatt, B. F.; Demarest, K.; Patricelli, M. P.; Bracey, M. H.; Giang, D. K.; Martin, B. R.; Lichtman, A. H. Supersensitivity to anandamide and enhanced endogenous cannabinoid signaling in mice lacking fatty acid

amide hydrolase. Proceedings of the National Academy of Sciences of the United States of America 2001, 98, 9371-6.

[42] Kathuria, S.; Gaetani, S.; Fegley, D.; Valiño, F.; Duranti, A.; Tontini, A.; Mor, M.; Tarzia, G.; La Rana, G.; Calignano, A.; Giustino, A.; Tattoli, M.; Palmery, M.; Cuomo, V.; Piomelli, D. Modulation of anxiety through blockade of anandamide hydrolysis. Nature medicine 2003, 9, 76-81.

[43] Wei, B. Q.; Mikkelsen, T. S.; McKinney, M. K.; Lander, E. S.; Cravatt, B. F. A second fatty acid amide hydrolase with variable distribution among placental mammals. The Journal of biological chemistry 2006, 281, 36569-78.

[44] Giang, D. K.; Cravatt, B. F. Molecular characterization of human and mouse fatty acid amide hydrolases. Proceedings of the National Academy of Sciences of the United States of America 1997, 94, 2238-42.

[45] Mileni, M.; Johnson, D. S.; Wang, Z.; Everdeen, D. S.; Liimatta, M.; Pabst, B.; Bhattacharya, K.; Nugent, R. a; Kamtekar, S.; Cravatt, B. F.; Ahn, K.; Stevens, R. C. Structure-guided inhibitor design for human FAAH by interspecies active site conversion. Proceedings of the National Academy of Sciences of the United States of America 2008, 105, 12820-4.

[46] Bracey, M. H.; Hanson, M. A.; Masuda, K. R.; Stevens, R. C.; Cravatt, B. F. Structural Adaptations in a Membrane Enzyme That Terminates Endocannabinoid Signaling. Science 2002, 298, 1793-1796.

[47] Patricelli, M. P.; Lashuel, H. a; Giang, D. K.; Kelly, J. W.; Cravatt, B. F. Comparative characterization of a wild type and transmembrane domain-deleted fatty acid amide hydrolase: identification of the transmembrane domain as a site for oligomerization. Biochemistry 1998, 37, 15177-87.

[48] Patricelli, M. P.; Lovato, M. A.; Cravatt, B. F. Chemical and mutagenic investigations of fatty acid amide hydrolase: evidence for a family of serine hydrolases with distinct catalytic properties. Biochemistry 1999, 38, 9804-9812.

[49] Patricelli, M. P.; Cravatt, B. F. Fatty acid amide hydrolase competitively degrades bioactive amides and esters through a nonconventional catalytic mechanism. Biochemistry 1999, 38, 14125-14130.

[50] Seierstad, M.; Breitenbucher, J. G. Discovery and development of fatty acid amide hydrolase (FAAH) inhibitors. Journal of medicinal chemistry 2008, 51, 7327-43.

[51] Patricelli, M. P.; Cravatt, B. F. Characterization and manipulation of the acyl chain selectivity of fatty acid amide hydrolase. Biochemistry 2001, 40, 6107-15.

[52] McKinney, M. K.; Cravatt, B. F. Evidence for distinct roles in catalysis for residues of the serine-serine-lysine catalytic triad of fatty acid amide hydrolase. The Journal of biological chemistry 2003, 278, 37393-9.

[53] Patricelli, M. P.; Cravatt, B. F. Clarifying the catalytic roles of conserved residues in the amidase signature family. The Journal of biological chemistry 2000, 275, 19177-84.

[54] Lodola, A.; Mor, M.; Hermann, J. C.; Tarzia, G.; Piomelli, D.; Mulholland, A. J. QM/MM modelling of oleamide hydrolysis in fatty acid amide hydrolase (FAAH) reveals a new mechanism of nucleophile activation. Chemical communications (Cambridge, England) 2005, 4399-401.

[55] Lodola, A.; Mor, M.; Sirirak, J.; Mulholland, A. J. Insights into the mechanism and inhibition of fatty acid amide hydrolase from quantum mechanics/molecular mechanics (QM/MM) modelling. Biochemical Society transactions 2009, 37, 363-7.

[56] Lodola, A.; Mor, M.; Rivara, S.; Christov, C.; Tarzia, G.; Piomelli, D.; Mulholland, A. J. Identification of productive inhibitor binding orientation in fatty acid amide hydrolase (FAAH) by QM/MM mechanistic modelling. Chemical communications 2008, 214-6.

[57] Tubert-Brohman, I.; Acevedo, O.; Jorgensen, W. L. Elucidation of hydrolysis mechanisms for fatty acid amide hydrolase and its Lys142Ala variant via QM/MM simulations. Journal of the American Chemical Society 2006, 128, 16904-13.

[58] Ahn, K.; Johnson, D. S.; Cravatt, B. F. Fatty acid amide hydrolase as a potential therapeutic target for the treatment of pain and CNS disorders. Expert opinion on drug discovery 2009, 4, 763-784.

[59] Boger, D. L.; Miyauchi, H.; Du, W.; Hardouin, C.; Fecik, R. A.; Cheng, H.; Hwang, I.; Hedrick, M. P.; Leung, D.; Acevedo, O.; Guimarães, C. R. W.; Jorgensen, W. L.; Cravatt, B. F. Discovery of a potent, selective, and efficacious class of reversible alpha-ketoheterocycle inhibitors of fatty acid amide hydrolase effective as analgesics. Journal of medicinal chemistry 2005, 48, 1849-56.

[60] Tarzia, G.; Duranti, A.; Tontini, A.; Piersanti, G.; Mor, M.; Rivara, S.; Plazzi, P. V.; Park, C.; Kathuria, S.; Piomelli, D. Design, synthesis, and structure-activity relationships of alkylcarbamic acid aryl esters, a new class of fatty acid amide hydrolase inhibitors. Journal of medicinal chemistry 2003, 46, 2352-60.

[61] Johnson, D. S.; Ahn, K.; Kesten, S.; Lazerwith, S. E.; Song, Y.; Morris, M.; Fay, L.; Gregory, T.; Stiff, C.; Dunbar, J. B.; Liimatta, M.; Beidler, D.; Smith, S.; Nomanbhoy, T. K.; Cravatt, B. F. Benzothiophene piperazine and piperidine urea inhibitors of fatty acid amide hydrolase (FAAH). Bioorganic & medicinal chemistry letters 2009, 19, 2865-9.

[62] Ahn, K.; Johnson, D. S.; Fitzgerald, L. R.; Liimatta, M.; Arendse, A.; Stevenson, T.; Lund, E. T.; Nugent, R. A.; Nomanbhoy, T. K.; Alexander, J. P.; Cravatt, B. F. Novel mechanistic class of fatty acid amide hydrolase inhibitors with remarkable selectivity. Biochemistry 2007, 46, 13019-30.

[63] Mor, M.; Rivara, S.; Lodola, A.; Plazzi, P. V.; Tarzia, G.; Duranti, A.; Tontini, A.; Piersanti, G.; Kathuria, S.; Piomelli, D. Cyclohexylcarbamic acid 3'- or 4'-substituted biphenyl-3-yl esters as fatty acid amide hydrolase inhibitors: synthesis, quantitative structure-activity relationships, and molecular modeling studies. Journal of medicinal chemistry 2004, 47, 4998-5008.

[64] Tarzia, G.; Duranti, A.; Gatti, G.; Piersanti, G.; Tontini, A.; Rivara, S.; Lodola, A.; Plazzi, P. V.; Mor, M.; Kathuria, S.; Piomelli, D. Synthesis and structure-activity relationships of FAAH inhibitors: cyclohexylcarbamic acid biphenyl esters with chemical modulation at the proximal phenyl ring. ChemMedChem 2006, 1, 130-9.

[65] Clapper, J. R.; Moreno-Sanz, G.; Russo, R.; Guijarro, A.; Vacondio, F.; Duranti, A.; Tontini, A.; Sanchini, S.; Sciolino, N. R.; Spradley, J. M.; Hohmann, A. G.; Calignano, A.; Mor, M.; Tarzia, G.; Piomelli, D. Anandamide suppresses pain initiation through a peripheral endocannabinoid mechanism. Nature neuroscience 2010, 13, 1265-70.

[66] Mor, M.; Lodola, A.; Rivara, S.; Vacondio, F.; Duranti, A.; Tontini, A.; Sanchini, S.; Piersanti, G.; Clapper, J. R.; King, A. R.; Tarzia, G.; Piomelli, D. Synthesis and quantitative structure-activity relationship of fatty acid amide hydrolase inhibitors: modulation at the N-portion of biphenyl-3-yl alkylcarbamates. Journal of medicinal chemistry 2008, 51, 3487-98.

4. Methods adopted during the study

The QM/MM method

In molecular modeling there are two main approaches that allow to estimate the internal energy of a system: molecular mechanics (MM) and quantum mechanics (QM).

In MM a molecular system, the energy of a system is described by an empirical mathematical function that expresses potential energy as a sum of energy terms, describing the deviation of bond lengths, bond angles and torsion angles from equilibrium values, plus terms for non-bonded pairs of atoms describing van der Waals and electrostatic interactions. The mathematical form of the expression, and the parameters in it, constitute the force field. Since this method makes no reference to the electrons, and so cannot throw light on electronic properties, such as charge distribution or nucleophilic or electrophilic behavior, the chief limitation of the MM level of theory is that it is not appropriate for the description of processes involving bond-making or bond-breaking, i.e., chemical reactions.

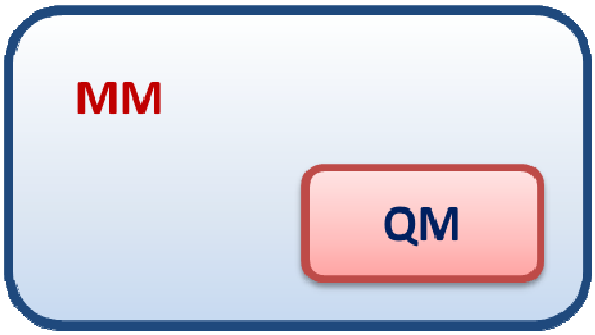

Figure 4.1 Schematic diagram depicting the partitioning of the system into a QM and an MM region

To adequately model such processes, QM methods are required. In fact, the fundamental postulate of quantum mechanics is that a so-called wave function exists for any (chemical) system, and its energy can be returned by an appropriate

operator, the Hamiltonian, as function of position and charge of the system elements only.

$$E\Psi = \widehat{H}\Psi \qquad \textit{(Eq. 4.1)}$$

However, the region of space within which significant changes in electronic structure occur, along the course of a reaction coordinate, is often relatively small compared to the size of the reacting system as a whole. For instance, an enzyme may catalyze the conversion of its substrate from one molecule to another, but the volume of space within which bonds are being made and broken is usually limited to the relatively small active site, while the remainder of the enzyme may exert important structural and stabilization functions. Thus, from a modeling perspective, it is possible to accurately model the electronic-structure problem by QM, retaining the electrostatic and van der Waals effects from the surrounding region, that are represented at the MM reduced level of theory[67].

This kind of framework was theorized by Levitt and Warshel in 1976 and take the name of hybrid QM/MM technique. The complete Hamiltonian for such system is:

$$H_{TOTAL} = H_{QM} + H_{MM} + H_{QM/MM} \qquad \textit{(Eq. 4.2)}$$

where H_{QM} accounts for the full interaction energy of all quantum mechanical particles, H_{MM} accounts for the full interaction energy of all classical particles and $H_{QM/MM}$ accounts for the energy of all interactions between the quantum mechanical and the classical particles. Different approaches allow the treatment of the $H_{QM/MM}$ term.

In the “Unpolarized” framework, the QM/MM interaction energy is computed in a fashion closely resembling the standard approach for MM non-bonded interactions, fixing a punctual charge on the QM atoms and assigning them the Lennard-Jones parameters in according to the force field applied to the MM region.

The most applied implementation is the “Polarized QM/Unpolarized MM”. In this case the electrostatic interaction has been separated into an operator acting on the QM electrons and the classical electrostatic and Lennard-Jones terms for the interaction of the MM atoms with the QM nuclei. In this way, the partial charges of the

MM atoms are included in the QM Hamiltonian, acting on the electrons such as QM nuclei.

When “fully polarized interactions” are computed, at each MM molecule or atom is assigned a polarizability tensor and an induced dipole at each polarizable center is determined by the electric field E created by both MM partial charges and the nuclei and electronic wave function of the QM system. The interaction of the induced dipoles between them and with the MM partial charges are added both in the H_{MM} and in the H_{QM} terms, where additional one-electron integrals for each dipoles are added to the Fock operator.

Boundary Region

When the boundary between the QM and MM regions of a QM/MM model is characterized by a very low level of electron density, that is no atoms on one side of the boundary are bonded to atoms on the other side, the $H_{QM/MM}$ term is restricted to non-bonded interactions. The situation is vastly more complicated when the boundary passes across one or more chemical bonds. Molecular mechanics methods are defined atom by atom, thus having a carbon atom without all of its bonds does not have a large affect on other atoms in the system. In contrast, quantum mechanical calculations use a wave function that can incorporate second atom effects, so an atom with a non-filled valence will behave differently than one with filled valence. The simplest solution is to define a boundary that does not pass through a covalent bond. Modeling the catalysis of an enzyme where generally catalytic residues are involved, this approach if unfeasible, since it would require to treat all the protein at QM level. Three main approaches were developed to fill the non-filled valence shell of the atoms when QM/MM boundary cuts covalent bonds.

Link atom scheme introduce an additional atomic center, usually an hydrogen bond, that is not part of the real system. It is covalently bound to the QM region and saturates its free valence, while it is interaction with MM region is not evaluate in the $H_{QM/MM}$ term.

In the boundary-atom schemes, the MM atom at the boundary is replaced by a special atom that appears in both H_{QM} and H_{MM} terms. In H_{QM} it mimics the electronic character of the MM moiety, while in the MM calculation it behaves as a normal MM atom.

Localized-orbital schemes place hybrid orbitals at the boundary, and keep some of them frozen. They serve to cap the QM region, replacing the cut bond.

In the CHARMM package, a standard QM/MM interface was implemented for semi-empirical and SCC-DFTB quantum methods[68,69]. A more detailed description about these quantum potentials will be dealt above in section 2.3. In the QM/MM approach, electrostatic effects as well as steric contributions from the environment are incorporated directly into the electronic structure calculations of the reactive region, resulting in a "QM polarized/MM unpolarized" framework. The interactions between the QM and MM regions are separated into an electrostatic term, arising from the electric field of the MM atoms, and a van der Waals component, accounting for dispersion interactions and Pauli repulsions. Although the electrostatic interaction Hamiltonian employs the standard partial atomic charges of the force field, the van der Waals term includes empirical parameters that depend from the QM model.

$$E_{TOT} = \langle \Psi | \hat{H}_{QM} + \hat{H}^{el}_{QM/MM} | \Psi \rangle + E^{vdW}_{QM/MM} + E_{MM} \qquad \textit{(Eq. 4.3)}$$

Two implementation allow the treatment of the QM/MM boundary: 1) hydrogen link atoms; 2) Generalized Hybrid Orbital (GHO), a frozen localized orbitals method.

Reaction modelling: the adiabatic mapping approach

In many cases, the mechanism of a reaction is known a priori, and it is easily described by one or more reaction coordinates that are function of several geometrical parameters. For example, hydrolytic reactions generally involve proton transfers that are well described by atomic distances. In these cases a reaction can be described exploring the potential energy along dimensions corresponding to the reaction coordinates. In adiabatic mapping methods, the system is restrained at fixed

values of the reaction coordinates that are gradually changed from the initial (the minimized structure of the reactants) to the final value (the products) in a stepwise way. At each step, the rest of the system is allowed to relax using minimization algorithms[70].

This approach allows to overpass the hills from reactants to products, and vice-versa, on the potential energy surfaces and localize approximated transition states (TS). Although widely used, this method present several limitations that must be taken into account. Firstly, it is valid only if one conformation of the protein is involved during the reaction, and the entropic term is negligible. Secondary, it permits to localize only approximated TS, since no vibrational analysis are performed. Finally, this method is highly dependent from the reaction coordinates: if a critical atom motion is not included in the coordinate, energy barriers are not reliable. Recalculating the path backwards from products is a useful test to ensure that a proper adiabatic, reversible profile has been modelled.

Furthermore, the choice of the starting conformation can heavily affect the energetics of a reaction: less stable is the starting conformation, lower will the energy barrier result. Accordingly to the Curtin-Hammett principle[71], a reaction is not controlled by the relative proportions of the conformational isomers of the reactants only, but it depends on the difference in standard Gibbs energies between them and the respective transition states. Exploration of the PES starting from several conformations that are accessible at ordinary temperature (e.g. different snapshots from a MD or MC equilibration) allows to locate the activated configurations of the system that, although thermodynamically less probable, can determine the rate of the reaction.

---

[67] Cramer CJ. Essential of computational chemistry: theories and models, 2nd edition. John Wiley & Sons Ltd, Chichester, 2004, Chapter 13

[68] Field, M. J.; Bash, P. A.; Karplus, M. A combined quantum mechanical and molecular mechanical potential for molecular dynamics simulations. Journal of Computational Chemistry 1990, 11, 700-733.

[69] Cui, Q.; Elstner, M.; Kaxiras, E.; Frauenheim, T.; Karplus, M. A QM/MM implementation of the Self-Consistent Charge Density Functional Tight Binding (SCC-DFTB) method. Journal of Physical Chemistry B 2001, 105, 569-585.

[70] Schlegel, H. B. Exploring potential energy surfaces for chemical reactions: an overview of some practical methods. Journal of computational chemistry 2003, 24, 1514-27.

[71] Seeman, J. I. Effect of conformational change on reactivity in organic chemistry. Evaluations, applications, and extensions of Curtin-Hammett Winstein-Holness kinetics. Chemical Reviews 1983, 83, 83-134.

5. Effect of the reactivity of cyclohexyl carbamic acids biphenyl-3-yl esters on the FAAH inhibitory potency

FAAH inhibitors from the class of O-aryl carbamate are being evaluated clinically for the treatment of pain and anxiety. Although they showed no sign of adverse effects in pre-clinical studies, interactions with carboxylesterases in liver might limit their usefulness[72]. In fact, URB597, the reference compound belonging to the class of carbamic acid O-aryl ester, displays remarkable target selectivity for FAAH both in vitro and in vivo[73]. Nevertheless, at concentrations that exceed those needed to fully block FAAH activity, the compound inhibits several broad-spectrum esterases in the liver. This may affect the pharmacokinetics of other therapeutic agents containing ester or amide bonds, that are normally substrates for liver carboxylesterases. Moreover, it had been shown that bioavailability of URB597 and its analogs is strongly affected by hydrolysis in plasma, catalysed by other esterases.

Two strategies can be applied to increase the selectivity of covalent inhibitors toward FAAH. The first is to improve the recognition for the target, by modulating the stereo-electronic complementarity with the binding site. The second involves modulation of the reactivity of the carbamate group with the scope of lowering its susceptibility to nucleophilic attack by generic hydrolases.

Structure–activity relationship (SAR) studies had shown that the introduction of electron-donor groups on the aryl portion, conjugated to the carbamic group of the reference compound URB524, enhanced compound stability both in alkaline buffer and in rat plasma. Conversely, the same substitution did not affect FAAH inhibitor potency in vitro. This resulted in the identification of a second generation of FAAH inhibitors, endowed with improved selectivity and in-vivo potency[74,75,76].

IC_{50} valies suggest that the catalytic machinery of FAAH is able to overcome the differences in reactivity of the three compounds reported in Table 5.1. To clarify the mechanism of action of this class of inhibitors, and elucidate the relationships between *in-vitro* potency and reactivity, a hybrid quantum mechanical/molecular

mechanics (QM/MM) approach was applied to model the carbamoylation reaction of FAAH by the reference inhibitor URB524 (IC_{50} = 63 nM) and by its p-OH (URB694, IC_{50} = 45 nM) and p-NH_2 (URB618, IC_{50} = 52 nM) derivatives.

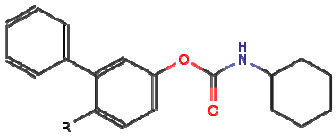	**R**	**IC_{50}**[74] (nM)	**$t_{1/2}$ pH9**[75] (min)	**$t_{1/2}$ rat plasma**[76] (min)	**ID_{50}**[76] (mg·Kg^{-1})
URB524	**H**	63	41	43	0.81
URB694	**OH**	45	255	950	0.16
URB618	**NH_2**	52	432	784	0.18

Table 5.1 In vitro and in vivo potency and stability of the O-aryl carbamate FAAH inhibitorsemployed in this investigation.

Moreover, differential transition state stabilization (DTSS) analysis[77], an emerging approach for identifying important interactions in enzyme-catalysed reactions[78], was applied to identify crucial residues (amino acids or water molecules) involved in FAAH inhibition.

The reliability of the adopted QM/MM approach was evaluated in a previous study, where the same QM/MM approach was able to identify the productive orientation of URB524 within the catalytic site of FAAH[79], that was confirmed by SAR studies[80] and by a crystallographic structure[81].

Methods

Model Building

The coordinates of FAAH were taken from those of a covalent adduct with methyl-arachidonyl-fluorophosphonate (MAPF), reported in the Protein Data Bank (PDB code: 1MT5). The atoms of the methyl-arachidonyl-phosphate (MAP) fragment were deleted and, after standard protein preparation, the three inhibitors were docked into

the catalytic site, selecting the energetically preferred and experimentally observed binding conformation II[79,80,81]. The partial charges of the ligand atoms were calculated by JAGUAR at B3LYP/6-31+G(d) level. The Michaelis Complexes (MC) were solvated by 25 Å-radius sphere of TIP3P water, minimized and equilibrated by 250 ps of classical molecular dynamic simulations. The equilibrated complexes were further minimized to an energy gradient of 0.01 kcal mol^{-1} $Å^{-1}$ with the ABNR method and employed for subsequent QM/MM reaction modeling.

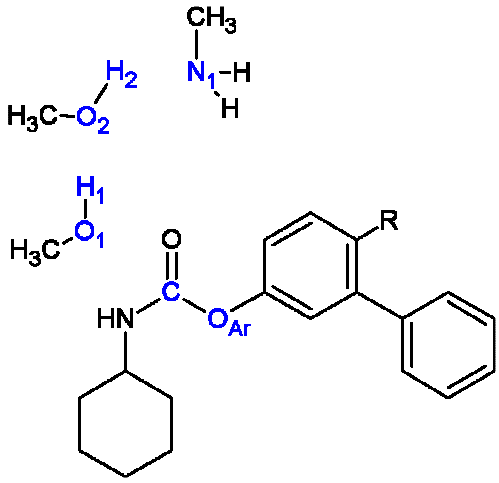

Figure 5.1 Structure of the QM region. It consists of the methylamine group of Lys142, the side chains of Ser217 and Ser241 and the whole URB inhibitors. Amino acids fragments were capped with 3 H-Link atoms.

Application of the QM/MM potential

The methylamine group of Lys142, the side chains of Ser217 and Ser241 and the carbamic inhibitors were treated at the PM3 quantum chemical level, while other atoms were treated at the MM level with the CHARMM all-atom force field, employing CHARMM22 parameters for the protein. Covalent bonds crossing the boundary between QM and MM regions were treated introducing three link atoms, which are included in the QM system.

Reaction model

The reaction was modelled in three steps, starting from the Michaelis complex (A): (**1**) formation of the TI (C); (**2**) m-biphenate expulsion with formation of carbamoylated Ser241 (E); (**3**) m-biphenate protonation and formation of neutral Lys142 (G). Stationary states were located on the potential energy surfaces (PESs) by a coordinate driving approach along appropriate reaction coordinates.

Step (1) was explored by means of two coordinates, R_X and R_Y, which describe proton abstraction from Ser241 by Ser217 and nucleophilic attack by Ser241 the first one, and the proton transfer between Ser217 and Lys142, the latter.

$$R_X = [\, d(O_1, H_1) - d(O_2, H_1) - d(O_1, C)\,] \qquad \textit{(Eq. 5.1)}$$

$$R_Y = [\, d(O_2, H_2) - d(N_1, H_2)] \qquad \textit{(Eq. 5.2)}$$

Step (2) was modelled by breaking the C-O bond (R_Z).

$$R_Z = [\, d(C, OAr)\,] \qquad \textit{(Eq. 5.3)}$$

In the last step (3), protonation of m-biphenate oxygen was explored by R_R, while the final proton transfer between Lys142 and Ser217 was described by R_S.

$$R_R = [\, d(O_2, H_1) - d(OAr, H_1)] \qquad \textit{(Eq. 5.4)}$$

$$R_S = [\, d(N_1, H_2) - d(O_2, H_2)] \qquad \textit{(Eq. 5.5)}$$

During PES exploration, atoms further than 14 Å from the Ser241 hydroxyl oxygen were fixed and R_X, R_Y, R_Z, R_R, and R_S were increased stepwise by 0.1 Å, applying harmonic restraints of 5000 kcal mol^{-1} $Å^{-2}$. At each step the rest of system was relaxed by ABNR method till an energy gradient of 0.01 kcal mol^{-1} $Å^{-1}$.

High-level corrections were applied on the stationary points: the corrected values were obtained subtracting the PM3 energy of the QM region at the total QM/MM energy and finally adding the energy of that region calculated by JAGUAR at B3LYP/6-31+G(d) level of theory.

Differential transition state stabilization (DTSS) calculations

The catalytic activity of a given molecular environment, R, can be defined as the lowering of activation energy barrier, Δ, which is equivalent to the difference in interaction energy of R with the transition state, ΔE_{TS-R}, and the substrate, ΔE_{S-R}:

$$\Delta = \Delta E_{TS-R} - \Delta E_{S-R} \qquad \textit{(Eq. 5.6)}$$

Accordingly, transition-state stabilization, relative to substrates, results in a negative value of Δ, giving rise to the catalytic effect (compared to the same reaction in the gas phase). When calculated separately for particular components of the catalytic environment (e.g. enzyme active site residues), differential transition state stabilization (DTSS) energy provides a quantitative measure of the residue's contribution to lowering of the barrier.

The structures of Michaelis complexes and transition states (TS)s for FAAH Ser241 carbamoylation by URB524, URB694, and URB618 inhibitors were taken from the QM/MM simulations described in the previous section and in the main text. To make the calculations feasible, FAAH active site models were built by selecting residues within 6 Å of the reaction centre (R) of the systems, defined as the centre of mass of the catalytic triad, formed by Lys142, Ser217 and Ser241. In addition to the catalytic triad members, the structures (Michaelis complexes and their relative TSs) resulted thus composed by 16 amino acids, two water molecules, and a carbamate inhibitor. All broken bonds were saturated with hydrogen atoms (with positions optimized at the HF/6-31G level). Such an approach has been shown to give useful results in analysing enzyme-catalysed reactions, as reported in recent publications[78,82]. Interaction energies were calculated in a pairwise fashion (i.e., for the reaction centre and each FAAH residue separately) at the MP2/6-31G(d) level of theory both for the Michaelis complexes (ΔE_{S-R}) and for the transition states (ΔE_{TS-R}). Basis set superposition error was accounted for by means of a counterpoise correction. Finally, the DTSS energy for each residue was obtained by applying equation 5.6.

It has been recently suggested that a water molecule interacting with p-OH or p-NH_2 groups might affect inhibitor potency, so DTSS analysis for the URB694 and URB618 inhibitors was also performed for this particular water molecule (Wat627).

Results and Discussion

Starting Structures

Visual inspection of the reactants (Michaelis complexes), optimized at the PM3-CHARMM22 level, revealed that the three inhibitors are similarly allocated in the FAAH active site, with the *O*-biphenyl moiety within the cytoplasmic access channel and the *N*-cyclohexyl group occupying the acyl-chain-binding pocket of FAAH (Figure 5.2). The inhibitor carbonyl oxygen is placed in the oxyanion hole, undertaking one hydrogen bond with Ile238 and three weaker polar interactions with backbone NHs of Gly239, Gly240 and Ser241. The hydroxyl of Ser241 is close to the carbamate carbon, while forming a hydrogen bond network with Ser217 and Lys142. In the case of URB694 (Figure 5-2) and URB618, the substituent in the para position forms a hydrogen bond with the NH backbone of Cys269 and Val270 through a water molecule (Wat627), conserved in crystallographic structures[81].

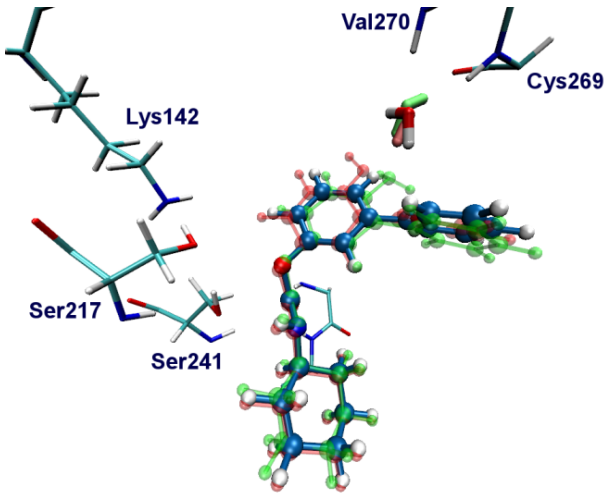

Figure 5.2 FAAH-URB524 michaelis complex. Carbon atoms of FAAH are coloured in cyan, and those of URB524 in blue. Structures of the other inhibitors are superposed in red (URB694) and green (URB618) transparencies. The para substituted inhibitors undertake additional interactions with residues of the catalytic site via a bridge water.

Reaction Mechanism at PM3-CHARMM22 level

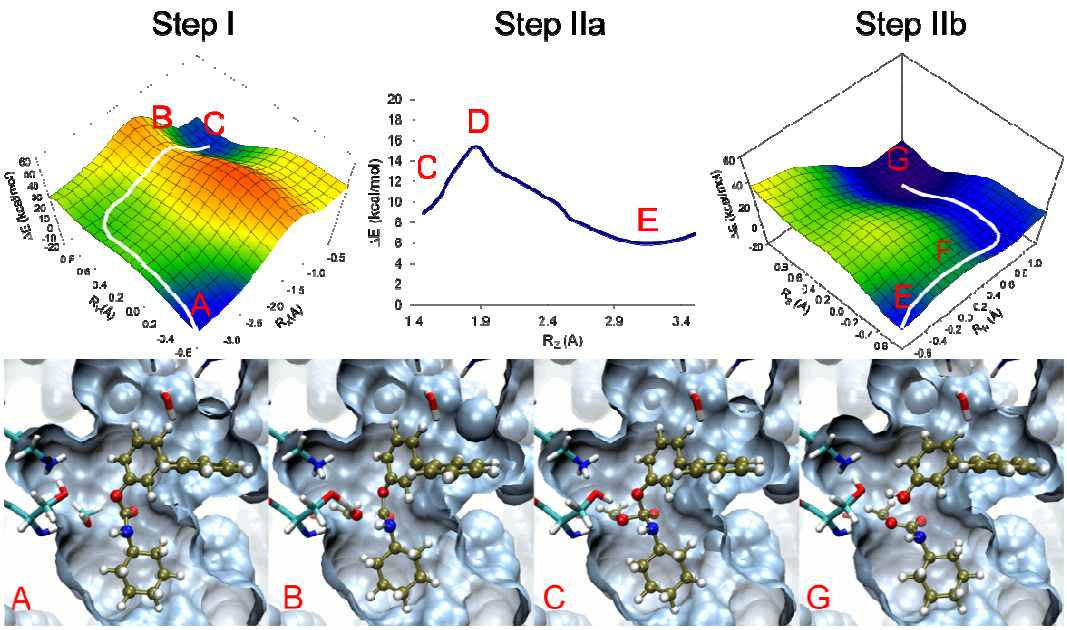

Figure 5.3 PM3-CHARMM27 QM/MM PESs (top) for FAAH carbamoylation in the reaction with URB524. The structures of some configurations are also shown: A (Michaelis complex), C (tetrahedral intermediate), G (carbamoylenzyme). FAAH active site residues are represented by cyan carbon atoms, while URB524 carbons are brown.

The PM3-CHARMM22 energetics of the carbamoylation of FAAH by the parent compound URB524 can be followed observing the potential energy surfaces (PESs) reported in Figure 5.3.

The reaction starts with a double proton transfer, in which Lys142, in cooperation with the bridging Ser217, deprotonates Ser241, triggering the nucleophilic attack and subsequent formation of the TI (configuration **C** on the PES of the left side of Figure 5-3). The energy required to overcome the highest point along the path - i.e. the transition state (TS) – is 40 kcal mol^{-1}. Visual inspection of the TS structure shows that deprotonation of Ser241 hydroxyl group is occurring at this stage (with H_1 found in between O_1 and O_2), while the nucleophile O_1 is still approaching the carbonyl carbon of the inhibitor (Table 5.2).

The TI (**C**) is a transient configuration along the carbamoylation pathway, significantly less stable than the reactants (**A**) by nearly 10 kcal mol^{-1}. Inspection of the TI structure shows that electrostatic interactions with backbone NH groups play a major role in stabilizing the system: there are two hydrogen bonds (Ile238, Gly239) and two strong interactions (Gly240, Ser241) between the negatively charged oxygen of URB524 and the oxyanion hole (not shown).

	A			B			C			E			F		
Atoms	URB 524	URB 694	URB 618	URB 524	URB 694	URB 618	URB 524	URB 694	URB 618	URB 524	URB 694	URB 618	URB 524	URB 694	URB 618
H_2 - N_1	1.77	1.77	1.77	1.06	1.04	1.05	1.02	1.02	1.02	1.02	1.02	1.02	1.75	1.75	1.75
O_2 - H_2	0.97	0.97	0.97	1.66	1.65	1.66	1.76	1.75	1.75	1.74	1.75	1.74	0.97	0.98	0.97
O_2 - H_1	1.81	1.80	1.80	1.09	1.33	1.26	0.98	0.98	0.98	0.98	0.98	0.98	1.76	1.83	1.76
O_1 - H_1	0.96	0.96	0.96	1.33	1.13	1.09	1.83	1.84	1.82	2.87	2.71	3.00	2.75	2.66	2.75
C – O_1	2.65	2.66	2.66	1.78	1.64	1.83	1.46	1.46	1.46	1.36	1.36	1.36	1.35	1.35	1.35

Table 5.2 Distances between reactant atoms (Å). Atom labels are consistent with Figure 5.1.

The following step (i.e. expulsion of the biphenate leaving group **E**) yields carbamoylated Ser241 overcoming a small energy barrier (Figure 5.3, step IIa). The energy of the TS for this step is 16 kcal mol^{-1} higher than that of the Michaelis complex.

Finally, protonation of the leaving group occurs with a very small barrier (Figure 5.3, step IIb). The energy of configuration **F** is 20 kcal mol^{-1} compared to the Michaelis complex, only 4 kcal mol^{-1} higher than configuration **E.** The **E** to **G** transformation is facilitated by Ser217, which is well oriented both to deprotonate the positively charged Lys142 and to protonate the oxygen of the biphenate anion.

Consistent with previous findings[79], formation of the TI, rather than LG expulsion and protonation, is found to be the rate limiting step (i.e. highest barrier) for FAAH inactivation at PM3-CHARMM level of theory.

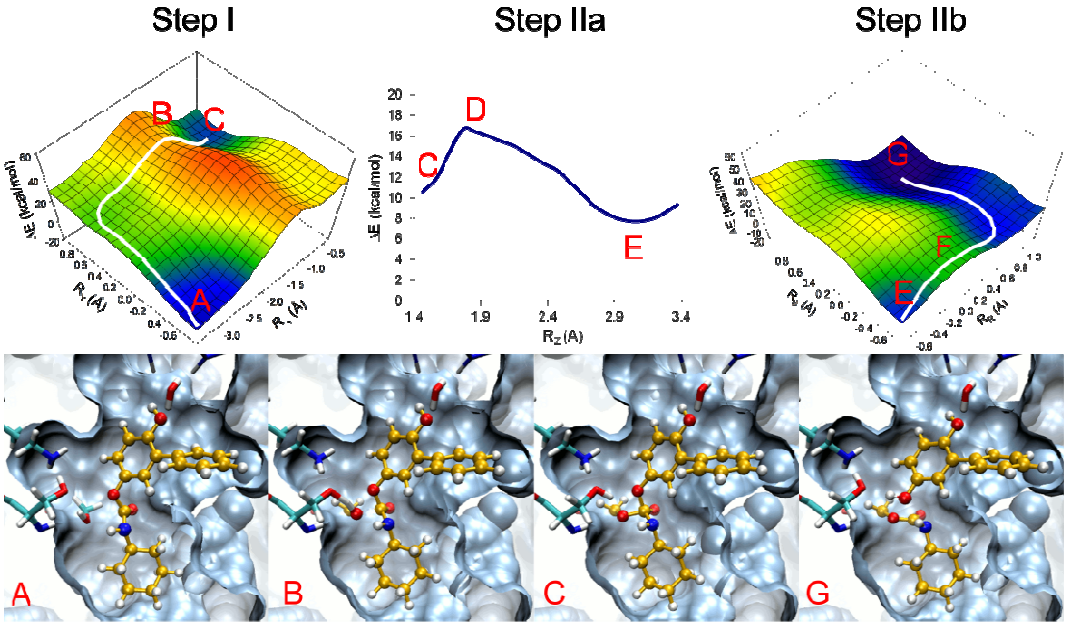

Figure 5.4 PM3-CHARMM27 QM/MM PESs (top) for FAAH carbamoylation in the reaction with URB694. The structures of shown configurations are: A (Michaelis complex), C (tetrahedral intermediate), G (carbamoylenzyme). URB694 carbons are shown in orange.

Carbamoylation reactions for *p*-substituted URB694 and URB618 show reaction pathways similar to that of the parent compound URB524 at PM3-CHARMM22 level of theory. The energetics of FAAH carbamoylation by URB694 is reported on the PES of Figure 5.4, while that one relative to FAAH carbamoylation by URB618 is reported in the PESs of Figure 5.5.

Analysis of these PM3-CHARMM22 surfaces shows that these three compounds share the same mechanism of inhibition. Indeed, also for URB618 and URB694 TI formation was found to be the rate-limiting step of the overall carbamoylation process, with the main TS of the reaction being dominated by proton trasfer between Ser217 and Ser241 (i.e. activation of the nucleophile).

As activation of the Ser41 nucleophile is a chemical event which is independent on the electronic state of the carbamate group of the inhibitor, the present calculations support the mechanistic hypothesis that introduction of electron donor groups in

conjugated position is not expected to energetically affect the carbamoylation pathway.

Furthermore, calculations also show that for all the three compounds, the LG leaves the TI (configuration **C**) as an anion. Indeed no prior protonation is required to achieve this step effectively. This finding is significantly different from what had been calculated for FAAH acylation by its substrates oleamide and oleoylmethylester[83], where protonation of the leaving group was the key element of the acylation pathway.

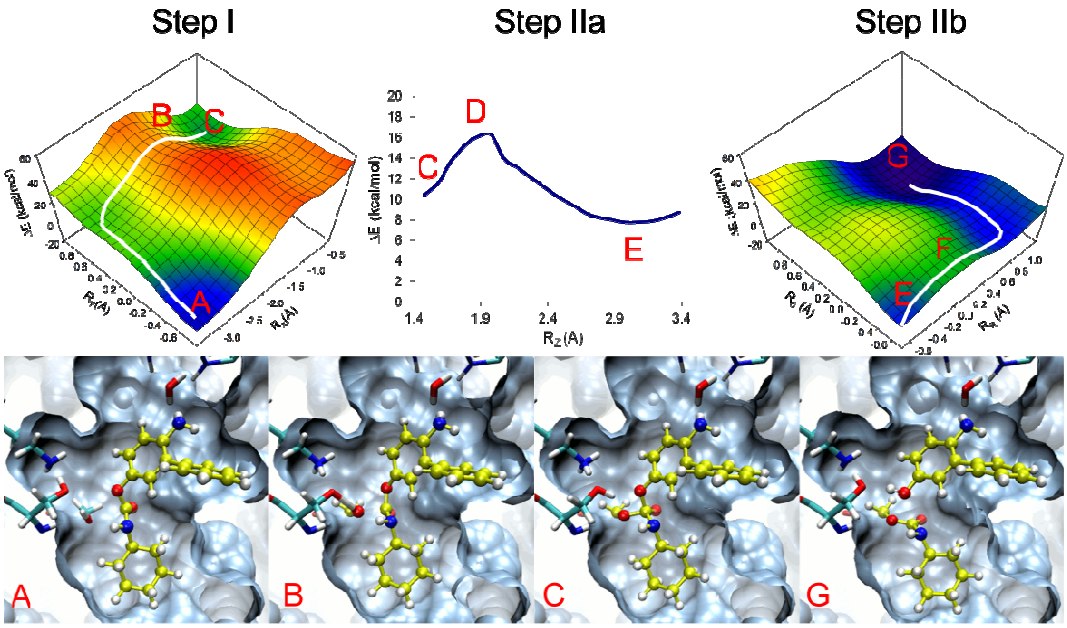

Figure 5.5 PM3-CHARMM27 QM/MM PESs (top) for FAAH carbamoylation in the reaction with URB618. The structures of shown configurations are: A (Michaelis complex), C (tetrahedral intermediate), G (carbamoylenzyme). URB618 carbons are shown in yellow.

To verify further this finding (that LG expulsion occurs without prior protonation for carbamic derivatives), we simulated an alternative carbamoylation pathways for URB694 and URB618, where protonation of the OAr oxygen was completed before the breaking of the C-OAr bond.

Calculations at PM3-CHARMM22 level show that when protonation of the biphenyl leaving group occurs before its expulsion the energy of the system increases up to

43 kcal mol^{-1} for URB694 and 44 kcal mol^{-1} for URB618. Following expulsion of the protonated LG results spontaneous, as no barrier was found between **E** and **G**. Taken together, these calculations confirm that breaking of the C-OAr followed by protonation is energetically favoured over OAr protonation followed by C-OAr breaking.

	URB694		**URB618**	
	LG expulsion followed by protonation	LG protonation followed by expulsion	LG expulsion followed by protonation	LG protonation followed by expulsion
A	0	0	0	0
B	42.08	42.08	44.61	44.61
C	10.57	10.57	10.38	10.38
D	16.73	43.44	16.23	44.36
E	7.67	21.55	7.73	31.36
F	20.49	no barrier	19.08	no barrier
G	-14.65	-14.38	-15.36	-15.43

Table 5.3 PM3-CHARMM27 energy values (kcal mol^{-1}) for key configurations obtained by simulating FAAH carbamoylation in the presence of URB694 and URB618 using different mechanisms: Mechanism (1) : TI formation (step I); LG expulsion (step IIa); LG protonation (step IIb). Mechanism (2): TI formation (step I); LG protonation (step IIa); TI collapse (step IIb).

To summarize the findings of calculations at PM3-CHARMM22 level of theory, it appears clearly that *i*) FAAH is not sensitive to the intrinsic reactivity of this class of aryl carbamates *ii*) TI formation represents the rate-limiting step of Ser241 carbamoylation iii) conjugated electron-donor groups have an effect only on step **IIb** of the reaction (LG protonation), which is not the rate-limiting one. The increment in electron density on the phenol oxygen (OAr), induced by p-OH or p-NH_2 groups of URB694 and URB618, respectively, makes its protonation easier with respect to the parent compound URB524.

Energy profiles at B3LYP/6-31+G(d)//PM3-CHARMM22 level

As semiempirical methods such as PM3 often overestimate energy barriers[84], higher-level calculations (B3LYP/6-31+G(d)) were applied to correct reaction energies. The corrected PES was obtained by subtracting the PM3 energy of the isolated QM region from the total QM/MM energy, and adding the B3LYP energy. This gives a surface with the energetics of the reaction described at a reliable level, relatively insensitive to geometry, also including the essential effects of the protein environment on the reaction.

After energy correction, the energy profiles for FAAH carbamoylation by URB524, URB694 and URB618 indicate that three carbamates undergo similar carbamoylation mechanisms, where TI formation is the rate-limiting step (Figure 5.6). This finding reinforces the conclusions drawn at lower level of theory, and it also suggests that these results are not method-dependent.

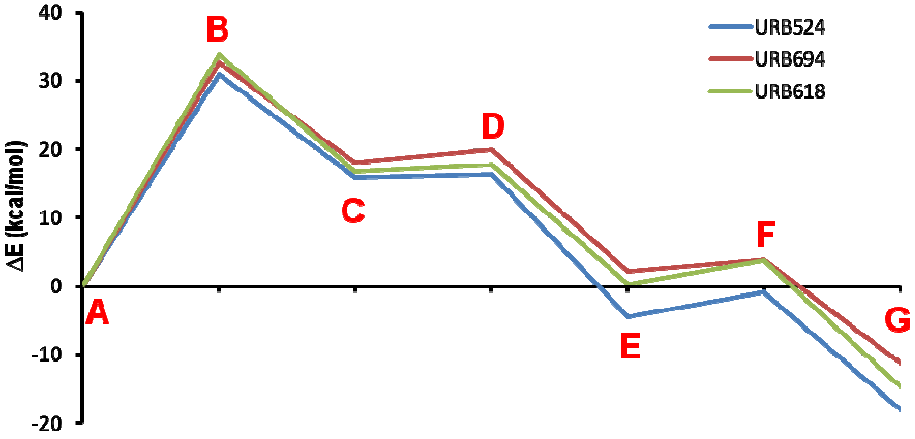

Figure 5.6 B3LYP/6-31+G(d)//PM3-CHARMM22 energy profiles for carbamoylation of Ser241 by carbamate inhibitors.

The B3LYP/6-31+G(d)//PM3-CHARMM22 barriers for this crucial step resulted similar for the three inhibitors (31.5 kcal mol^{-1} for URB524, 32.7 kcal mol^{-1} for URB694 and 33.6 kcal mol^{-1} for URB618), despite their different chemical structure and reactivity. Interestingly, the main TS is characterized by deprotonation of Ser241, similarly to what observed at PM3-CHARMM22 level of theory.

The TI (**C**) is a transient configuration along the carbamoylation pathway, significantly less stable than the reactants (**A**). It lies 18.0 kcal mol^{-1} above the reactants for the p-OH analogue, compared to 16.8 kcal mol^{-1} for the p-NH_2 variant,

and 15.8 kcal mol^{-1} for URB524. Expulsion of the biphenate leaving group gives carbamoylated Ser241 (**E**) overcoming small energy barriers (lower than 2 kcal mol^{-1}), suggesting that formation and collapse of TI are highly concerted. However, protonation of the leaving group is required to conclude the catalytic cycle. Energy barriers for this step are small, ~3 kcal mol^{-1} for URB524, ~2 kcal mol^{-1} for URB694 and ~3 kcal mol^{-1} for URB618, with respect to E. The final product (**G**) is the most stable configuration of the pathway. Configuration **G** is 17 kcal mol^{-1} lower in energy than **A** for URB524, and by 13 and 11 kcal mol^{-1} for URB618 and URB694, respectively. All the covalently inhibited complexes are predicted to be relatively very stable.

DTSS calculation

DTSS calculations were performed for FAAH carbamoylation in the presence of the three inhibitors for residues at the active site that are potentially important for catalysis. These calculations indicate that the identified TS stuctures for Ser241 carbamoylation are greatly stabilized by the enzyme, when compared to the corresponding Michaelis complexes. This stabilization is mainly related to residues involved in the proton transfer from Ser241 to Lys142, through Ser217. A FAAH active-site model, consisting of 16 residues and two water molecules (see methods), provides comparable DTSS for the three inhibitors (−25.1, −24.0, and −25.4 kcal mol^{-1} for URB524, URB694, and URB618, respectively).

The highest contribution to the lowering of activation barriers comes from Thr236 (~ −7.5 kcal mol^{-1}, see Figure 7). This residue accepts a H-bond from Lys142, possibly favoring its protonation, critical for Ser241 activation. Moreover, Ser218 (which also accepts a H-bond from Lys142), Ile238, Gly239 and Gly240 (which are the fundamental element of the oxyanion hole) contribute comparable amounts of DTSS for the three inhibitors. Other amino acids show negligible contributions, with the exception of Asp237, which shows a small destabilizing effect on the TS of URB618. The water molecule (Wat627), involved in the recognition of p-OH and p-NH_2 substituents, has negligible contribution to TS stabilization (DTSS of −0.4 and −0.7 kcal mol^{-1} for URB694 and URB618, respectively).

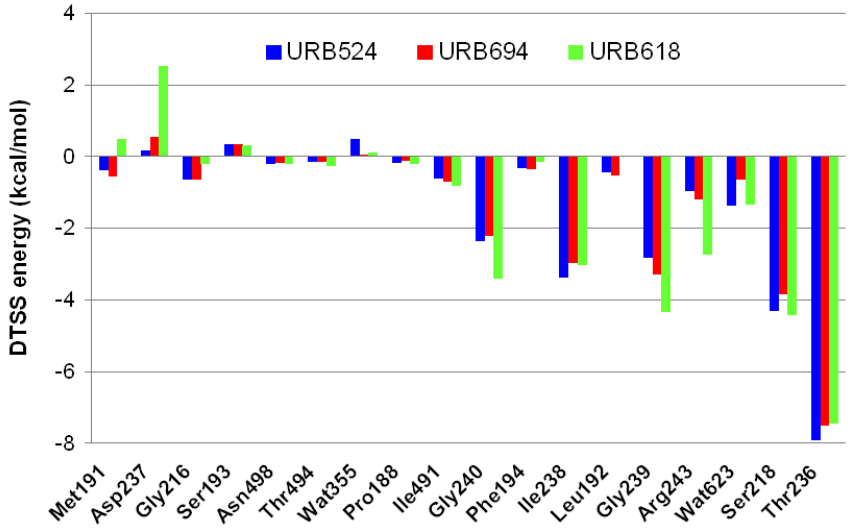

Figure 5.7 DTSS energies at the MP2/6-31G(d) level of theory, for the carbamoylation of Ser241 with the three carbamate inhibitors.

Conclusions

The QM/MM results presented here provide a mechanistic explanation for the lack of correlation between the in-vitro inhibitor potency and the reactivity of these carbamates. In spite of the different intrinsic reactivity of URB524 and its para-substituted derivatives, negligible effects on activation barrier for Ser241 carbamoylation are observed. The three compounds undergo the same reaction mechanism, with similar energy barrier heights, sincethe rate-limiting step for FAAH carbamoylation is deprotonation of Ser241, instead of nucleophilic attack.

Since intrinsic reactivity of compounds belonging to this class of inhibitors does not affect the potency on FAAH, while it strongly affects their chemical and biological stability, these QM/MM calculations indicates that reduction of the carbamate reactivity represents a good strategy for the design of new inhibitors with improved pharmaceutical properties, e.g. improved in vivo potency and better selectivity versus putative off-targets.

Finally, this QM/MM protocol has been demonstrated to be a reliable procedure for quantitative estimation of the contribution of covalent binding to *in vitro* potency, providing a useful tool for in-silico activity predictions of new compounds.

[72] Zhang, D.; Saraf, A.; Kolasa, T.; Bhatia, P.; Zheng, G. Z.; Patel, M.; Lannoye, G. S.; Richardson, P.; Stewart, A.; Rogers, J. C.; Brioni, J. D.; Surowy, C. S. Fatty acid amide hydrolase inhibitors display broad selectivity and inhibit multiple carboxylesterases as off-targets. Neuropharmacology 2007, 52, 1095-105.

[73] Piomelli, D.; Tarzia, G.; Duranti, A.; Tontini, A.; Mor, M.; Compton, T. R.; Dasse, O.; Monaghan, E. P.; Parrott, J. a; Putman, D. Pharmacological profile of the selective FAAH inhibitor KDS-4103 (URB597). CNS drug reviews 2006, 12, 21-38.

[74] Tarzia, G.; Duranti, A.; Gatti, G.; Piersanti, G.; Tontini, A.; Rivara, S.; Lodola, A.; Plazzi, P. V.; Mor, M.; Kathuria, S.; Piomelli, D. Synthesis and structure-activity relationships of FAAH inhibitors: cyclohexylcarbamic acid biphenyl esters with chemical modulation at the proximal phenyl ring. ChemMedChem 2006, 1, 130-9.

[75] Vacondio, F.; Silva, C.; Lodola, A.; Fioni, A.; Rivara, S.; Duranti, A.; Tontini, A.; Sanchini, S.; Clapper, J. R.; Piomelli, D.; Mor, M.; Tarzia, G. Structure-property relationships of a class of carbamate-based fatty acid amide hydrolase (FAAH) inhibitors: chemical and biological stability. ChemMedChem 2009, 4, 1495-504.

[76] Clapper, J. R.; Vacondio, F.; King, A. R.; Duranti, A.; Tontini, A.; Silva, C.; Sanchini, S.; Tarzia, G.; Mor, M.; Piomelli, D. A second generation of carbamate-based fatty acid amide hydrolase inhibitors with improved activity in vivo. ChemMedChem 2009, 4, 1505-13.

[77] Sokalski, A. W. The physical nature of catalytic activity due to the molecular environment in terms of intermolecular interaction theory: derivation of simplified models. Journal of molecular catalysis 1985, 30, 395-410.

[78] Szefczyk, B.; Mulholland, A. J.; Ranaghan, K. E.; Sokalski, W. A. Differential transition-state stabilization in enzyme catalysis: quantum chemical analysis of interactions in the chorismate mutase reaction and prediction of the optimal catalytic field. Journal of the American Chemical Society 2004, 126, 16148-59.

[79] Lodola, A.; Mor, M.; Rivara, S.; Christov, C.; Tarzia, G.; Piomelli, D.; Mulholland, A. J. Identification of productive inhibitor binding orientation in fatty acid amide hydrolase (FAAH) by QM/MM mechanistic modelling. Chemical communications 2008, 214-6.

[80] Mor, M.; Lodola, A.; Rivara, S.; Vacondio, F.; Duranti, A.; Tontini, A.; Sanchini, S.; Piersanti, G.; Clapper, J. R.; King, A. R.; Tarzia, G.; Piomelli, D. Synthesis and quantitative structure-activity relationship of fatty acid amide hydrolase inhibitors: modulation at the N-portion of biphenyl-3-yl alkylcarbamates. Journal of medicinal chemistry 2008, 51, 3487-98.

[81] Mileni, M.; Kamtekar, S.; Wood, D. C.; Benson, T. E.; Cravatt, B. F.; Stevens, R. C. Crystal structure of fatty acid amide hydrolase bound to the carbamate inhibitor URB597: discovery of a deacylating water molecule and insight into enzyme inactivation. Journal of molecular biology 2010, 400, 743–754.

[82] Szarek, P.; Dyguda-Kazimierowicz, E.; Tachibana, A.; Sokalski, W. A. Physical nature of intermolecular interactions within cAMP-dependent protein kinase active site: differential transition state stabilization in phosphoryl transfer reaction. The journal of physical chemistry. B 2008, 112, 11819-26.

[83] Lodola, A.; Mor, M.; Sirirak, J.; Mulholland, A. J. Insights into the mechanism and inhibition of fatty acid amide hydrolase from quantum mechanics/molecular mechanics (QM/MM) modelling. Biochemical Society transactions 2009, 37, 363-7.

[84] Mulholland, A. J.; Lyne, P. D.; Karplus, M. Ab Initio QM/MM Study of the Citrate Synthase Mechanism. A Low-Barrier Hydrogen Bond Is not Involved. Journal of the American Chemical Society 2000, 122, 534-535.

6. Application of a SCC-DFTB QM/MM approach to the investigation of the catalytic mechanism of Fatty Acid Amide Hydrolase

Mechanistic simulation of enzyme-catalyzed reactions within a realistic environment (composed by a full protein structure and solvent molecules) are made possible by the application of the hybrid quantum mechanics/molecular mechanics (QM/MM) method. As described previously in the QM/MM framework, the simulation system (e.g. the enzyme-substrate complex) is divided into two linked regions: i) the core region which contains the reacting fragments and it is described by quantum mechanics; ii) the surrounding protein, represented by classical molecular mechanics force field[85,86]. In this way, it is possible to treat systems composed by thousand of atoms and to describe the potential energy surfaces (PESs) relevant to enzymatic chemistry[87,88].

Reliable calculations have increasingly been made possible by the development of QM/MM methods based on electron correlation approaches such as the MP2 perturbation method and coupled-cluster theory[89,90], often resulting in successful reproduction of experimental results. Unfortunately, these methods can result too heavy to allow sufficient sampling or to perform costly reaction-path calculations. On the other hand, semiempirical (SE) molecular-orbital techniques, while not suitable for all systems, allow to treat large QM regions and to perform more extensive simulations (e.g. testing alternative reaction mechanisms or exploring multiple reaction paths[91]) at the cost of limited accuracy in reproducing experimental data[92]. The most popular among these methods are based on neglect of diatomic differential overlap (NDDO) and are known with the acronyms MNDO, AM1, PM3. These methods are based on the Hartree–Fock formalism, but make several approximation substituting some differential equations with parametrized polynomials that reproduce empirical data. Density functional theory (DFT) has become popular for computational studies because of its generally good and robust performance at reasonable cost. DFT calculations are, however, significantly more expensive than semiempirical MNDO calculation.

An attractive alternative to *ab initio* and traditional semiempirical methods within the context of hybrid QM/MM simulations is represented by the self-consistent charge density functional tight binding (SCC-DFTB) method[93,94]. This is a semiempirical methodology density-functional based, which incorporates tight binding principles, that is parametrized using results based on the local density approximation (LDA). The SCC-DFTB has proved to be excellent for geometries and to perform well for many biological systems[95], and in the best cases, it performed similar to DFT calculations based on hybrid functionals[96]. Furthermore, since its implementation in widely used QM/MM packages, such as CHARMM[97] or AMBER[98], SCC-DFTB has provided results in approximate agreement with QM/MM calculations performed at higher level of theory[99]. Furthermore, since this method is parameterized on DFT calculations and not on experimental values, it is expected to provide more reliable structures for high-level corrections. Despite these encouraging results, SCC-DFTB has been used less extensively than earlier semiempirical methods for enzyme reaction modelling and thus its reliability in this field is somehow unexplored[99].

In the previous chapters, the mechanism of action[100] and inhibition[101] of fatty acid amide hydrolase (FAAH) was elucidated by means of QM/MM simulations based on PM3 hamiltonian. In literature is possible to find several deficiencies in NDDO methods, such as PM3: (i) erroneous prediction of branched chain hydrocarbons being less stable than their straight chain analogs; (ii) poor treatment of the energetics of bonds in which one or more atomic component possess lone-pair electrons; (iii) flawed energetics for molecules with multiple rings; (iv) underestimation of the stabilization energy of delocalized systems; (v) general overestimation of the energy associated with the methylene fragment, which rapidly skews heats of formation of molecules containing long alkyl chains; (vi) inaccurate description of intermolecular interactions, especially hydrogen bonding; (vii) poor treatment of conformational energetics including cis-trans isomers and rotomeric energies; (viii) incorrectly predicted molecular geometries for a number of molecules including hydrogen peroxide and cyclobutane; (ix) significant errors in proton affinities[102].

To overcome these known limits of PM3, PESs of the modelled reactions were initially built at PM3-CHARMM level and the energetic was corrected with DFT single point calculations. Although this approach has shown to give reliable results in many

cases[85], it has some explicit drawbacks: i) it is computationally demanding as hundred of single point DFT calculations are required[103] ii) it relies on the assumption that DFT methods are relatively insensitive to the quality of the geometry of the system under consideration, which may not be always the case.

The availability of a DTFB-based QM/MM potential, which may retain DFT-type accuracy at reduced computational costs, represents a tempting opportunity to improve our QM/MM model about FAAH catalytic and inhibition reactions. In order to verify the reliability of this potential on the biological system of interest, the acylation reaction of FAAH in presence of oleamide (OA) and oleoylmethyl ester (OME) substrates was investigated applying the SCC-DFTB-CHARMM potential implemented in CHARMM30b2[104]. PESs for the reactions were calculated for multiple starting structures and compared with previous calculations at PM3-CHARMM and B3LYP/6-31+G(d)//PM3-CHARMM level of theory[105]. The work here reported shows that SCC-DFTB-CHARMM significantly outperforms calculations on FAAH based on SE methods, with energetic barriers in reasonable agreement with the experimental values. More importantly, the remarkable experimental preference of FAAH in hydrolyzing OA faster that OME was satisfactorily reproduced by the SCC-DFTB-CHARMM protocol here applied.

Methods

Models Building

The cartesian coordinates of the reactants (Michaelis complexes) were taken from those used in our previous studies [100,105], which were based on the crystal structure of rat FAAH in its covalent adduct with methyl arachidonyl phosphonate[106]. The FAAH-OA and FAAH-OME complexes were firstly minimized to an energy gradient of 0.01 kcal mol^{-1} $Å^{-1}$ applying the SCC-DFTB-CHARMM27 potential and thus equilibrated by stochastic boundary molecular dynamics (SBMD)[107].

The SCC-DFTB-CHARMM27 potential was used to generate a trajectory using a time step of 0.1 ps for the integration, and a cut-off distance for non bonded interactions of 12 Å. During the simulation, all atoms further than 21 Å away from the Ser241 hydroxyl oxygen were harmonically restrained to their crystallographic

coordinates with force constants based on model average B-factors[108]. Frictional coefficients of 250 ps^{-1} for non-hydrogen protein atoms and 62 ps^{-1} on water oxygen atoms were applied on a buffer region and a deformable boundary potential was also applied for the water oxygens.

The simulation was divided into three phases: (i) a heating phase of 10 ps needed to increase the temperature from 0 to 300 K; (ii) an equilibration phase of 200 ps at 300 K; (iii) a production phase of 150 ps at 300 K.

One snapshot every 25 picoseconds of the SCC-DFTB-CHARMM27 MD production phase was considered for modelling investigation, for a total of six equally-spaced starting structures. The equilibrated structures were newly minimized and thus employed for mechanistic QM/MM calculations. Both for OA and OME, the minimum energy pathway with the lowest energy barriers was found with the Michaelis complex obtained after 75 ps of MD production phase.

Application of the QM/MM potential

The SCC-DFTB-CHARMM27 QM/MM potential was employed to model the acylation reaction of FAAH. The quantum-mechanical region includes the methylamine group of Lys142, the side chains of Ser217 and Ser241 and the butanamide fragment for OA and the butanoyl methyl ester one for OME. All the other atoms of the system were treated with the CHARMM27 MM force field[109,110]. The covalent bonds crossing the boundary between the QM and MM regions were treated by introducing four 'HQ' link atoms which are included in the QM system. Van der Waals and bonded interactions between the QM and MM region were described by MM terms, with standard CHARMM27 parameters for the QM atoms, while electrostatic interactions were treated following the coulombic interaction between the Mulliken charges of the QM atoms and the MM partial charges[97].

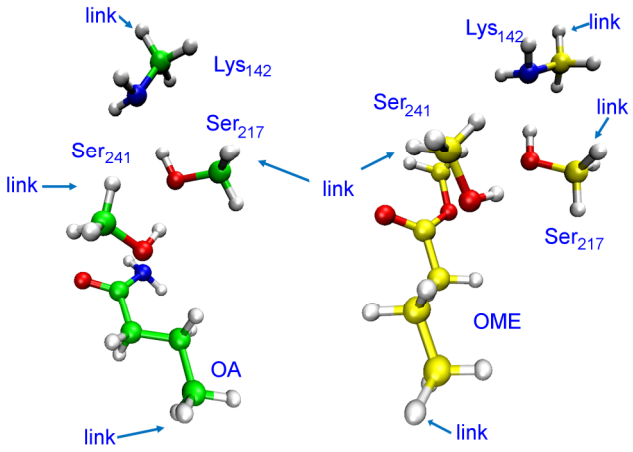

Figure 6.1 QM regions employed in the QM/MM simulations with OA (left, green carbons) and OME (right, yellow carbons).

Calculation of potential energy surfaces.

The reaction was modeled by means of adiabatic mapping approach in three main steps starting from the FAAH-OA and FAAH-OME Michaelis complexes, accordingly to Figure 6.2: (**I**) formation of the TI; (**IIa**) leaving group protonation; (**IIb**) leaving group expulsion and formation of the acylated Ser241.

Reaction coordinates were defined for every reaction step and restrained sequentially to move the system along a given reaction path, while atoms further than 14 Å from the Ser241 hydroxyl oxygen were fixed. With the exception of these constraints, all the other atoms were free to move during PES exploration. A harmonic potential with a constant of 5000 kcal mol^{-1} $Å^{-2}$ was used to restrain all the defined coordinates step-wise. The values for the restrained distances were increased continuously to force the system across the barrier of a specific reaction step. Energy minimizations of all structures were performed to a gradient tolerance of 0.01 kcal mol^{-1} $Å^{-1}$ by ABNR method. The structures of energy minima (i.e. stable structures) were determined more precisely by performing additional geometry optimizations with none of the reaction coordinates restrained. The final energy of a structure (as indicated on the potential energy surfaces, for example) was obtained by single point energy calculations where the energy contribution derived from any restraints was left out.

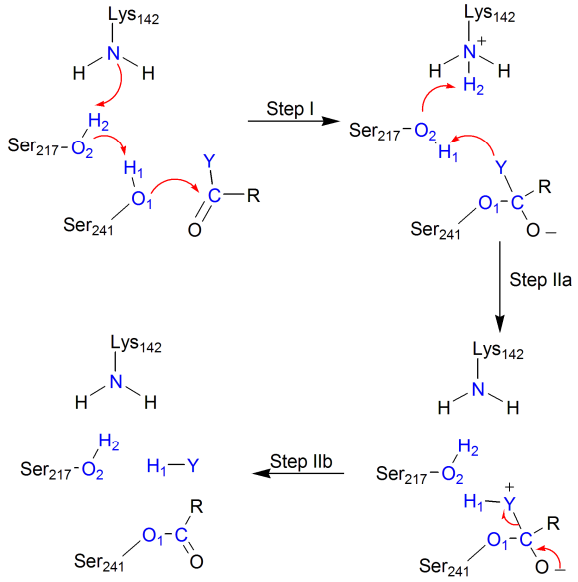

Figure 6.2 Acylation mechanism of FAAH [105] in the presence of oleamide (OA) and for oleoylmethyl ester (OME). Y is -NH_2 for OA (the label N_{am} is used for its leaving group nitrogen in the text) and -OCH_3 for OME (O_{es} is used as a label for its leaving group oxygen in the text). Labels are also consistent with the definition of the reaction coordinates employed in the calculations.

Step **I** of the acylation reaction consists of multiple events: a proton is abstracted from Ser241 and *via* the bridging residue Ser217 is transferred to the general base Lys142. Thus, the activated Ser241 attacks the carbonyl group of the substrate, leading to the formation of the TI. It was modelled by restraining the following two reaction coordinates: R_X includes proton abstraction from Ser241 by Ser217 and the nucleophilic attack by Ser241, while R_Y describes the proton transfer between Ser217 and Lys142. R_X and R_Y were increased respectively in steps of 0.15 Å and 0.1 Å till reaching the next stationary state along the PES.

$$R_X = [d(O_1, H_1) - d(O_2, H_1) - d(O_1, C)] \qquad \textit{(Eq. 6.1)}$$

$$R_Y = [d(O_2, H_2) - d(N, H_2)] \qquad \textit{(Eq. 6.2)}$$

Modelling of acylenzyme formation from the TI (Step **II**) was separated into two sub-events: protonation of the leaving group (a) and its consequent expulsion (b).

In the case of OA, step **IIa** was modelled using the following reaction coordinates: R_T defines the proton transfer from Ser217 to N_{am} of OA, while R_S the proton transfer from Lys142 back to Ser217.

$$R_T = [d(O_2, H_1) - d(N_{am}, H_1)] \qquad \textit{(Eq. 6.3)}$$

$$R_S = [d(N, H_2) - d(O_2, H_2)] \qquad \textit{(Eq. 6.4)}$$

Step **IIb** was explored by restraining R_R, describing the breaking of the bond between the carbonyl carbon and the amide nitrogen.

$$R_R = d(N_{am}, C) \qquad \textit{(Eq. 6.5)}$$

R_T, R_S and R_R were increased in steps of 0.1 Å with an harmonic potential with constant of 5000 kcal mol^{-1} Å^{-2}.

A similar approach was employed to model the second step of FAAH acylation in presence of OME, with the following differences: In the step **IIa**, protonation of the leaving group involved the alcoholic oxygen O_{es}, while in the step **IIb**, expulsion of leaving group requires the breaking of a C-O bond. The two coordinates assume this new form:

$$R_T = [d(O_2, H_1) - d(O_{es}, H_1)] \qquad \textit{(Eq. 6.6)}$$

$$R_R = d(O_{es}, C) \qquad \textit{(Eq. 6.7)}$$

Results and Discussion

The SCC-DFTB-CHARMM PESs of FAAH acylation in presence of OA is reported in Figure 3. The surface relative to the step **I** is reported on the left panel. The change in energy during Ser241 deprotonation and subsequent nucleophilic attack can be followed along R_X, while the change of the energy during the protonation of Lys142 can be observed along R_Y. The minimum energy path (MEP) connecting the Michaelis complex (A) to the tetrahedral intermediate (TI, C) on the SCC-DFTB-CHARMM surface shows the presence of a concerted process, similarly to what observed in our previous B3LYP/6-31+G(d)//PM3-CHARMM calculations. It is worth note that the SCC-DFTB-CHARMM step **I** occurs overcoming a energy barrier of 16.1 kcal mol^{-1}, that is in good agreement with the B3LYP/6-31+G(d)//PM3-CHARMM calculated one (18.0, kcal mol^{-1}), and significantly smaller than the one calculated at PM3-CHARMM level of theory (36.0 kcal mol^{-1})[100]. It is also worth note that SCC-DFTB-CHARMM PES resembles much more the B3LYP/6-31+G(d)//PM3-CHARMM surface than the PM3-CHARMM one, reported in ref 100 indicating that SCC-DFTB fairly reproduces B3LYP potential energy values.

Visual inspection of the approximate TS (B) suggests that the main event of the process is represented by Ser241 activation with proton H_1 being transferred from O_1 to O_2 (Table 6.1). Conversely, at the TS, the proton transfer involving Ser217 and Lys142 results nearly complete, (N-H_2 distance of 1.1 Å) while the nucleophilic attack is only at its begin with a O_1-C distance close to value observed in the Michaelis complex. Even though the predicted TS involves proton transfer rather than nucleophilic attack, the absence of a energetic barrier between **B** and **C** indicates that Ser241 deprotonation and nucleophilic attack are effectively concerted.

The product of step **I,** the TI, results less stable than the Michaelis complex by 11.5 kcal mol^{-1}, indicating its transient character. On the other hands, this configuration is greatly stabilized by FAAH oxyanion hole, which forms hydrogen bonds with the negatively charged oxygen of the substrate, as also reported in previous calculations[100,111]. Interestingly, a water molecule (conserved in FAAH[112]) was found to interact with the carbonyl oxygen of OA both in the TS and in TI, and assisting the stabilization of the incoming negative charge on the oxygen atom.

Visual inspection of the TI structure confirms the presence of a new bond between Ser241 O_1 and carbonyl carbon of OA (O_1-C = 1.62 Å) as well as the presence of a protonated and positively charged Lys142 (N-H_1 = 1.07 Å) at the active site. Furthermore, in the TI leaving group N_{am} atom is correctly oriented towards the hydroxyl group of Ser217 for initiating the second step of the acylation (Figure 6.3). This finding differs from what observed at PM3-CHARMM22 level, where a rearrangement of the TI due to the pyramidal inversion of N_{am} was required to start step **II** [105].

The SCC-DFTB-CHARMM27 PES relative to step **IIa** is reported in the central panel of Figure . The change in energy during protonation of the basic nitrogen of OA (N_{am}) by Ser217 can be followed along R_T, while the change of the energy during the transfer of H_2 from Lys142 to Ser217 can be observed along R_S. The MEP identified on the surface showed a mechanism where protonation of the basic nitrogen of OA (N_{am}) by Ser217 is nearly completed, before H_2 transfer from Lys142 to Ser217 has begun. However, as this second event takes place with no barrier, the double proton transfer of step **IIa** can be considered a concerted process. These events lead to configuration **E** overcoming a barrier of 18.8 kcal mol^{-1} (relative to the Michaelis complex), ~3 kcal mol^{-1} higher than that calculated for the deprotonation of Ser241.

Visual inspection of the approximate TS structure **E** shows H_1 being transferred from O_2 to N_{am}, (N_{am}-H_1 = 1.19 Å; O_2-H_1 = 1.37 Å), suggesting that leaving group protonation is the rate-liming event for FAAH acylation. The activation barrier of 18.8 kcal mol^{-1} results in good agreement with the experimentally deduced one of 16.0 kcal mol^{-1} and it is significantly smaller than the calculated one at PM3-CHARMM level (40.0 kcal mol^{-1} [105]).

As a consequence of the protonation of N_{am}, configuration **E** results characterized by a slightly longer C-N_{am} bond and by a shorter O_1-C than what observed in the TI (Table 6.1). This finding suggests that **E** is ready for being converted in the acylenzyme ester **G**.

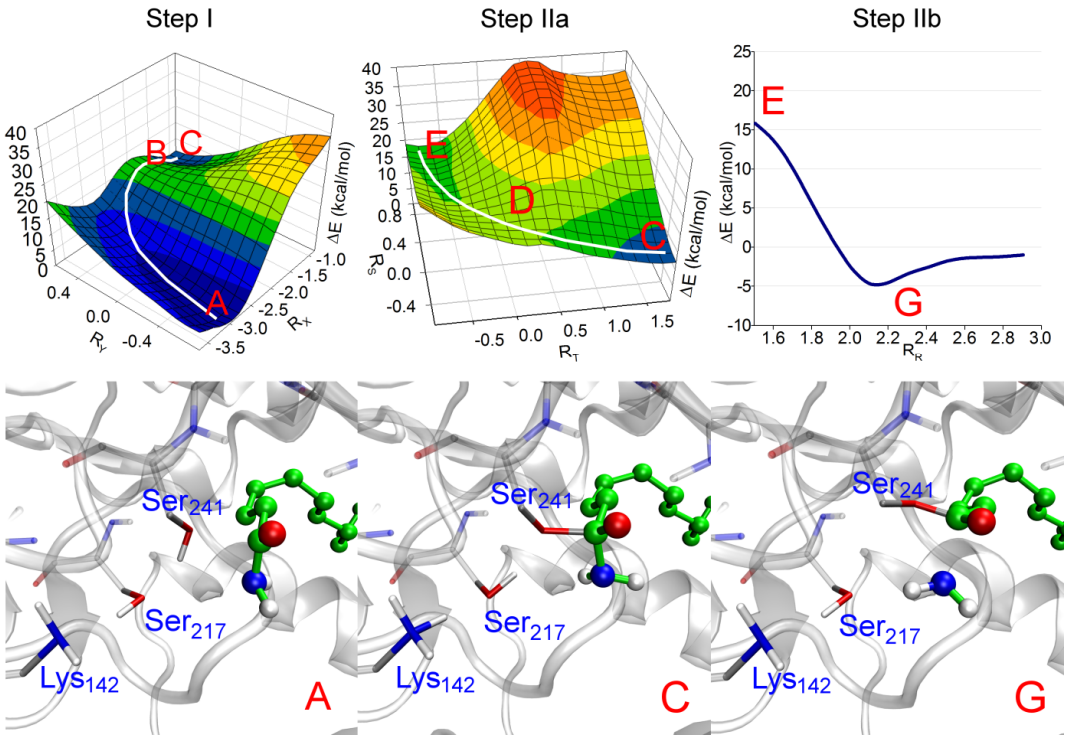

Figure 6.3 SCC-DFTB-CHARMM27 QM/MM PES for FAAH acylation in presence of OA. The geometry of relevant configurations are also reported: A (Michaelis complex), C (tetrahedral intermediate), G (acylenzyme).

Step **IIb** occurs with no barrier (Figure 6.3 SCC-DFTB-CHARMM27 QM/MM PES for FAAH acylation in presence of OA. The geometry of relevant configurations are also reported: A (Michaelis complex), C (tetrahedral intermediate), G (acylenzyme). Figure 6.3, upper right panel), leading to the formation of the acylenzyme **G**. Protonation and the expulsion of the leaving group (i.e., neutral ammonia) are thus

highly concerted. The acylenzyme is characterized by a planar carbonyl bond and by a short O_1-C distance (1.38 Å), while the ammonia group remains quite close to Ser217 even after its expulsion (Figure 6.3, lower right panel). Finally **G** is calculated to be more stable than the Michaelis complex by 4.7 kcal/mol, indicating the presence of an exothermic overall profile.

STATE	O1•••C		O1•••H1		O2•••H1		O2•••H2		N•••H2		C•••Y		Y•••H1	
	OA	OME	OA	OME	OA	OME	OA	OME	OA	OME	OA	OME	OA	OME
A	2.18	2.13	0.99	1.01	1.76	1.73	1.00	1.01	1.97	1.91	1.39	1.39	2.45	2.35
B	2.04	1.87	1.41	1.54	1.25	1.16	1.63	1.45	1.09	1.15	1.41	1.46	2.96	2.45
C	1.62	1.59	1.66	1.72	1.03	1.03	1.71	1.68	1.07	1.07	1.46	1.50	2.81	2.21
D	1.49	1.49	2.48	2.26	1.37	1.50	1.40	1.14	1.17	1.44	1.50	1.51	1.19	1.06
E	1.49	1.48	2.35	2.22	1.70	1.75	1.01	1.01	1.88	1.91	1.51	1.51	1.07	1.01
G	1.38	1.35	2.60	2.49	1.90	1.82	1.01	1.01	1.89	1.89	2.11	2.41	1.04	1.00

Table 6.1 Distances between reactant atoms (Å). Atom labels are consistent with Figure 6.2

The acylation mechanism of FAAH in presence of OME substrate was modelled applying the same procedure described for OA. The SCC-DFTB-CHARMM PESs for FAAH acylation by OME are reported in Figure 6.4. The PES for Step **I,** explored applying the reaction coordinates R_X and R_Y, is reported on the left panel of the same figure. The MEP connecting the Michaelis complex (**A**) and the TI (**C**) is similar to that one observed for OA. The energetic barrier required for the formation of the TI (**C**) results of 18.9 kcal mol^{-1}, relative to the substrate complex **A**, significantly lower than the one calculated at PM3-CHARMM level (44 kcal mol^{-1} [105]).

The examination of the approximate TS geometry (**B**) shows Ser241 deprotonation as the crucial event of the first step of acylation. However the proton transfer of H_1 to Ser217 O_2 is less advanced than for OA (Table 6.1). Ser241 deprotonation and the subsequent nucleophilic attack results tightly coupled as no barrier is found between **B** and **C**. Although stabilized by the oxyanion hole, the TI (**C**) results less stable than the Michaelis complex of 12.5 kcal mol^{-1}. Differently to what observed for OA, in

configurations **B** and **C** no water molecule is found to interact with the carbonyl oxygen of OME. Visual inspection of FAAH-OME and FAAH-OA TI structures suggests that the methoxy group of OME actually displaces this important water molecule. The lack of an additional hydrogen bond can thus account for the slightly higher barrier found in the first step of FAAH acylation by OME.

The subsequent formation of the acylenzyme from the TI is again a complex multiproton-transfer process. The SCC-DFTB-CHARMM27 PES relative to step **IIa** is reported in the central panel of Figure .

The highest energy point along the MEP (**D**) is the TS for protonation of the leaving group oxygen (O_{es}). This process leads to **E** overcoming a barrier of 20.8 kcal mol^{-1} relative to the substrate complex **A**. Calculation at PM3-CHARMM22 level predicted for step IIa an energy barrier of 47.0 kcal mol^{-1} [105].

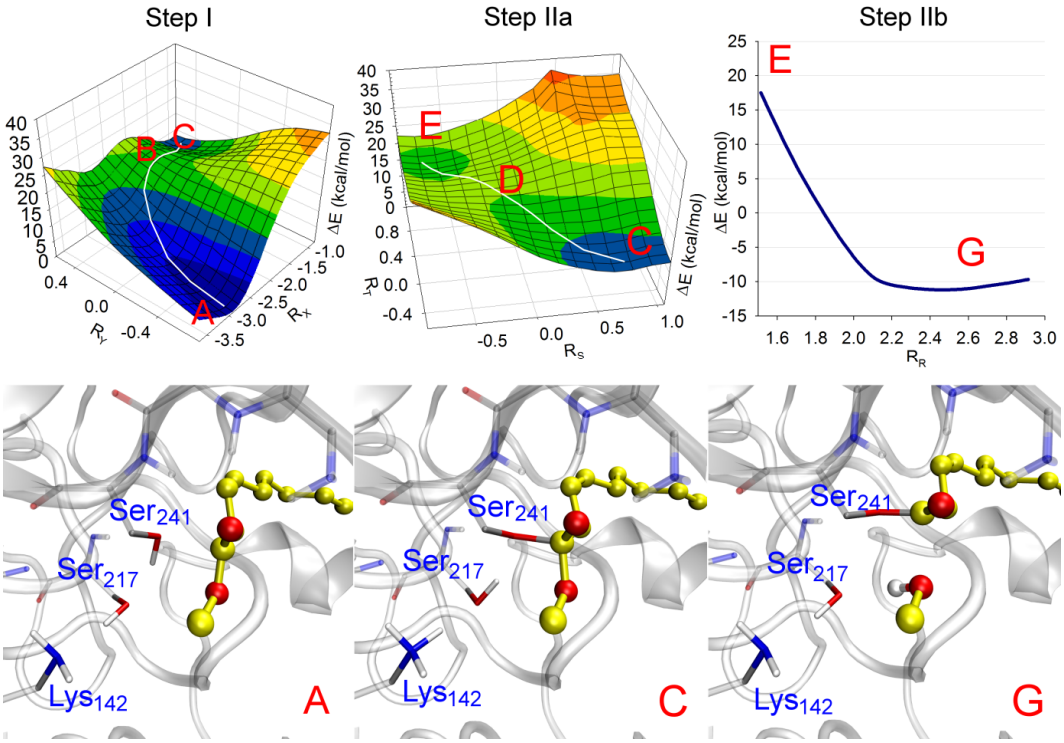

Figure 6.4 SCC-DFTB-CHARMM27 QM/MM PES for FAAH acylation in presence of OME. The geometry relevant configurations are also reported: A (Michaelis complex), C (tetrahedral intermediate), G (acylenzyme).

The subsequent expulsion of methanol happened spontaneously as no effective barrier divides **E** from the acylenzyme **G**. Also in this case, **G** is calculated to be more

stable than the Michaelis complex (by 11.0 kcal mol^{-1}), indicating the presence of an exothermic overall profile.

Figure 6.5 summarizes the potential energy profiles for acylation of FAAH in presence OA and OME at the SCC-DFTB-CHARMM27 level. The calculations indicate that these substrates follow a similar mechanism of FAAH acylation, with TI collapse being the rate-limiting step of the process.

The overall calculated barrier (relative to **A**) for the amide cleavage is 18.8 kcal mol^{-1}, 2.0 kcal mol^{-1} smaller then the barrier for the ester. These findings are in agreement with kinetic investigations on OA and OME substrates: the experimental barrier for the hydrolysis of oleamide is lower by ~1 kcal/mol than that for oleoylmethyl ester. The calculations suggest that this unique preference for the amide depend both on a more efficient stabilization of the TS for the deprotonation of Ser241 and on higher basicity of the nitrogen N_{am} compared to that of oxygen O_{es} in the TI.

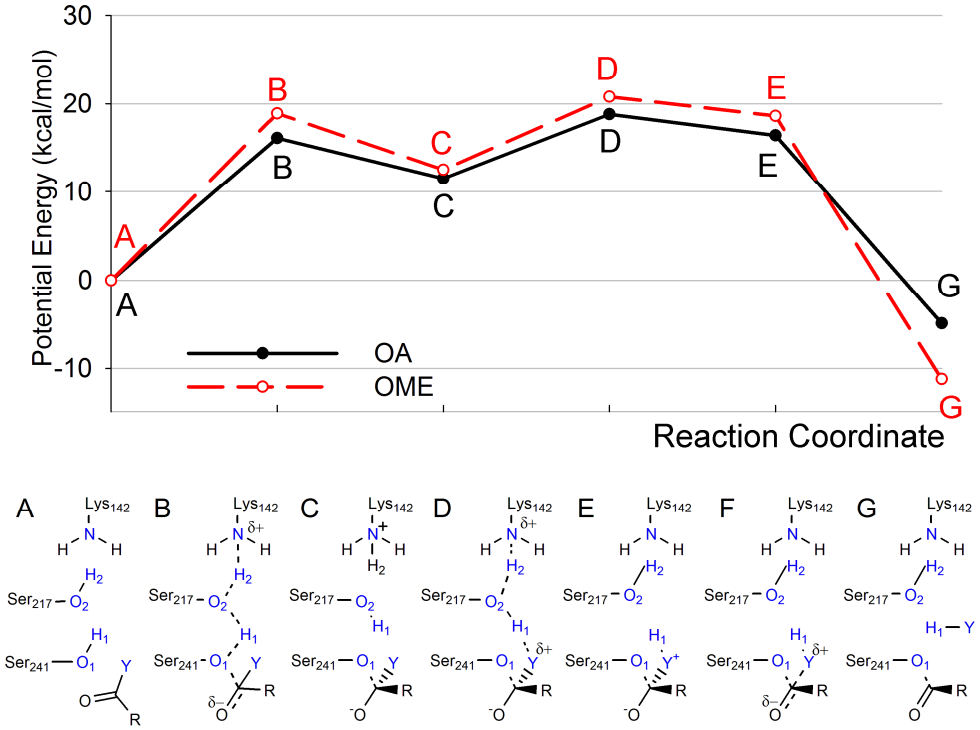

Figure 6.5 SCC-DFTB-CHARMM27 QM/MM potential energy profiles for FAAH acylation by OA (solid line) and OME (dashed line). The relevant configurations are: Michaelis complex (A), TS for TI formation (B), TI (C), TS for leaving group protonation (D), protonated TI (E), acylenzyme (G).

As QM/MM calculations based on adiabatic mapping along a reaction coordinate may hide potential pitfalls due to conformational transitions at the protein active site[113], the SCC-DFTB-CHARMM27 calculations were repeated for others starting conformations of FAAH in complex with the two considered substrates.

Five additional FAAH-OA and FAAH-OME Michaelis complexes were extracted from the MD trajectory (see Method section) and employed to build PESs for the acylation reaction. The same adiabatic mapping protocol described above was employed to drive the systems from the reactants to the products. Although PESs and the relative positions of the stationary points were not affected by the geometry of the starting points, moderate differences were observed in the energy of key stationary points.

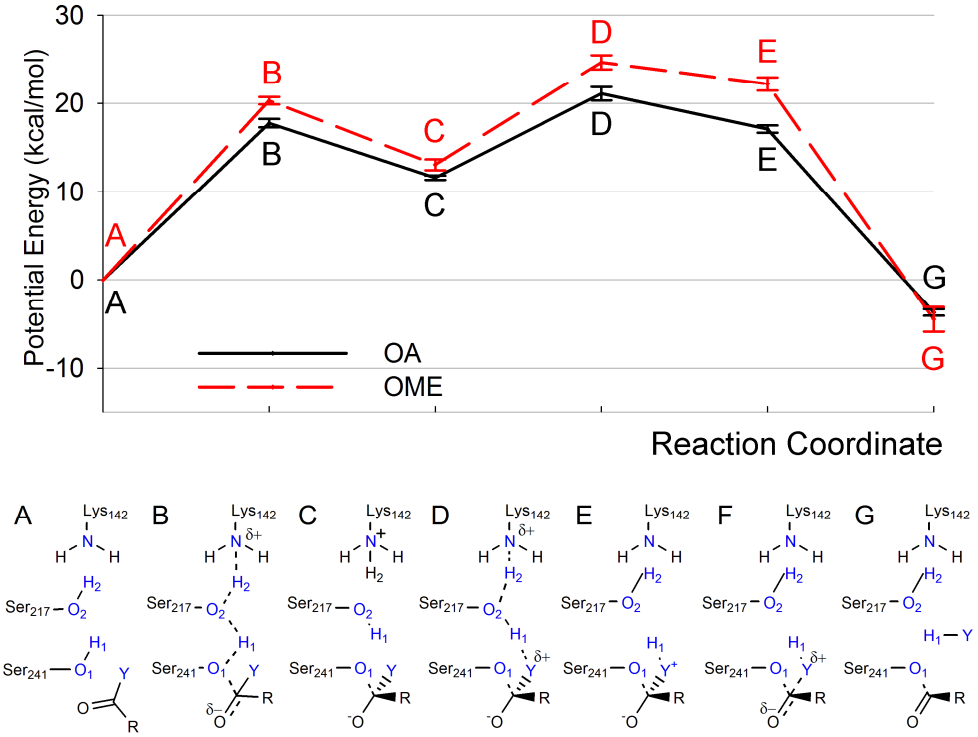

Figure 6.6 SCC-DFTB-CHARMM27 QM/MM potential energy profiles for FAAH acylation by OA (solid line) and OME (dashed line). The relevant configurations are: Michaelis complex (A), TS for TI formation (B), TI (C), TS for leaving group protonation (D), protonated TI (E), acylenzyme (G). Potential energy values are reported as mean value ± SEM (kcal mol^{-1}) of six independent simulations of the acylation reactions.

The results of these simulations are summarized in the potential energy profiles reported in Figure 6.6, where energy values of intermediates, TSs and products are reported as mean values ± standard errors of the mean (SEM). The energy profiles

are consistent with those reported in Figure 6.5, confirming that TI collapse controls the reaction-rate of FAAH acylation both for OA and OME. The key energy barrier for OA acylation results lower than that one for OME also when multiple starting conformations are considered, suggesting that a difference of 2-3 kcal mol^{-1} can be considered significant at this level of theory.

For OA, the activation barriers of the main TS (configuration **D)** can significantly changes among the six simulations, with an absolute range of variation of 4.6 kcal mol^{-1} (calculated as the difference between the highest and lowest E_{att} obtained). This is also the case for OME, with an absolute range of variation of 5.6 kcal mol^{-1} (for configuration **D**).

Conclusions

To improve the applicability of QM/MM methods to enzyme-catalyzed reaction, it is necessary to improve their accuracy at a reasonable computational cost. As QM/MM approaches based on SCC-DFTB theory seem to meet this requirement, we evaluated the performance of a SCC-DFTB-CHARMM27 method by modelling the mechanism of the previously-explored acylation of FAAH in presence of OA and OME substrates.

The exploration of the PESs for FAAH acylation indicates that the collapse of the tetrahedral intermediate is the rate-limiting step of the reaction for both OA and OME substrates, with calculated barriers of 18.8 and 20.8 kcal mol^{-1}, in reasonable agreement with the experimentally deduced ones of 16.0 and 17.0 kcal mol^{-1}. It should be stressed that the PESs here obtained do not include zero point energy, nor the influence of hydrogen-tunnelling effects, that may lower the calculated barriers by few kcal mol^{-1} [114]. Regardless of the possible role played by quantum effects in FAAH catalysis, the SCC-DFTB-CHARMM27 activation barriers resulted significantly lower than the ones calculated at PM3-CHARMM[100,105] and PDDG/PM3-OPLS[111] levels, previously reported in literature.

The present calculations show that collapse of the TI follows a concerted reaction mechanism, where Lys142 and Ser217 cooperate in the protonation of the leaving group heteroatom (nitrogen for OA, oxygen for OME). Protonation of the leaving

group is identified as the key event of acylation for both OA and OME, a finding that provides a theoretical explanation for the remarkable ability of FAAH in hydrolyzing amides faster than esters.

Taken together, these findings indicates that SCC-DFTB-CHARMM27 calculations can provide reliable results for enzyme catalysis, particularly for FAAH. Future mechanistic investigations on this and similar enzymes may thus benefit of the present validation study.

[85] Cavalli A, Carloni P, Recanatini M (2006) Target-related applications of first principles quantum chemical methods in drug design. Chem Rev 106:3497-3519.

[86] Field MJ, Bash PA, Karplus M (1990) A combined quantum mechanical and molecular mechanical potential for molecular dynamics simulations. J Comput Chem 11:700-733.

[87] Warshel A (2003) Computer simulations of enzyme catalysis: methods, progress, and insights. Annu Rev Biophys Biomol Struct 32:425-443.

[88] Senn HM, Thiel W (2009) QM/MM methods for biomolecular systems. Angew Chem Int Ed Engl. 48:1198-1229.

[89] Claeyssens, F., Harvey, J.N., Manby, F.R., Mata, R.A., Mulholland, A.J., Ranaghan, K.E., Schütz, M., Thiel, S., Thiel, W. and Werner, H.-J. (2006) High accuracy computation of reaction barriers in enzymes. Angewandte Chemie Intl. Edn. **45**, 6856-6859

[90] Mulholland, A.J. (2007) Chemical accuracy in QM/MM calculations on enzyme-catalysed reactions, Chemistry Central Journal. **1**, 1-19.

[91] Lodola A, Sirirak J, Fey N, Rivara S, Mor M, Mulholland AJ (2010) Structural Fluctuations in Enzyme-Catalyzed Reactions: Determinants of Reactivity in Fatty Acid Amide Hydrolase from Multivariate Statistical Analysis of Quantum Mechanics/Molecular Mechanics Paths. J Chem Theory Comput 6:2948–2960.

[92] Ridder L, Mulholland AJ (2003) Modeling biotransformation reactions by combined quantum mechanical/molecular mechanical approaches: from structure to activity. Curr Top Med Chem 3: 1241-1256.

[93] Elstner M, Porezag D, Jungnickel G, Elsner J, Haugk M, Frauenheim T, Suhai S, Seifert G (1998) Self-consistent-charge density-functional tight-binding method for simulations of complex materials properties. Phys Rev B 58:7260-7268.

[94] Otte N, Scholten M, Thiel W (2007) Looking at self-consistent-charge density functional tight binding from a semiempirical perspective. J Phys Chem A 111:5751-5755.

[95] Elstner M (2006) The SCC-DFTB method and its application to biological systems. Theor Chem Acc 116:316-325.

[96] Xu D, Guo H, Cui Q (2007) Antibiotic Binding to Dizinc β-Lactamase L1 from Stenotrophomonas maltophilia: SCC-DFTB/CHARMM and DFT Studies. J Phys Chem A 111:5630-5636.

[97] Cui Q, Elstner M, Kaxiras E, Frauenheim T, Karplus M (2001) A QM/MM Implementation of the Self-Consistent Charge Density Functional Tight Binding (SCC-DFTB). Method. J Phys Chem B 105:569-585.

[98] Seabra G, Walker RC, Elstner M, Case DA, Roitberg AE (2007) Implementation of the SCC-DFTB method for hybrid QM/MM simulations within the amber molecular dynamics package. J Phys Chem A 26:5655-5664.

[99] Riccardi D, Schaefer P, Yang Y, Yu H, Ghosh N, Prat-Resina X, König P, Li G, Xu D, Guo H, Elstner M, Cui Q (2006) Development of effective quantum mechanical/molecular mechanical (QM/MM) methods for complex biological processes. J Phys Chem B. 110:6458-6469.

[100] Lodola A, Mor M, Hermann JC, Tarzia G, Piomelli D, Mulholland AJ (2005) QM/MM modelling of oleamide hydrolysis in fatty acid amide hydrolase (FAAH) reveals a new mechanism of nucleophile activation. Chem Commun 35: 4399-4401.

[101] Lodola A, Mor M, Rivara S, Christov C, Tarzia G, Piomelli D, Mulholland AJ (2008) Identification of productive inhibitor binding orientation in fatty acid amide hydrolase (FAAH) by QM/MM mechanistic modelling. Chem Commun 2:214-216.

[102] Repasky, M. P.; Chandrasekhar, J.; Jorgensen, W. L. PDDG/PM3 and PDDG/MNDO: improved semiempirical methods. Journal of computational chemistry 2002, 23, 1601-22.

[103] Lodola A, Mor M, Zurek J, Tarzia G, Piomelli D, Harvey JN, Mulholland AJ (2007) Conformational effects in enzyme catalysis: reaction via a high energy conformation in fatty acid amide hydrolase. Biophys J 92:L20-L22

[104] Brooks BR, Bruccoleri RE, Olafson BD, States DJ, Swaminathan S, Karplus M. (1983) CHARMM: A program for macromolecular energy, minimization, and dynamics calculations. J Comput Chem 4:187–217.

[105] Lodola A, Mor M, Sirirak J, Mulholland AJ (2009) Insights into the mechanism and inhibition of fatty acid amide hydrolase from quantum mechanics/molecular mechanics (QM/MM) modelling. Biochem Soc Trans 37(Pt 2):363-367.

[106] Bracey MH, Hanson MA, Masuda KR, Stevens RC, Cravatt BF (2002) Structural adaptation in a membrane enzyme that terminates endocannabinoid signaling. Science 298:1793-1796.

[107] Brooks CL, Karplus M (1989). Solvent effects on protein motion and protein effects on solvent motion. Dynamics of the active site region of lysozyme J Mol. Biol. 208: 159-181

[108] Mulholland AJ, Richards WG (1997) Acetyl-CoA enolization in citrate synthase: a quantum mechanical/molecular mechanical (QM/MM) study. Proteins 27:9-25.

[109] MacKerell AD Jr, Bashford D, Bellott M, Dunbrack RL Jr, Evanseck JD, Field MJ, Fischer S, Gao J, Guo H, Ha S, Joseph-McCarthy D, Kuchnir L, Kuczera K, Lau FTK, Mattos C, Michnick S, Ngo T, Nguyen DT, Prodhom B, Reiher WE III, Roux B, Schlenkrich M, Smith JC, Stote R, Straub J, Watanabe M, Wiorkiewicz-Kuczera J, Yin D, Karplus M (1998) All-atom empirical potential for molecular modeling and dynamics Studies of proteins. J Phys Chem B 102:3586–3616.

[110] Yin D, MacKerell AD Jr (1998) Combined Ab initio/Empirical Approach for the Optimization of Lennard-Jones Parameters. J Comput Chem 19: 334-338.

[111] Tubert-Brohman I, Acevedo O, Jorgensen WL (2006) Elucidation of hydrolysis mechanisms for fatty acid amide hydrolase and its Lys142Ala variant via QM/MM simulations. J Am Chem Soc 128:16904-16913.

[112] Mileni M, Garfunkle J., Ezzili C, Kimball FS, Cravatt BF, Stevens RC, Boger DL (2010). X-ray Crystallographic analysis of α-ketoheterocycle inhibitors bound to a humanized variant of fatty acid amide hydrolase J Med Chem 53:230-240

[113] Klähn M, Braun-Sand S, Rosta E, Warshel A (2005) On possible pitfalls in *ab initio* quantum mechanics/molecular mechanics minimization approaches for studies of enzymatic reactions. J Phys Chem B 109:15645-15650.

[114] Garcia-Viloca M, Gao J, Karplus M, Truhlar DG (2005) How Enzymes Work: Analysis by Modern Rate Theory and Computer Simulations. Science 303:186-195.

7. Insights into the covalent mechanism of FAAH inhibitors

As discussed in the previous chapters, FAAH possesses a unique catalytic triad consisting of two serine residues and one lysine residue, that is responsible for its ability to cleave amides and esters at similar rates.[115] The catalytic mechanism of FAAH has been widely investigated with both experimental[116] and computational methods.[117] These investigations, mainly performed with 9Z-octadecenamide (oleamide, OAE, 1) as a substrate, showed that the catalytic process is initiated by the activation of the Ser241 nucleophile by a cooperative action of Ser217 and Lys142.[116,117] Then, the Ser241 nucleophile anion attacks the carbonyl group of the substrate, leading to the formation of a tetrahedral intermediate (TI). The reaction proceeds through the protonation of the leaving group, again by a combined action of Lys142 and Ser217, which triggers its departure and leads to the formation of an acyl-enzyme intermediate. Lys142 is a key element of this mechanism, as emphasized by the identification of a novel FAAH variant, which lacks amidase activity due to a structural perturbation in the proximity of this residue.[118]

The hydrolysis of acylated Ser241 is a necessary event for the regeneration of a catalytically competent FAAH form. The recent crystallization of FAAH carbamoylated by different covalent inhibitors,[119] allowed to identify a water molecule that may participate in the hydrolysis of carbamoylated and acylated Ser241, called "deacylating water molecule". This water molecule (W1) occupies a conserved position in different crystal structures, it is involved in a complex hydrogen-bond network with the catalytic triad, and it is well positioned to perform a nucleophilic attack on Ser 241.[119] The mechanism proposed by Mileni *et al.* for FAAH deacylation resembles that of acylation (Figure 7.1A). After deprotonation performed by Lys142 and Ser217, W1 is supposed to attack the acylating carbon generating a novel TI (Figure 7.1A). This intermediate is expected to rapidly collapse, triggered by a protonation reaction performed by Lys142 and Ser217, leading to the expulsion of Ser241 hydroxyl and thus restoring a functional enzyme.

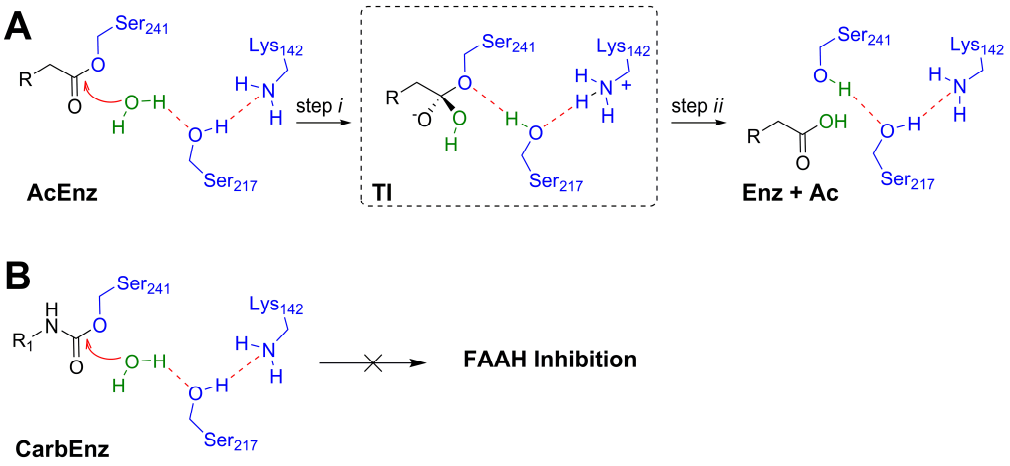

Figure 7.1 Mechanism of hydrolysis of acylated- (A) and carbamoylated-FAAH (B). The water molecule depicted in green corresponds to the deacylating water molecule W1 identified in the FAAH-URB597 crystal structure.[119]

In the recent years, the search for selective and potent inhibitors of FAAH has been the subject of an intense medicinal chemistry effort.[120] Many promising inhibitors identified so far are covalent modifiers of the enzyme such as *O*-aryl carbamates and the tertiary ureas (Figure 7.2). *O*-aryl carbamates, including the reference compound cyclohexylcarbamic acid 3′-carbamoylbiphenyl-3-yl ester (URB597, 2)[121,122] inhibit FAAH through carbamoylation of Ser241,[123] following a mechanism where Lys142 works as a base and as an acid in distinct steps of the catalytic process.[124,125] X-ray crystallography and mass spectrometry experiments have recently shown that also tertiary ureas, including the piperidinyl derivative PF-750[126] or the piperazinyl one, N-phenyl-4-(3-phenyl-1,2,4-thiadiazol-5-yl)-1-piperazine-carboxamide (JNJ1661010, 3),[127] inhibit FAAH through carbamoylation of Ser241. Indeed, the aniline moiety of these compounds served as a leaving group during catalysis, with the piperidine- or piperazine-1-carboxylic acid fragment forming a tertiary carbamate with Ser241.[128]

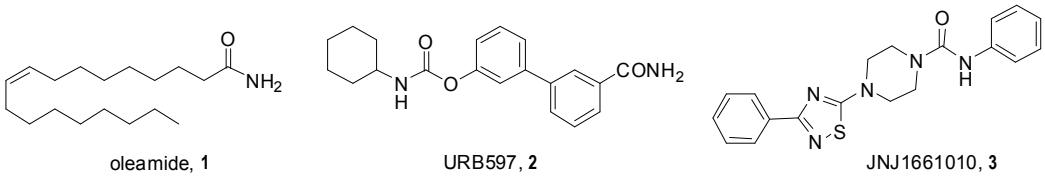

Figure 7.2 Structures of the FAAH substrate oleamide and of covalent inhibitors (URB597, JNJ1661010) employed in this study.

Generally, carbamoylating compounds block the catalytic activity of serine hydrolases by trapping the nucleophile residue of the enzyme within an acylenzyme-like intermediate (a carbamate) that is resistant to further hydrolysis (Figure 7.1B). In other words, the structure of the carbamoylated enzyme is such that regeneration of the enzyme, by its further reaction with nucleophiles, becomes a slow process, leading to effective inhibition.[129]

Recently, scientists at Johnson&Johnson have pointed out that, in the case of FAAH, the ability of the carbamoylated enzyme to recover activity depends on the chemical structure of the inhibitor.[127] Indeed, while the adduct between FAAH and compound URB597 failed to recover amidase activity after 18-hrs dialysis, that with JNJ1661010 recovered activity in the same conditions, suggesting a release of the carbamoylating fragment from the active site.[130] Thus, inhibition of FAAH by the piperazinyl urea JNJ1661010 results reversible, with potential consequences for the *in vivo* behavior of this compound.

As a last step of my PhD research, starting from the FAAH-URB597 and FAAH-JNJ1661010 covalent adducts, I focused on the mechanism of Ser241 decarbamoylation, applying a hybrid quantum mechanical/molecular mechanical (QM/MM) approach.[131] Potential energy surfaces (PES) of the decarbamoylation reaction were explored at SCC-DFTB/CHARMM27 level of theory, by means of the adiabatic mapping method, already described in the previous chapters. To have further insights into the mechanism of FAAH inhibition, the energetic of FAAH decarbamoylation was compared with that of FAAH deacylation in the presence of the substrate. Experimentally, it is not clear if the rate-limiting step of FAAH-catalyzed hydrolysis of OEA resides in the acylation or in the deacylation step. Observation that it is possible to isolate a small, but significant, level of the acylenzyme intermediate suggested that the energy barrier for FAAH deacylation should be in the range of the one found for acylation, i.e. ~ 16 kcal mol^{-1}.[132]

QM/MM simulations were performed to investigate if a mechanism involving the conserved water W1 as a critical element of the Lys-Ser-Wat triad is energetically and structurally reasonable, and in agreement with experimental data.

Methods

Application of the QM/MM potential

The CHARMM program (version c30b2)[133] was employed to build FAAH-substrate or FAAH inhibitor systems, as well as to perform energy minimization (constrained or unconstrained) and molecular dynamics simulations. The CHARMM27 all-atom force field[134] was used in combination with the self-consistent charge-density functional tight binding (SCC-DFTB) method, as implemented in the QM/MM module of CHARMM.[135]. The SCC-DFTB method is an approximate DFT method and it is more efficient than *ab initio* QM/MM approaches.[136] The SCC-DFTB model has been tested for several enzymes,[137] including FAAH. In particular, the remarkable preference of FAAH in hydrolyzing the amide substrate faster than the ester one has been found to be satisfactorily reproduced by the SCC-DFTB/CHARMM27 protocol, here applied.

A relatively large quantum mechanical region of 73 atoms was defined for the FAAH-OEA covalent adduct (1) (Figure 7.3). These includes the catalytic water W1, the (Z)-heptadec-8-enyl fragment of OEA and parts of the side chains of Lys142, Ser217, Ser241. In the FAAH-URB597 system (2), the cyclohexyl carbamic acid portion of URB597 parts of Lys142, Ser217 and Ser241 side chains and water W1 were included in QM regions, for a total of 42 atoms (Figure 7.3). In the case of the FAAH-JNJ1661010 system (3), the 4-(3-phenyl-1,2,4-thiadiazol-5-yl)piperazin-1-yl carbamic acid of JNJ1661010, parts of Lys142, Ser217, Ser241 side chains and W1 molecule were included in QM selection, for a total of 53 atoms (Figure 7.3). For all these systems, the QM-region had a neutral total charge and in all of them, three HQ link atoms were introduced to saturate the shells of QM-atoms covalently bonded to MM-atoms. The QM/MM approach used here includes bonded and nonbonded interactions between the QM and MM systems and accounts for the essential effect of the protein on the modeled reactions.[135] Van der Waals and bonded interactions were described by MM terms, with standard CHARMM27 parameters used for the QM atoms. Electrostatic interactions were treated by calculating the Coulombic interactions between the Mulliken charges of the QM atoms and the MM partial atomic charges.[135] A group-based nonbonded cut-off of 12 Å was applied and atoms further than 16 Å from the Ser241 hydroxyl oxygen were fixed. With the exception of these boundary restraints, all the other atoms were free to move during the calculations.

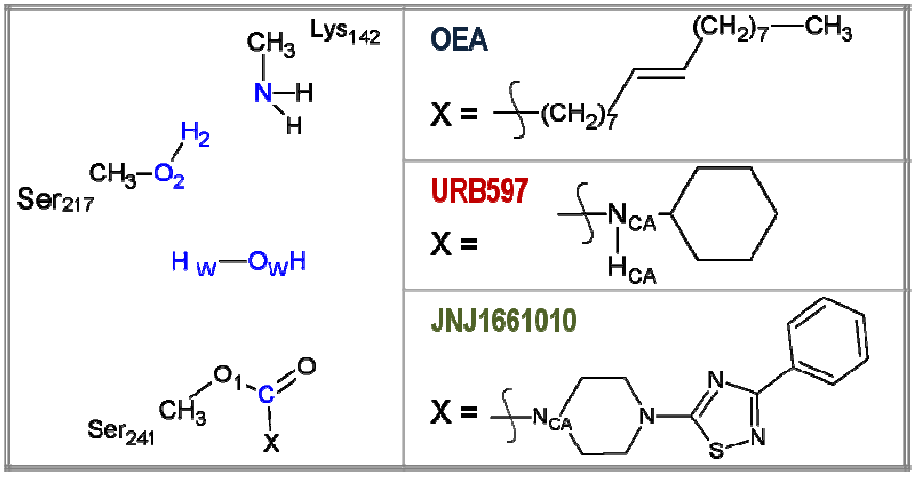

Figure 7.3 Structure of the QM region for the three system : It consists of the methylamine group of Lys142, the side chains of Ser217 and Ser241 and the whole substrate/inhibitors fragments. Amino acids fragments were capped with 3 H-Link atoms.

Preparation of the protein-ligand models

The structures of the covalent adducts of FAAH with 1 and with 3 were prepared starting from the X-ray coordinates of the adduct between the humanized-rat (h/r) variant of FAAH and the inhibitor PF-3845 (PDB code 3LJ6). The Ser241 carbamoylating fragment of PF-3845 was transformed into the (Z)-heptadec-8-enyl group of 1 or into the 4-(3-phenyl-1,2,4-thiadiazol-5-yl)piperazin-1-yl group of 3. The coordinates of FAAH-2 adduct were taken from the X-ray crystal structure of the h/r variant of FAAH-URB597 (PDB entry 3LJ7).[119] Hydrogen atoms were added with the HBUILD routine in CHARMM. Conventional protonation states (physiological pH) were assigned to all the amino acids, except for Lys142 that was modeled in its neutral form. All protein residues and the crystal water molecules containing at least one atom within 25 Å of the system centre (defined as the side chain oxygen of Ser241) were included in the models. The three systems were solvated by superimposing a 25 Å radius sphere of pre-equilibrated TIPS3P water molecules (CHARMM-type variant of TIP3P waters).[138] After solvation, the systems resulted composed by 7756 atoms in case of 1, 7610 for 2 and 7741 for 3.

Energy minimization with all non-water atoms fixed was then carried out with 500 steps of steepest descent (SD) followed by 2500 steps of Adopted Basis Newton–Raphson (ABNR). Finally, the three systems were fully minimized (1500 steps SD,

2500 steps ABNR), in absence of any constraints to a gradient tolerance of 0.01 kcal mol^{-1}.

Protein-ligand adducts were prepared for stochastic boundary molecular dynamics simulation (SBMD).[139] Stochastic boundary conditions, were applied by separating the systems into two regions: the reaction region, consisting of all atoms within 21 Å from the system centre, and the buffer region, containing all other atoms in the 25 Å sphere. While the reaction region was treated with Newtonian dynamics, the buffer region was described by Langevin dynamics. Furthermore, a deformable boundary potential was imposed on the water molecule to prevent their diffusion away from the reactive site. In the buffer region, the Langevin equations of motion impose both a friction coefficient and a random force on all heavy atoms, which allows the buffer region to act as a heat bath. Friction coefficients of 250 ps^{-1} for non-hydrogen protein atoms and 62 ps^{-1} on water oxygen atoms were used, similarly to what performed in previous simulations on FAAH[117].

The FAAH-based systems were then heated from 10 to 310 K in three separate but consecutive steps of 50 ps: *i*) from 10 to 100 K, *ii*) from 100 to 200 K, and, *iii*) from 200 to 310 K. Finally, these three systems were equilibrated for 2 ns at 310 K, in the SBMD regime. The SHAKE algorithm was applied allowing the employment of a time step for integration of 1 fs.

For each system, after 600 ps of simulation, one snapshot every 200 ps of SCC-DFTB/CHARMM27 SBMD simulation was considered for the mechanistic study, for a total of 8 equally-spaced starting structures. The resulting 24 structures were minimized to a gradient tolerance of 0.01 kcal mol^{-1} $Å^{-1}$ with the QM/MM potential, freezing all heavy atoms further than 16 Å from the reaction center, and then employed to model the deacylation (1) or decarbamoylation (2, 3) reaction.

Calculation of the Potential Energy Surfaces

Reaction coordinates were defined for every reaction step and restrained sequentially to move the system along the given reaction path. Reaction coordinate restraints were applied by means of the RESD command implemented in CHARMM program. A force constant of k=5000 kcal mol^{-1} $Å^{-2}$ was used to restrain all the defined coordinates. The values for the restrained distances were increased in step

of 0.1 Å to force the system across the barrier for a specific reaction step. ABNR energy minimizations of all the generated structures were performed to a gradient tolerance of 0.01 kcal mol^{-1} $Å^{-1}$ using a SCC-DTFB/CHARMM27 potential. Furthermore, the structures of energy minima were determined more accurately by performing additional geometry optimizations with none of the reaction coordinates restrained. The final energy of a structure (as indicated on the potential energy surfaces) was obtained by performing single-point energy calculations at SCC-DFTB/CHARMM27 level, excluding the energy contribution coming from the applied restraint. The PESs explored here allow to determine the basic mechanistic features of a given reaction, such as the identification of approximate transition states and intermediates. However, they do not account for zero-point energy, nor for the influence of hydrogen tunneling effects that are expected to lower the calculated barriers by few kcal mol^{-1}.

Single-point calculations *in vacuo* and enzyme stabilization energy

To quantify the relative stabilization provided by FAAH along the simulated pathways, the SCC-DFTB energy of the QM region alone ($E_{QMvacuo}$), at the corresponding QM/MM optimized geometry, was re-calculated for each stationary point identified along the deacylation/decarbamoylation of FAAH. We then defined the stabilization energy of the MM part of the enzyme on the QM part as:

$$E_{stabilization} = E_{total} - E_{QMvacuo} \qquad \textit{(Eq. 7.1)}$$

where the total energy of each system has the form of a potential energy and it is defined as:

$$E_{total} = E_{QM/MM} + E_{MM} \qquad \textit{(Eq. 7.2)}$$

The $E_{QM/MM}$ includes the self-consistent energy of the QM atoms and the interaction energy between the QM and MM regions, including electrostatic and polarization effects as well as an MM term which includes van der Waals interactions between QM and MM atoms. E_{MM} is the classical contribution of the energy arising from MM part. The so-defined stabilization energy is the amount by which a QM region structure is stabilized by the environment relative to the reactant.[140]

Amino-acid Decomposition Analysis

Important structures along the deacylation and decarbamoylation pathways were investigated the by decomposition analysis approach.[141] In brief, conserved FAAH active site residues (amino acids or water molecules included in the MM part) were removed from the simulation system. After every deletion, the total energy of the system was recalculated by single point calculations. The calculated change in the total energy gives an estimate of the contribution provided by an amino acid or by a water molecule to the stabilization of the structure. This approach can help to identify vital interactions of the enzyme and the substrate or quantum mechanically treated active site residues.

Results and Discussion

Reaction path calculations

The deacylation or decarbamoylation reaction was modeled in two main steps, starting from the FAAH-acylated adduct (heptadec-8-enyl fragment for compound 1) or from the two FAAH-carbamoylated adducts, including carbamoylating fragments of compound 2 and 3. According to the mechanism depicted in Figure 7.4, these steps were: (*i*) attack of a conserved water molecule (W1) and formation of a TI; (*ii*) protonation of the leaving group followed by its subsequent expulsion with formation of free Ser241.

Step (*i*) consisted of several events: a proton was initially abstracted from the water molecule W1 and transferred to the neutral Lys142, *via* the bridging residue Ser217 (events *x* and *y*). Then, the activated water W1 attacked the carbonyl carbon of the carbamoylating (acylating) group (C), leading to the formation of the TI. For this purpose, step (*i*) was modeled by restraining the following two reaction coordinates: Rx, defined as [d(O_w, H_w) − d(O_2, H_w) − d(O_w, C)], describing proton abstraction from water W1 by Ser217 and nucleophile attack by W1; and Ry, defined as [(dO_2, H_2)] − d[(N, H_2)], which described the proton transfer between Ser217 and Lys142.

Also step *ii* was a complex process, as it involved the breakage of the bond between the hydroxyl oxygen of Ser241 and the carbonyl carbon of carbamoylating

(acylating) fragment (event *r*), assisted by a double proton transfer involving Ser217 (*s*) and Lys142 (*t*). Step (*ii*) was thus modeled using Rs, defined as $d[O_1, H_W] - d[O_2, H_W] + d[O_2,C]$), describing protonation and expulsion of Ser241, and R_t defined as ($d[N, H_1]- d[O_1,H_1]$) which accounted for the movement of proton H_1 on Lys142 to Ser217.

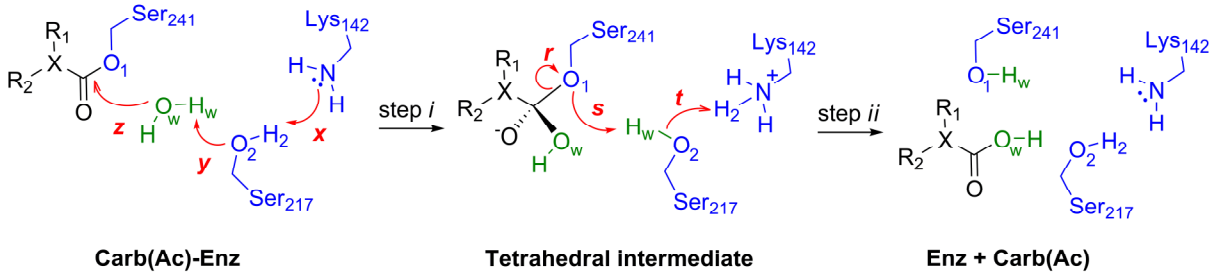

Figure 7.4 Individual reaction processes (*x*, *y*, *z*, *r*, *s*, *t*) involved in the deacylation or decarbamoylation of FAAH. General formulas of catalytic residues with the adduct product of Ser241 and oleamide, X = C, R_1=H R_2 = (Z)-heptadec-8-enyl; JNJ1661010, X = N, R_1 R_2 X = (4-(3-phenyl-1,2,4-thiadiazol-5-yl)piperazin-1-yl); URB597, X = N; R_1= H, R_2 = cyclohexyl.

Deacylation of FAAH-oleamide adduct

The SCC-DFTB/CHARMM27 PESs of FAAH deacylation are reported in Figure 7.5. The potential energy surface has a smooth shape, indicating that the employed reaction coordinates and modeling procedure are able describe the essential details of the reaction. The PES relative to step *i* (formation of the TI) is reported in the left panel. The change in energy during the nucleophilic attack of water molecule W1 (event *z*), assisted by deprotonation of Ser217 (event *y*), can be followed along Rx, while the change in potential energy during the protonation of Lys142 (event *x*) can be observed along Ry. The minimum energy path (MEP) for step *i* indicated the presence of a concerted mechanism. Indeed, the MEP connecting the Ac-Enz (A) with the TI (C) goes approximately through the middle of the surface. The highest point along the MEP, corresponding to the transition state (TS, B), has an energy of 16.6 kcal mol^{-1} compared to the acylenzyme. Visual inspection of B shows that the proton abstraction from the water molecule to Ser217 is nearly complete on this configuration. The distance of the moving proton H_w to the oxygen of Ser217 (H_w–O_2) is 1.11 Å (1.02 Å at the TI), while the distance to the water oxygen O_w is still 1.38 Å (Table 7.1). In the TS, the proton transfer involving Ser217 and Lys142 is already complete, being the H_2–N distance at the same value of the TI (1.06 Å).

The distance of the W1 oxygen (O_W) to the carbonyl carbon decreases from 2.48 Å in the acylenzyme to 1.84 Å of the TS, indicating that the nucleophilic attack is occurring. The C–O_w distance shortens constantly from the TS to the TI, where it reaches its equilibrium distance of 1.47 Å at the TI (Table 7.1).

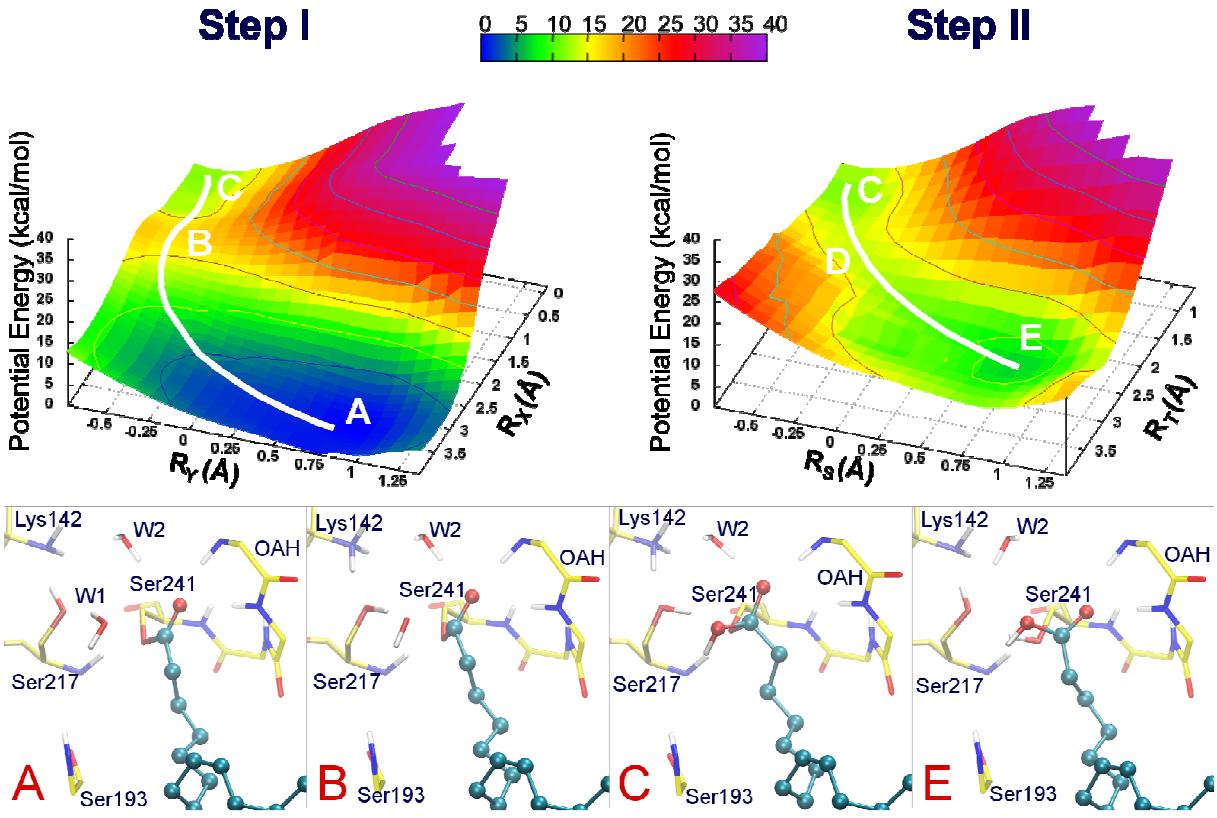

Figure 7.5 SCC-DFTB/CHARMM27 QM/MM PESs (top) for the deacylation in presence of the (Z)-heptadec-8-enyl fragment of 1. The structures of some configurations (bottom) are also shown: A (Acyl Enzyme), B (transition state) C (tetrahedral intermediate), E (free enzyme and oleic acid). FAAH active site residues are represented by yellow carbon atoms, while the carbons of the (Z)-heptadec-8-enyl fragment of 1 are depicted in cyan.

The TI (C) is less stable than the acylenzyme adduct by 12.5 kcal mol^{-1}, indicating its transient character. On the other hand, this configuration is stabilized by the FAAH oxyanion hole, which forms hydrogen bonds with the negatively charged oxygen of the substrate (Figure 4), as also reported in previous calculations.[117] Interestingly, an accessory water molecule (W2)[119] was found to interact with the carbonyl oxygen of the acylating portion of 1 in both the TS and TI (Figure 7.5), assisting the stabilization of the incoming negative charge on the oxygen atom.

The SCC-DFTB/CHARMM27 PES associated with step *ii* of the reaction (TI collapse) is reported in Figure 7.5. The change in energy during the expulsion of Ser241 side chain from the TI (*r*), assisted by protonation performed by Ser217 (*s*), can be followed along Rs. The change in energy during the proton transfer of H_2 from Lys142 to Ser217 (*t*) can be observed along Rt. The PES of step *ii* showed a MEP that connects the TI (C) with the product of the reaction (the free enzyme E), moving approximately across the middle of the surface. No stable species are found during this reaction, suggesting that the two protonation events (*s* and *t*) are tightly coupled with the expulsion of the leaving group (*r*).

	O_w-C	O_w- H_w	O_2-H_w	O_2-H_2	N-H_2	O_1-C	O_1-H_w	O-C
Ac-Enz (**A**)	2.478	0.991	1.783	1.009	1.885	1.360	2.529	1.241
TS1 (**B**)	1.840	1.382	1.113	1.690	1.065	1.438	2.450	1.286
TI (**C**)	1.467	1.656	1.019	1.690	1.065	1.614	2.486	1.336
TS2 (**D**)	1.412	2.646	1.151	1.533	1.108	1.912	1.286	1.285
Products (**E**)	1.405	2.448	1.797	1.026	1.801	2.173	0.994	1.234

Table 7.1 Distances in Å between atoms involved in the formation or in the breakage of covalent bonds for relevant configuration indentified during the deacylation of FAAH in presence of Oleamide. Atom labels are consistent with Figure 7.4.

However, visual inspection of the TS structure (D), indicates that protonation of the Ser241 O_1 by Ser217 (H_w–O_1 distance 1.29 Å) is occurring during the breakage of the O_1-C bond (O_1-C distance 1.91 Å). On the contrary, the transfer of H_2 from Lys142 back to Ser217 only begins at this point of the reaction (N–H_2 distance 1.11 Å). The energy of the identified TS (D) is 14.3 kcal mol^{-1} (relative to the acylenzyme), ~2 kcal mol^{-1} lower than that calculated here for the formation of the TI, suggesting that step *i*, rather than step *ii*, is the rate-liming event for FAAH deacylation. However, the finding that TI occupies a rather flat area of the overall PES suggests that formation and collapse of TI are tightly coupled events. Finally, the product of the reaction E (composed by the free enzyme and oleic acid) is calculated to be less stable than the acylenzyme by 8.2 kcal mol^{-1}.

Decarbamoylation of FAAH-URB597 adduct

The SCC-DFTB/CHARMM27 PESs of FAAH decarbamoylation in the presence of the carbamoylating portion of 2 are reported in Figure 7.6. The surface relative to step *i* is reported in the left panel. The change in energy during W1 deprotonation by Ser217 (*y*) and the subsequent nucleophilic attack on the carbamoylated Ser241 (*z*) can be followed along Rx, while the change in the energy during the Ser217-Lys142 proton transfer (*x*) can be observed along Ry. Also in the case of carbamoylation, the minimum energy path (MEP) connecting the reactant (Carb-Enz, A) to the tetrahedral intermediate B goes diagonally on the PES surface, indicating that reaction processes *x*, *y* and *z* are concerted. The SCC-DFTB/CHARMM27 energy barrier for the first step resulted 28.3 kcal mol^{-1} significantly higher (~12 kcal mol^{-1}) than the barrier found for the first step of FAAH deacylation in presence of 1.

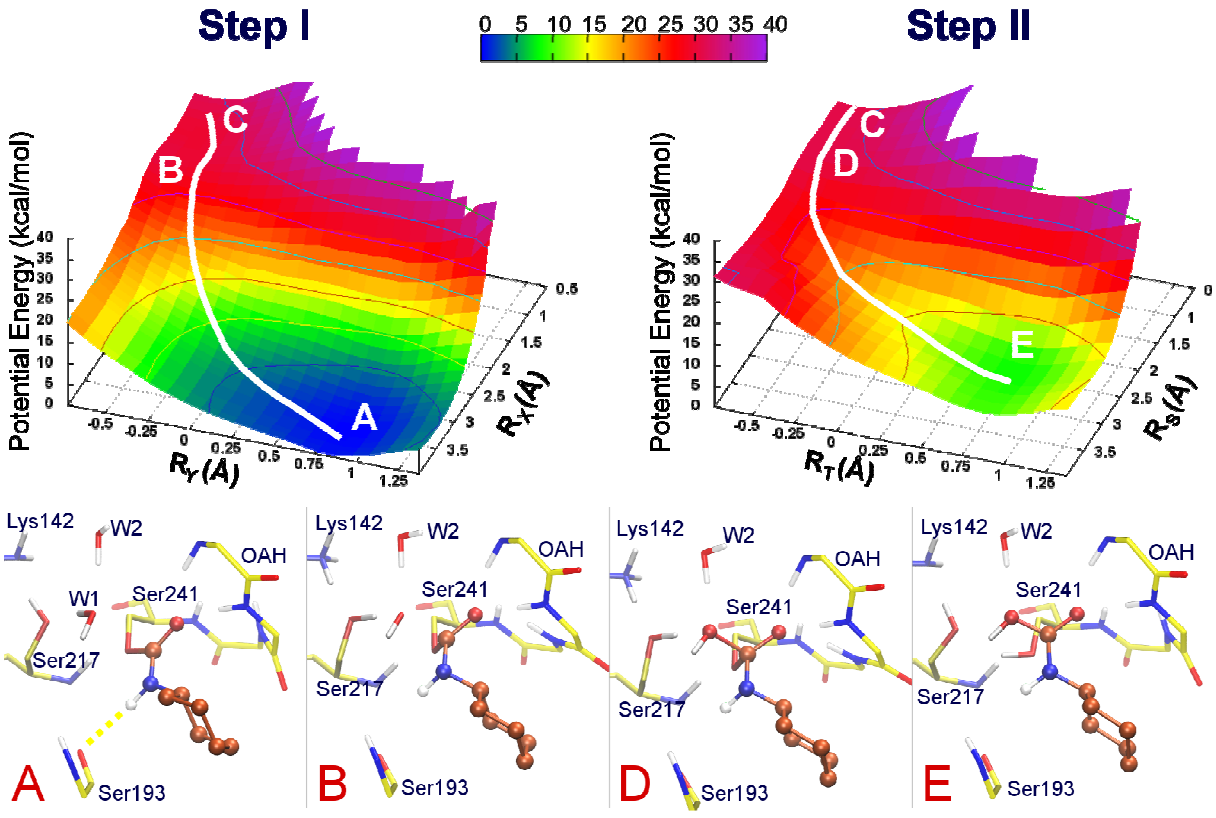

Figure 7.6 SCC-DFTB/CHARMM27 QM/MM PESs (top) for the decarbamoylation reaction starting from the cyclohexylaminocarbonyl derivative of FAAH at Ser241. The structures of some configurations (bottom) are also shown: A (carbmoyl-enzyme), B (transition state) C (tetrahedral intermediate), E (free enzyme and cyclohexylcarbamic acid). FAAH active-site residues are represented by yellow carbon atoms, while the carbons of carbamoylating fragment of 2 are depicted in orange.

Analysis of the first TS (B) shows that the proton H_w resulted nearly transferred to the accepting oxygen (O_2) of Ser217 (O_2-H_w distance = 1.09 Å, Table 2) on this configuration, while the removal of H_w from the W1 oxygen (O_w-H_w distance = 1.44 Å) is not yet complete. Proton H_2 is almost bound to the side-chain nitrogen atom (N) of Lys142 (N-H_2 distance = 1.06 Å), bearing a positive charge at this stage of the reaction. The distance between the W1 oxygen (O_w) and the carbonyl carbon of the carbamoylating portion is considerably decreased from the 2.66 Å at the covalent adduct to 1.82 Å at the TS. Furthermore, the finding that carbamate group is significantly deviating from planarity confirmes that the nucleophilic attack is here occurring. Visual inspection of the TI structure confirmes the presence of a new bond between the water molecule W1 and the carbonyl carbon of the inhibitor (O_w–C distance = 1.57 Å). Conversely, the O_2-H_w and N-H_2 distances underwent only minor adjustments (Table 7.2), indicating that the geometry of the TI closely resembles that of the TS, accordingly to their close positions on the PES. As a consequence the TI has a very high energy contents, only 1 kcal mol^{-1} less than the energy of TS.

	O_w-C	O_w- H_w	O_2-H_w	O_2-H_2	N-H_2	O_1-C	O_1-H_w	O-C
Carb-Enz (**A**)	2.657	0.987	1.803	1.007	1.878	1.375	2.456	1.248
TS1 (**B**)	1.816	1.436	1.093	1.690	1.061	1.459	2.500	1.289
TI (**C**)	1.571	1.798	1.011	1.693	1.064	1.544	2.396	1.316
TS2 (**D**)	1.471	2.393	1.066	1.699	1.070	1.794	1.503	1.290
Products (**E**)	1.388	2.444	1.882	1.012	1.884	2.265	0.991	1.246

Table 7.2 Distances in Å between atoms involved in the formation or in the breakage of covalent bonds for relevant configuration indentified during the decarbamoylation of FAAH in presence of URB597.

The PES for step *ii* is reported in the right panel of Figure 7.6. The change in potential energy during protonation of the leaving group (event *s*) and its expulsion (event r) is described by reaction coordinate R_s, while the change in the energy during the deprotonation of Lys142 (event t) can be observed along R_t. Analysis of the second TS (D) shows that, at this stage of the reaction, the events s and r are almost complete, as indicated by O_2-H_W, O_1–H_W, and C-O_1 distances of 1.07 Å and 1.50 Å, respectively. On the contrary, the proton transfer from Lys142 to Ser217 has not occurring yet, as the H_2 was still bound to Lys142 (O_2-H_2 = 1.70 Å; N-H_2 = 1.07).

The energy of D is 28.9 kcal mol^{-1}, only ~1 kcal mol^{-1} higher than TI, confirming that step *i* and *ii* are tightly coupled, similarly to what observed for FAAH deacylation. The conclusive proton transfer (*t*) is spontaneous, as no barrier is found between D and E on the PES. Configuration E, resulted ~9 kcal mol^{-1} less stable than the cabamoylated enzyme A.

Decarbamoylation of FAAH-JNJ1661010 adduct

The SCC-DFTB/CHARMM27 PESs of FAAH decarbamoylation in the presence of the carbamoylating portion of 3 are reported in Figure 7.7. The surface relative to step *i* is reported on the left panel. The change in energy during W1 deprotonation and subsequent nucleophilic attack can be followed along Rx, while the change in the potential energy during the protonation of Lys142 can be observed along Ry. Similarly to what observed for decarbamoylation of 2, the MEP connecting the reactant A to the TI (C) on the SCC-DFTB/CHARMM27 surface shows the presence of a concerted reaction. At the TS (B), proton H_2 is still bound to Lys142 (O_2-H_2 = 1.74 Å; N-H_2 = 1.06 Å), while the proton abstraction of Hw (from W1) by Ser217 is almost complete, with O_2-H_W distance of 1.10 Å, similar to 1.01 Å distance at the TI. The TS shows an incoming nucleophilic attack being the O_W-C distance only 1.83 Å, similar to the final value of 1.53 Å at the TI. The energy content of the TS (B) is 21.9 kcal mol^{-1} relative to the Carb-enz A. The TI (C) has an energy of only few kcal mol^{-1} smaller than the TS (19.6 kcal mol^{-1} compared to A), as observed in the case of decarbamoylation of FAAH in presence of the carbamoylating portion of compound 2.

The reaction energetics of step *ii* is reported on the PES of Figure 7.7 (right panel). Protonation (event *s*) and expulsion (event *r*) of the Ser241 leaving group are described by the reaction coordinate Rs, while the Lys142-Ser217 proton transfer (events *t*) is described by Rt. The MEP links the TI (C) with the product of the reaction (E) moving approximately across the middle of the surface. No stable species are found during this reaction, suggesting that two protonation events (*s* and *t*) are tightly coupled with the expulsion of the leaving group (*r*). Analysis of the second TS (D) shows that the expulsion of leaving group Ser241 is advanced (O_1-C = 2.12 Å, Table 7.3) on this configuration. This process is assisted by a double proton transfer (involving Ser217 and Lys142, Figure 2) as shown by the O_1-H_W and N–H_2 distances of 1.04 Å and 1.18 Å respectively at the TS (Table 7.3). The potential

energy barrier required to overcome D is 23 kcal mol^{-1} (relative to the Carb-Enz A), ~3 kcal mol^{-1} higher than that the barrier found for step *i*. Finally, the product of the reaction E (composed by the free enzyme and the 4-(3-phenyl-1,2,4-thiadiazol-5-yl)piperazin-1-yl carbamic acid fragment of 3) is calculated to be less stable than the carbamoylenzyme A by 15.8 kcal mol^{-1}.

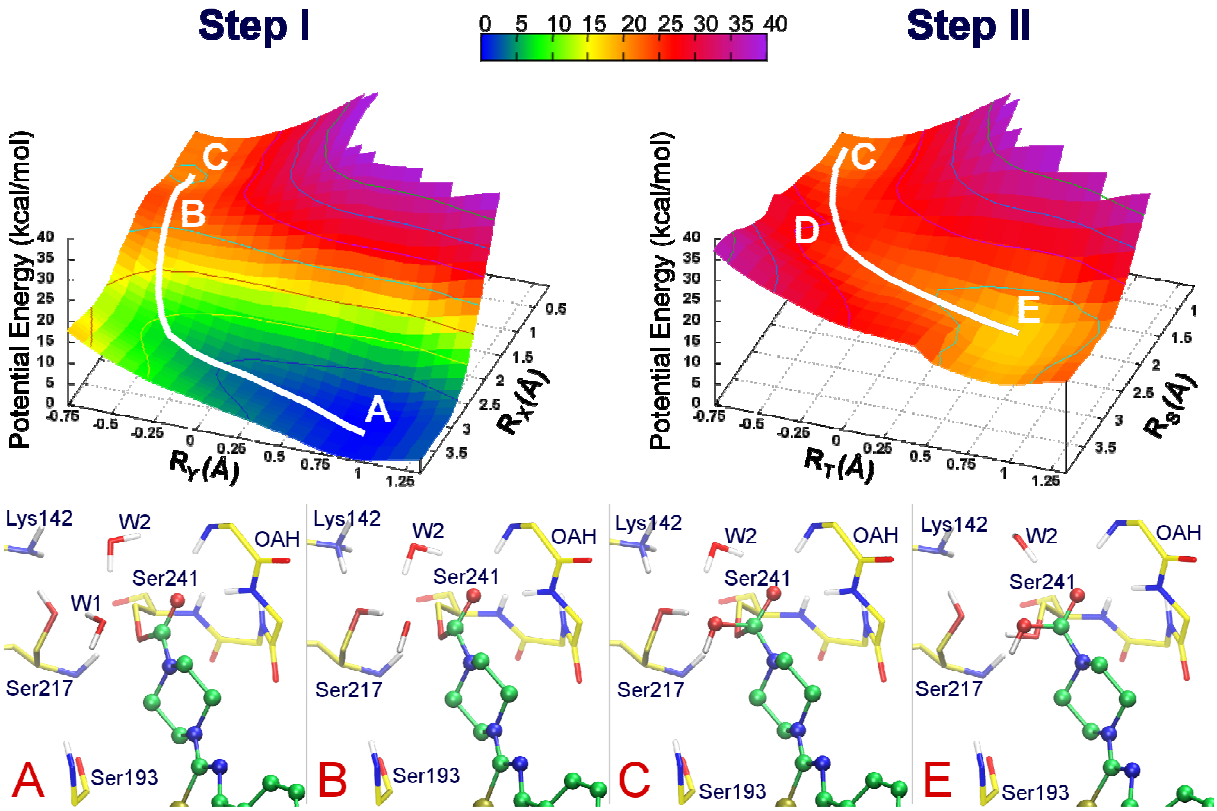

Figure 7.7 SCC-DFTB/CHARMM27 QM/MM PESs (top) for the decarbamoylation reaction in presence of the 4-(3-phenyl-1,2,4-thiadiazol-5-yl)piperazin-1-yl carbamic acid FAAH ester on Ser241. The structures of some configurations (bottom) are also shown: A (Acyl Enzyme), B (transition state) C (tetrahedral intermediate), E (free enzyme and 4-(3-phenyl-1,2,4-thiadiazol-5-yl)piperazin-1-yl carbamic acid). FAAH active site residues are represented by yellow carbon atoms, while the carbons of carbamoylating fragment of 3 are depicted in green.

	O_w-C	O_w- H_w	O_2-H_w	O_2-H_2	N-H_2	O_1-C	O_1-H_w	O-C
Carb-Enz (A)	2.492	0.985	1.822	0.990	2.007	1.373	2.460	1.242
TS1 (B)	1.829	1.403	1.100	1.735	1.056	1.438	2.427	1.293
TI (C)	1.526	1.799	1.008	1.737	1.057	1.529	2.316	1.325
TS2 (D)	1.383	2.400	1.550	1.365	1.184	2.115	1.044	1.243
Products (E)	1.396	2.311	1.686	1.004	1.921	2.139	1.006	1.230

Table 7.3 Distances in Å between atoms involved in the formation or in the breakage of covalent bonds for relevant configuration indentified during the decarbamoylation of FAAH in presence of JNJ1661010.

Overall deacylation and decarbamoylation reaction profiles

Figure 7.8 summarizes the SCC-DFTB-CHARMM27 potential energy profiles for FAAH deacylation in presence of the acylating portion of the substrate 1 and FAAH decarbamoylation in presence of the carbamoylationg portions of the irreversible inhibitor 2 and of the slowly reversible one 3. The calculations indicate that for FAAH deacylation, formation of TI, rather than its collapse, represents the rate-limiting step of the process. Conversely, the energy profile for FAAH decarbamoylation indicates that this process depends on both TI formation and collapse, with no single step being clearly rate-limiting. Decarbamoylation of FAAH adducts needs to overcome a significantly higher energy barrier than deacylation, accordingly with the expected different behaviour between a covalent inhibitor and a substrate.

The energy barrier for decarbamoylation of the covalent adduct formed by FAAH and compound 2 was found to be significantly higher than that obtained for FAAH-3 adduct (28.6 kcal mol^{-1} *vs* 22.9 kcal mol^{-1}. This result is consistent with the kinetic behavior of compounds 2 and 3, as observed in dialysis experiments, where the two compounds act as irreversible and slowly-reversible inhibitors of FAAH respectively.

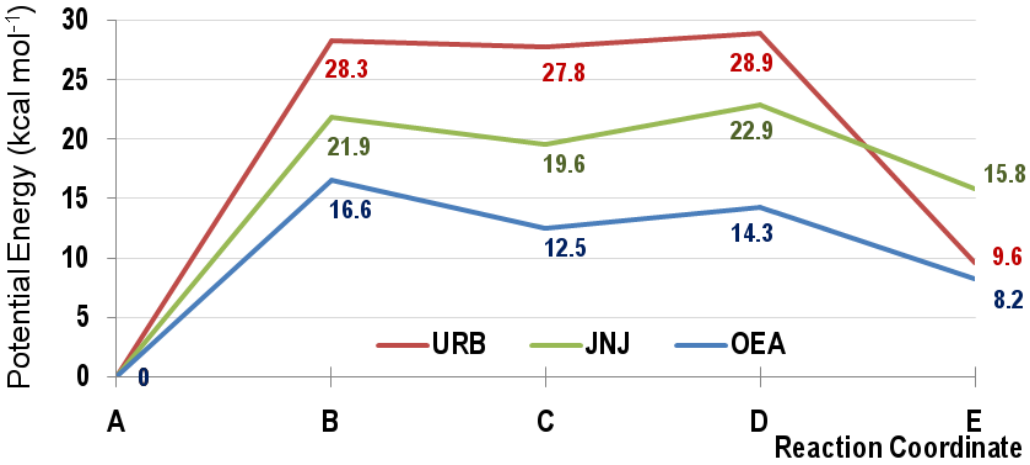

Figure 7.8 SCC-DFTB-CHARMM27 potential energy profiles for deacylation/decarbamoylation of the covalent adduct of FAAH with OA (blue), URB594 (red) and JNJ1661010 (green). The relevant configurations are: acyl/Carbamoyl Enzyme (A), TS for TI formation (B), TI (C), TS for TI collapse (D), free enzyme and acid (E).

QM/MM calculations based on adiabatic mapping approach can be considerably affected by the starting geometry of the reactants.[142] To reinforce the present computational findings, SCC-DFTB/CHARMM27 calculations were performed for alternative conformations of FAAH covalent adducts. For each system, seven

additional FAAH structures were extracted from the corresponding QM/MM MD trajectory (see Method section) and employed to build PESs for the deacylation or decarbamoylation reaction. Even if PESs and the relative positions of the stationary points were not significantly influenced by the starting geometry of the reactants (configurations A), moderate differences were observed in their calculated energy. The results of these additional simulations are summarized in the potential energy profiles reported in Figure 7.9, where energy values of intermediates, TSs and products are reported as a mean values ± standard errors of the mean (SEM). The obtained energy profiles are consistent with those reported in Figure 7.8, confirming that *i)* Ser241 deacylation is energetically cheaper than decarbamoylation, *ii)* the barrier for Ser241 decarbamoylation of the irreversible inhibitor 2 remains higher than the one for Ser241 decarbamoylation with the reversible inhibitor 3.

Furthermore, the use of multiple starting conformations confirms that, while the rate of deacylation mainly depends on the energy required to form TI, in case of decarbamoylation processes TI collapse appears as much as important as TI formation.

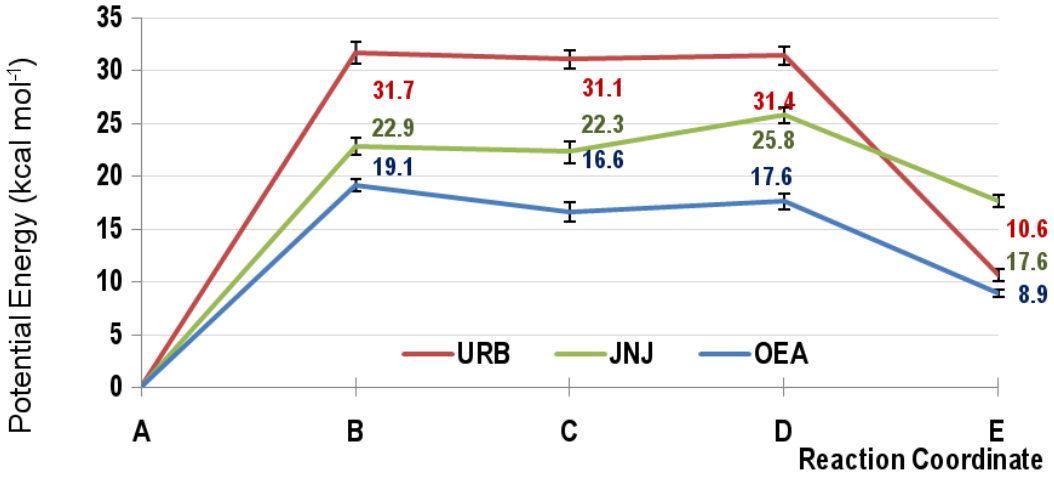

Figure 7.9 SCC-DFTB-CHARMM27 potential energy profiles for deacylation/decarbamoylation of the covalent adduct of FAAH with OA (blue), URB594 (red) and JNJ1661010 (green). Energy values are expressed as mean value ± standard error of the mean The relevant configurations are: acyl/carbamoyl Enzyme (A), TS for TI formation (B), TI (C), TS for TI collapse (D), free enzyme and acid (E).

Comparison with single point calculation in gas phase: the effect of enzyme stabilization

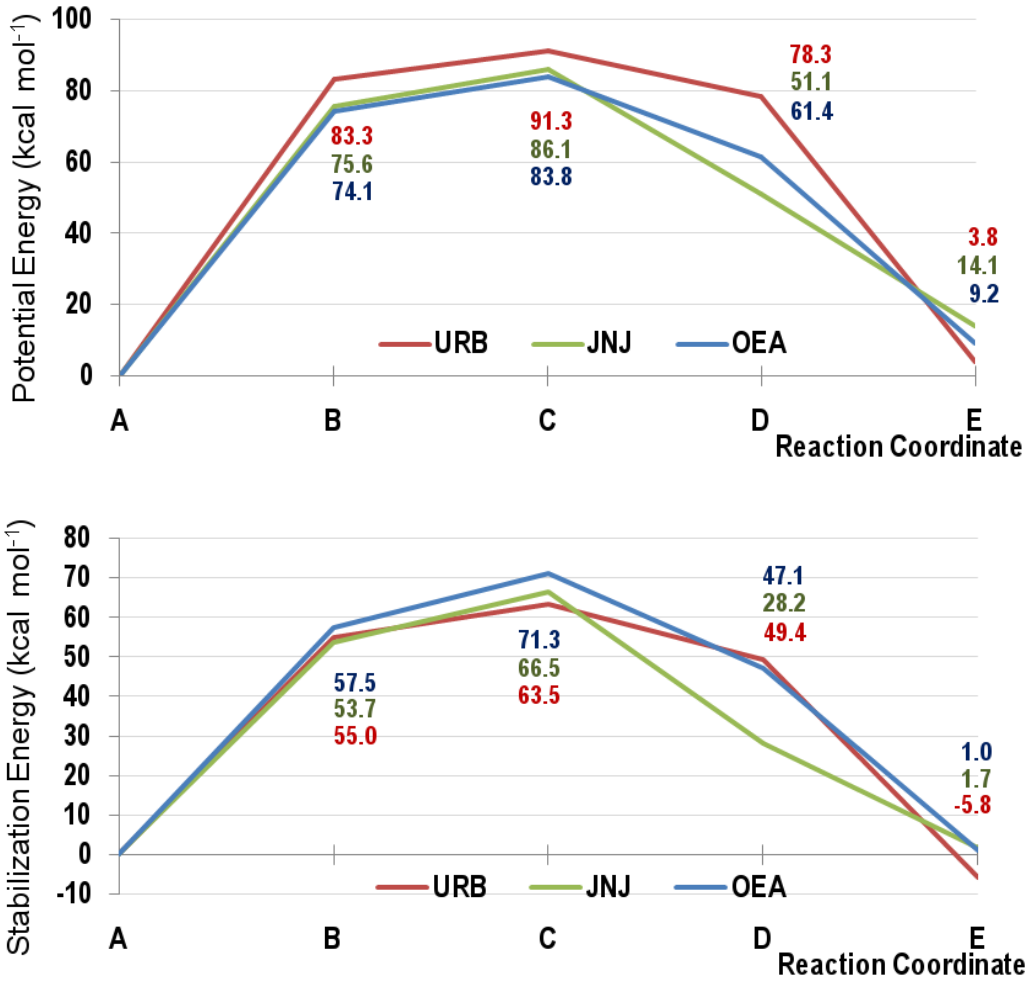

Figure 7.10. Top panel. Gas-phase SCC-DFTB potential energy profile of the QM region. The reported values are derived from single-point calculations on the QM regions of the relevant configurations for the deacylation/decarbamoylation of the covalent adduct of FAAH with OA (blue), URB594 (red) and JNJ1661010 (green): acyl/carbamoyl Enzyme (A), TS for TI formation (B), TI (C), TS for TI collapse (D), free enzyme and acid (E). Bottom panel. Stabilization energy along the reaction coordinate (relative to the acyl/carbamoyl enzyme) for OA (blue), URB597 (red), JNJ1661010 (green).

To examine the stabilization provided by FAAH during the reaction of deacylation/decarbamoylation, single-point calculations on the isolated QM region were carried out for the QM/MM optimized geometries along the different reaction paths (i.e. calculating the energy of the reacting system without the effects of the protein, see methods). The resulting gas-phase SCC-DTFB profiles are reported in Figure 7.10. The three curves here represented have similar shapes and show significantly higher energy values for the TSs compared to those calculated for the corresponding reaction in FAAH. More importantly, the analysis of the gas-phase

curves indicates that the TI is not a low-energy configuration on the PES surface in absence of the enzyme structure, regardless of the chemical nature of the acylating or carbamoylating portion of Ser241. The TI is indeed the point along the reaction path with highest SCC-DFTB potential energy. While for the deacylation of 1 the TI resulted destabilized by 80.4 kcal mol^{-1} compared to the acylenzyme A, in the case of decarbamoylation the energy of the TI resulted. of 91.3 kcal mol^{-1} for compound 2 and 86.1 kcal mol^{-1} for compound 3, when compared to their corresponding starting structure A. This indicates that the two carbamoylated serines are less prone to react with the water molecule W1 than the acylated one, reflecting the intrinsic higher stabilization of alkylcarbamic acid *O*-alkyl ester over carboxylic acid *O*-alkyl ester.

Enzymes usually posses a specific environment which electrostatically complement the changes in the electronic structure of the "substrate" during the catalyzed reactions.[130] This provides a simple and effective way of reducing the activation energies of a chemical transformation. The environmental effect provided by FAAH during the reaction of deacylation and decarbamoylation can be roughly estimated by subtracting the SCC-DFTB energy of the isolated QM region from the total SCC-DTFB/CHARMM27 energy. In this way, stabilization energy curves as those of Figure 7.10 can be obtained, showing the contribution played by the active site along the reaction path.

As found in earlier simulations of FAAH acylation,[117] the active site of FAAH provides an increasing stabilization of the reacting system as the deacylation or decarbamoylation proceeds (and as negative charge increases on the carbonyl oxygen), until the TI is reached. It is evident that FAAH stabilizes the TSs (B), but it stabilizes the TIs (C) even more, thanks to its oxyanion hole. This is mainly because the negative charge of the carbonyl oxygen is greatest at the TI both in the case of deacylation and decarbamoylation (Table 7.4). Analysis of the curves also shows that the deacylation reaction is much more stabilized by FAAH than the decarbamoylation ones. Again this seems to depend on the extent of the negative charge on the carbonyl oxygen (O) of the acylating/carbamoylating portion at TI. Indeed, the calculated stabilization energy parallels the absolute value of the mulliken charge on this oxygen atom.

	O_w cpd **1**	C cpd **1**	O_1 cpd **1**	O cpd **1**	O_w cpd **2**	C cpd **2**	O_1 cpd **2**	O cpd **2**	O_w cpd **3**	C cpd **3**	O_1 cpd **3**	O cpd **3**
Carb(Ac-Enz (**A**)	-0.70	0.68	-0.29	**-0.65**	-0.70	0.76	-0.49	**-0.71**	-0.66	0.75	-0.48	**-0.68**
TS (**B**)	-0.76	0.72	-0.37	**-0.83**	-0.77	0.84	-0.59	**-0.86**	-0.74	0.82	-0.60	**-0.86**
TI (**C**)	-0.61	0.76	-0.48	**-0.99**	-0.71	0.87	-0.53	**-0.93**	-0.63	0.85	-0.52	**-0.96**
TS (**D**)	-0.53	0.70	-0.54	**-0.81**	-0.62	0.83	-0.56	**-0.86**	-0.48	0.78	-0.74	**-0.68**
Products (**E**)	-0.53	0.68	-0.45	**-0.62**	-0.52	0.78	-0.50	**-0.70**	-0.50	0.78	-0.48	**-0.63**

Table 7.4 Mulliken charges of selected heavy atoms involved in the formation and/or in the breakage of covalent bonds, or subject to a change in the hybridization state during FAAH deacylation or decarbamoylation. Atom labels are consistent with Figure 7.4.

Decomposition Analysis

The contributions of individual residues to the stabilization of the TI with respect to reactants (state A), were also analyzed by decomposition analysis (see method section). The TI is the most important configuration along the deacylation and decarbamoylation reaction in presence of FAAH, where the stabilizing effect of the enzyme reaches is highest contribution. It is thus meaningful to consider this stationary point as a reference state to look at the effect of individual residues.

In the case of deacylation of 1, the decomposition analysis indicated that the highest contribution in the lowering the energy of the TI is from the auxiliary water W2 (Figure 7.11). This water molecule is a structurally conserved component of the FAAH active site and it is found here to form a very short hydrogen bond with the carbonyl oxygen of the acylating group in the TI. Other important residues in the TI stabilization are Thr236 and Ser218. These two residue accept hydrogen-bond from the positively charged Lys142. The components of the oxyanion hole, which in FAAH is composed by the NH backbone groups of four consecutive residues, namely Ile238, Gly239, Gly240 and Ser241, are expected to participate actively to the stabilization. However, in the case of deacylation of compound 1, only Ile238 and Ser241 have a significant role in the TI stabilization. On the other hands, Arg243 which places its positively charged side chain just behind the oxyanion hole, it is also found to have an important stabilizing effect. Other amino acids show negligible contributions, with the exception of Asp237, which shows a small destabilizing effect on the TI.

A similar effect is observed also for decarbamoylation reactions in presence of compounds 2 and 3, with the important exception of the role played by the auxiliary

water molecule W2. Indeed, in the case of the decarbamoylation of the irreversible inhibitor 2, this water molecule is found to have a less important role in stabilizing the TI. Visual inspection of the structures along the decarbamoylation pathway of 2 indicates that W2 remains far away from the carbonyl oxygen of the carbamoylating group. This is mainly due the presence of an accessory hydrogen bond at the active site, between the NH group of the carbamoylated Ser241 and the carbonyl oxygen of Ser193, that changes the relative position of the carbamic moiety in the active site, when compared to the acylating group of 1. Notably, the effect of this hydrogen bond on the stabilization of the TI is indirect, as its contribution is energetically negligible. In fact, removal of Ser193 from the active site does not influence the potential energy of the system, as obtained by single point calculation. In the case of decarbamoylation of compound 3, the stabilizing effect of FAAH is similar to that observed for deacylation of 1. Compound 3 forms a tertiary carbamate with Ser241, being its carbamic N included in piperizine ring. As a consequence, no hydrogen bond can be formed with Ser193 backbone oxygen, and thus the water molecule W2 can access the former carbonyl oxygen at the TI, stabilizing its energy.

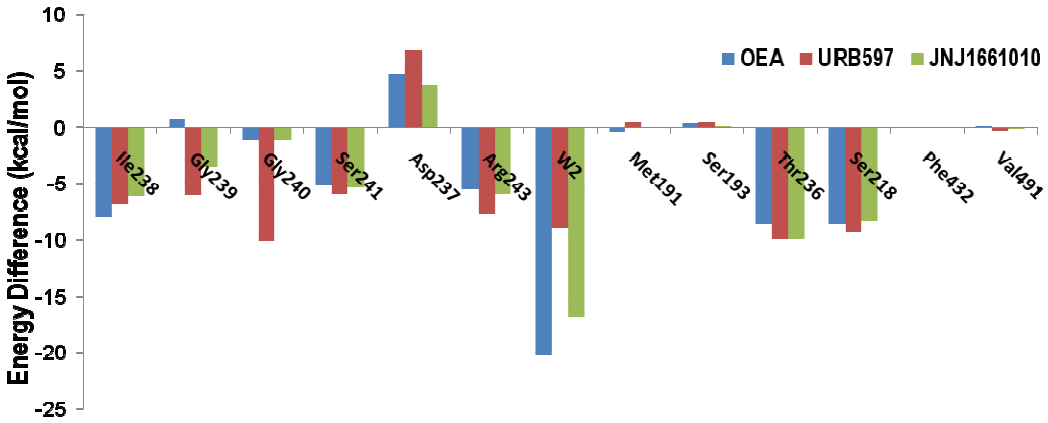

Figure 7.11 Amino acid decomposition analysis showing the energy contribution of MM-residue on SCC-DFTB/CHARMM27 energy of the TI (state **C**). Negative values correspond to stabilization, positive ones to destabilization. Energies are relative to the acyl/carbamoyl-enzyme.

Conclusions

Carbamoylating compounds block the catalytic activity of serine hydrolases by trapping the nucleophile residue of the enzyme, within an acylenzyme-like intermediate that, differently from the substrate-based one, is resistant to chemoenzymatic hydrolysis. In the present work, a QM/MM protocol validated for

FAAH catalyzed reactions is applied to understand the chemical determinats of reversible and irreversible inhibition of FAAH by carbamoylating agents. To this purpose, the energetics for the deacylation reaction in presence of a FAAH substrate 1 was investigated and used as a reference reaction.

Calculations show that deacylation of FAAH occurs with a significantly lower activation barrier than decarbamoylation, both starting from the adducts with the irreversible and the reversible inhibitors 2 and 3. Calculations indicate that deacylation is energetically favoured for two main reasons: *i)* the TI generated from an ester is more accessible than that generated from a carbamate; *ii*) the active site of FAAH stabilizes the anionic TI much more for the deacylation pathway rather than for decarbamoylation pathways, with a fundamental role played by those FAAH residues which are involved in the stabilization of the negative charge of this intermediate. Among these residues, the conserved W2 molecule emerged as a discriminating element between reversible and irreversible carbamoylating inhibitors. Compound 2 inhibits FAAH producing a secondary serine carbamate, where the cyclohexylamine portion forms a hydrogen-bond with Ser193, which assumes a geometry that does not allow to W2 to interact closely with carbamate carbonyl oxygen. This results in significant increment of the TI energy, making the decarbamoylation reaction unlikely to take place, according to experimental data on cyclohexyl carbamic acid *O*-biphen-3-yl esters.[143] This is not the case for compound 3, being unable to donate hydrogen bond to Ser193 assumes a position at the active site that is comparable to that of the acylating portion of the substrate, taking thus advantage of the stabilizing effect given by water molecule W2. In conclusion, this computational study has been able to well reproduce the experimentally observed kinetic differences among the following processes: *i)* deacylation of a substrate; *ii)* decarbamoylation of a reversible inhibitor; *iii)* decarbamoylation of an irreversible inhibitor. The atomistic insight here obtained may help the design of novel reversible and irreversible FAAH inhibitors.

[115] McKinney, M. K.; Cravatt, B. F. Structure and function of fatty acid amide hydrolase. Annu Rev Biochem 2005, 74, 411-432.

[116] (a) Cravatt, B. F.; Giang, D. K.; Mayfield, S. P.; Boger, D. L.; Lerner, R. A.; Gilula, N. B. Molecular characterization of an enzyme that degrades neuromodulatory fatty-acid amides. Nature 1996, 384, 83–87. (b) Patricelli, M. P.; Cravatt, B. F. Clarifying the catalytic roles of conserved residues in the amidase signature family. J Biol Chem 2000, 275, 19177–19184. (c) McKinney, M. K.; Cravatt, B. F. Evidence for distinct roles in

catalysis for residues of the serine-serine-lysine catalytic triad of fatty acid amide hydrolase. J Biol Chem 2003, 278, 37393-37399.

[117] (a) Lodola, A.; Mor, M.; Hermann, J. C.; Tarzia, G.; Piomelli, D.; Mulholland, A. J. QM/MM modelling of oleamide hydrolysis in fatty acid amide hydrolase (FAAH) reveals a new mechanism of nucleophile activation. Chem Commun 2005, 4399-4401. (b) Tubert-Brohman, I.; Acevedo, O.; Jorgensen, W. L. Elucidation of hydrolysis mechanisms for fatty acid amide hydrolase and its Lys142Ala variant via QM/MM simulations. J Am Chem Soc 2006, 128, 16904-16913. (c) Lodola, A.; Mor, M.; Sirirak, J.; Mulholland, A. J. Insights into the mechanism and inhibition of fatty acid amide hydrolase from quantum mechanics/molecular mechanics (QM/MM) modelling. Biochem Soc Trans 2009, 37, 363-367. (d) Lodola, A.; Sirirak, J.; Fey, N.; Rivara, S.; Mor, M.; Mulholland, A. J. Structural fluctuations in enzyme-catalyzed reactions: Determinants of reactivity in fatty acid amide hydrolase from multivariate statistical analysis of quantum mechanics/molecular mechanics paths. J. Chem. Theory Comput. 2010, 6, 2948-2960.

[118] Fu, J.; Bottegoni, G.; Sasso, O.; Bertorelli, R.; Rocchia, W.; Masetti, M.; Guijarro, A.; Lodola, A.; Armirotti, A.; Garau, G.; Bandiera, T.; Reggiani, A.; Mor, M.; Cavalli, A.; Piomelli, D. A catalytically silent FAAH-1 variant drives anandamide transport in neurons. Nat Neurosci. 2012. 15, 64-69.

[119] Mileni, M.; Kamtekar, S.; Wood, D. C.; Benson, T. E.; Cravatt, B. F.; Stevens, R. C. Crystal structure of fatty acid amide hydrolase bound to the carbamate inhibitor URB597: discovery of a deacylating water molecule and insight into enzyme inactivation. J Mol Biol. 2010, 400, 743-754.

[120] (a) Otrubova, K.; Ezzili, C.; Boger, D. L. The discovery and development of inhibitors of fatty acid amide hydrolase (FAAH). Bioorg Med Chem Lett 2011, 21, 4674-4685. (b) Minkkilä, A.; Saario, S.; Nevalainen T. Discovery and development of endocannabinoid-hydrolyzing enzyme inhibitors. Curr Top Med Chem. 2010, 10, 828-858. (c) Seierstad, M.; Breitenbucher, J. G. Discovery and development of fatty acid amide hydrolase (FAAH) inhibitors. J Med Chem 2008, 51, 7327-7343. (d) Vandevoorde, S. Overview of the chemical families of fatty acid amide hydrolase and monoacylglycerol lipase inhibitors. Curr Top Med Chem. 2008, 8, 247-267. (e) Lambert, D. M.; Fowler, C. J. The endocannabinoid system: drug targets, lead compounds, and potential therapeutic applications. J Med Chem 2005, 48, 5059-5087.

[121] Mor, M.; Rivara, S.; Lodola, A.; Plazzi, P. V.; Tarzia, G.; Duranti, A.; Tontini, A.; Piersanti, G.; Kathuria, S.; Piomelli, D., Cyclohexylcarbamic acid 3'- or 4'-substituted biphenyl-3-yl esters as fatty acid amide hydrolase inhibitors: synthesis, quantitative structure-activity relationships, and molecular modeling studies. J Med Chem 2004, 47, 4998-5008.

[122] Lodola, A.; Rivara, S.; Mor, M. Application of computational methods to the design of fatty acid amide hydrolase (FAAH) inhibitors based on a carbamic template structure. Adv Protein Chem Struct Biol. 2011, 85, 1-26.

[123] Alexander, J. P.; Cravatt, B. F. Mechanism of carbamate inactivation of FAAH: implications for the design of covalent inhibitors and in vivo functional probes for enzymes. Chem Biol 2005, 12, 1179-1187.

[124] Lodola, A.; Mor, M.; Rivara, S.; Christov, C.; Tarzia, G.; Piomelli, D.; Mulholland, A. J., Identification of productive inhibitor binding orientation in fatty acid amide hydrolase (FAAH) by QM/MM mechanistic modelling. Chem Commun 2008, 214-216.

[125] Lodola, A.; Capoferri, L.; Rivara, S.; Chudyk, E.; Sirirak, J.; Dyguda-Kazimierowicz, E.; Sokalski, W. A.; Mileni, M.; Tarzia, G.; Piomelli, D.; Mor, M.; Mulholland, A. J. Understanding the role of carbamate reactivity in fatty acid amide hydrolase inhibition by QM/MM mechanistic modelling. Chem Commun 2011, 47 , 214-216.

[126] Mileni, M.; Johnson, D. S.; Wang, Z.; Everdeen, D. S.; Liimatta, M.; Pabst, B.; Bhattacharya, K.; Nugent, R. A.; Kamtekar, S.; Cravatt, B. F.; Ahn, K.; Stevens, R. C.. Structure-guided inhibitor design for human FAAH by interspecies active site conversion. Proc Natl Acad Sci USA 2008, 105, 12820-12824.

[127] Keith, J. M.; Apodaca, R.; Xiao, W.; Seierstad, M.; Pattabiraman, K.; Wu, J.; Webb, M.; Karbarz, M. J.; Brown, S.; Wilson, S.; Scott, B.; Tham, C. S.; Luo, L.; Palmer, J.; Wennerholm, M.; Chaplan, S.; Breitenbucher, J. G., Thiadiazolopiperazinyl ureas as inhibitors of fatty acid amide hydrolase. Bioorg Med Chem Lett 2008, 18, 4838-4843.

[128] Ahn, K.; Johnson, D. S.; Fitzgerald, L. R.; Liimatta, M.; Arendse, A.; Stevenson, T.; Lund, E. T.; Nugent, R. A.; Nomanbhoy, T. K.; Alexander, J. P.; Cravatt, B. F. Novel mechanistic class of fatty acid amide hydrolase inhibitors with remarkable selectivity. Biochemistry 2007, 46, 13019–13030.

[129] Sykes, N. O.; Macdonald, S. J.; Page, M. I. Acylating agents as enzyme inhibitors and understanding their reactivity for drug design. J Med Chem 2002, 45, 2850-2856.

[130] Karbarz, M. J.; Luo, L.; Chang, L.; Tham, C. S.; Palmer, J. A.; Wilson, S. J.; Wennerholm, M. L.; Brown, S. M.; Scott, B. P.; Apodaca, R. L.; Keith, J. M.; Wu, J.; Breitenbucher, J. G.; Chaplan, S. R.; Webb, M. Biochemical and biological properties of 4-(3-phenyl-[1,2,4] thiadiazol-5-yl)-piperazine-1-carboxylic acid phenylamide, a mechanism-based inhibitor of fatty acid amide hydrolase. Anesth Analg. 2009, 108, 316-329.

[131] (a) Warshel, A.; Levitt, M. Theoretical studies of enzymic reactions: dielectric, electrostatic and steric stabilization of the carbonium ion in the reaction of lysozyme. J Mol Biol 1976, 103, 227-249. (b) Field, M. J.; Bash, P. A.; Karplus, M. A combined quantum mechanical and molecular mechanical potential for molecular dynamics simulations. J Comput Chem 1990, 11, 700-733. (c) Gao, J. In Reviews in Computational Chemistry; Lipkowitz, K. B., Boyd, D. R., Eds.; VCH Publishers: New York, 1996; Vol. 7, pp 119-185. (d) Warshel, A. Computer simulations of enzyme catalysis: methods, progress, and insights. Annu Rev Biophys Biomol Struct 2005, 32, 425-443.

[132] Patricelli, M. P.; Lovato, M. A.; Cravatt, B. F. Chemical and mutagenic investigations of fatty acid amide hydrolase: evidence for a family of serine hydrolases with distinct catalytic properties. Biochemistry 1999, 38, 9804–9812.

[133] Brooks, B. R.; Bruccoleri, R. E.; Olafson, B. D.; States, D. J.; Swaminathan, S.; Karplus, M. Charmm - A Program for Macromolecular Energy, Minimization, and Dynamics Calculations. J. Comput. Chem. 1983, 4, 187-217. www.charmm.org

[134] MacKerell, A. D.; Bashford, D.; Bellott, M.; Dunbrack, R. L.; Evanseck, J. D.; Field, M. J.; Fischer, S.; Gao, J.; Guo, H.; Ha, S.; Joseph-McCarthy, D.; Kuchnir, L.; Kuczera, K.; Lau, F. T. K.; Mattos, C.; Michnick, S.; Ngo, T.; Nguyen, D. T.; Prodhom, B.; Reiher, W. E.; Roux, B.; Schlenkrich, M.; Smith, J. C.; Stote, R.; Straub, J.; Watanabe, M.; Wiorkiewicz-Kuczera, J.; Yin, D.; Karplus, M. All-Atom Empirical Potential for Molecular Modeling and Dynamics Studies of Proteins. J. Phys. Chem. A 1998, 102, 3586-3616.

[135] Cui, Q.; Elstner, M.; Kaxiras, E.; Frauenheim, T.; Karplus, M. A QM/MM Implementation of the Self-Consistent Charge Density Functional Tight Binding (SCC-DFTB) Method. J. Phys. Chem. B 2001, 105, 569-585.

[136] Elstner, M. The SCC-DFTB method and its application to biological systems. Theor. Chem. Acc. 2006, 116, 316–325

[137] (a) Woodcock, H, L.; Hodoscek, M.; Brooks, B. R. Exploring SCC-DFTB paths for mapping QM/MM reaction mechanisms. J. Phys. Chem. A 2007, 111, 5720-5728. (b) Riccardi, D.; Schaefer, P.; Yang, Y.; Yu, H.; Ghosh, N.; Prat-Resina, X.; König, P.; Li, G.; Xu, D.; Guo, H.; Elstner, M.; Cui, Q. Development of effective quantum mechanical/molecular mechanical (QM/MM) methods for complex biological processes. J. Phys. Chem. B 2006, 110, 6458–6469. (c) Xu, D.; Guo, H.; Cui, Q. Antibiotic deactivation by a dizinc beta-lactamase: mechanistic insights from QM/MM and DFT studies. J. Am. Chem. Soc. 2007, 129, 10814-10822. (d) Barnett, C. B.; Wilkinson, K. A.; Naidoo, K. J. Molecular details from computational reaction dynamics for the cellobiohydrolase I glycosylation reaction. J. Am. Chem. Soc. 2011, 133:19474-19482. (e) Mujika, J. I.; Lopez, X.; Mulholland, A. J. Mechanism of C-terminal intein cleavage in protein splicing from QM/MM molecular dynamics simulations. Org. Biomol. Chem. 2011, in press. (f) Lodola, A.; Branduardi, D.; Capoferri, L.; De Vivo, M.; Mor, M.; Piomelli, D. A catalytic mechanism for cysteine N-terminal nucleophile hydrolases, as revealed by free energy simulations Plos One, 2012, accepted for revision.

[138] Jorgensen, W. L.; Chandrasekhar, J.; Madura, J. D.; Impey, R. W.; Klein, M. L. Comparison of Simple Potential Functions for Simulating Liquid Water J. Chem. Phys. 1983, 79, 926-935.

[139] Brooks, C. L. III.; Karplus, M. Deformable stochastic boundaries in molecular dynamics. J. Chem. Phys, 1983, 79, 6312-6325.

[140] Claeyssens F, Ranaghan KE, Lawan N, Macrae SJ, Manby FR, Harvey JN, Mulholland AJ. Analysis of chorismate mutase catalysis by QM/MM modelling of enzyme-catalysed and uncatalysed reactions. Org. Biomol. Chem. 2011, 9, 1578-1590

[141] Mulholland, A.J.; Richards, G. Acetyl-CoA enolization in citrate synthase: a quantum mechanical/molecular mechanical (QM/MM) study. Proteins 1997, 27, 9-25.

[142] Klahn, M.; Braun-Sand, S.; Rosta, E.; Warshel, A. On Possible Pitfalls in ab Initio Quantum Mechanics/Molecular Mechanics Minimization Approaches for Studies of Enzymatic Reactions. J. Phys. Chem. B 2005, 109, 15645–15650

[143] Tarzia, G.; Duranti, A.; Tontini, A.; Piersanti, G.; Mor, M.; Rivara, S.; Plazzi, P. V.; Park, C.; Kathuria, S.; Piomelli, D. Design, synthesis, and structure-activity relationship of alkylcarbamic acid aryl esters, a new class of fatty acid amide hydrolase inhibitors. J. Med. Chem. 2003, 46, 2352-2360.

8. Conclusions

Fatty acid amide hydrolase (FAAH) is an integral membrane enzyme that hydrolyzes the endocannabinoid anandamide and related signaling lipid amides. Pharmacological inactivation of FAAH produces analgesic, anti-inflammatory, anxiolytic, and antidepressant effects, without showing the undesirable side effects of direct cannabinoid receptor agonists. These findings suggest that FAAH may represent an attractive therapeutic target for treatment of pain, inflammation, and central nervous system (CNS) disorders. Over the past several years, drug-discovery efforts have led to potent FAAH inhibitors with varying mechanisms of action, potencies, and selectivities. Most promising classes of inhibitors form a covalent bond with Ser241. Among these molecules are O-aryl carbamates, including the reference compound cyclohexylcarbamic acid 3′-carbamoylbiphenyl-3-yl ester (URB597), and tertiary ureas, including the piperidinyl derivative PF-750 or the piperazinyl one, N-phenyl-4-(3-phenyl-1,2,4-thiadiazol-5-yl)-1-piperazine-carboxamide (JNJ1661010).

Potency and selectivity of an irreversible inhibitor can be optimized by altering the structure of the compound to modulate either its non-covalent binding to the target, or the rate at which it reacts with the target itself and with off-targets. This dual approach allows the potency and selectivity of covalent inhibitors to be fine-tuned. The reversibility of inhibition is another key aspect of the enzyme-inhibition since it has important consequences for drug pharmacodynamics, particularly when the extent and duration of target inhibition affects the level and frequency of doses required to achieve the desired pharmacological effect. Moreover, reactivity of covalent inhibitors affect their pharmacokinetics, and in-vivo potency also depends on the exposure of target to the drug. For FAAH inhibitors, highest in-vivo potency was obtained combining sufficient target affinity and in-vitro potency and stabilization of the key carbamate group toward hydrolysis by generic esterases, as in the case of second-generation aryl carbamates, including the para-hydroxyphenyl derivative, URB694. The development of this compound, performed at the University of Parma, in collaboration with University of Urbino and University of California at Irvine, was the result of structure–activity relationship (SAR) studies showing that the

introduction of electron-donor groups on conjugated position to the carbamic group of the reference compound URB524 enhanced compound stability both in alkaline buffer and in rat plasma. Conversely, this substitution did not affect FAAH inhibitor potency in vitro. The overall effect was an improved in vivo potency of these compounds.

Modelling the carbamoylation reaction of FAAH by URB524 and its derivative by means of a QM/MM approach provides a mechanistic explanation for the lack of correlation between the in-vitro inhibitory potency and the reactivity of these carbamates. The computational protocol described in the present thesis is a reliable tool for in-silico prediction of in-vitro potency for new FAAH inhibitors of this class, that can be applied to the modulation of additional biological properties, such as in-vivo potency or tissue distribution. In spite of their different intrinsic reactivity, URB524 and its derivatives undergo the similar reaction mechanisms, since the rate-limiting step for FAAH carbamoylation by such compounds is activation of Ser241, instead of nucleophilic attack.

To improve the accuracy of QM/MM approach, maintaining a reasonable computational cost, the performance of the potential was also evaluated. SCC-DFTB proved to be excellent for geometries and energetics, performing, in the best cases, like DFT calculations. Since SCC-DFTB-CHARMM27 is a parametrized functional, its reliability on a biological system of interest needs to be assessed by extensive tests. The present thesis provide evidences that it works accurately for FAAH acylation by the substrates oleylamide and oleylmethylester. Taken together, these findings indicated that SCC-DFTB-CHARMM27 calculations can provide reliable results for enzyme catalysis for FAAH and similar enzymes.

This level of theory was finally employed to study another crucial aspect of FAAH inhibition, i.e. reversibility. Scientists at Johnson&Johnson have recently found that, while FAAH inhibited by URB597 did not recover amidase activity after 18-h dialysis, inhibition by JNJ1661010 was reversed in the same condition. The two inhibitors act

in a similar way, forming respectively a secondary and a tertiary carbamate at nucleophile Ser241. For the first time, deacylation reaction was here modeled for the oleylethanolamide substrate, providing energy barriers (16.6 kcal mol^{-1}) consistent with experimental results. The same protocol applied to decarbamoylation of the covalent adducts of FAAH with URB597 and JNJ1661010, respectively. Results indicated that the two adducts can undergo similar hydrolysis paths, with energy barriers for the reversible JNJ1661010 (23 kcal mol^{-1}) and for the irreversible URB597 (29 kcal mol^{-1}) consistent with their kinetic in dialysis experiments. Analysis of reaction paths showed that an accessory hydrogen bond between the inhibitor fragment and a residue close to the active site is crucial for stabilization of the covalent adduct formed by the secondary carbamate with nucleophilic serine in FAAH, thus providing a clue to design new inhibitors with tailored inhibition kinetics.